2012-10-03

Mathematical Modeling of Craniospinal Hydrodynamics: Investigation of CSF Dynamics and Compliance Function

Rong-Wen Tain
University of Miami, taylor27@gmail.com

UNIVERSITY OF MIAMI

MATHEMATICAL MODELING OF CRANIOSPINAL HYDRODYNAMICS: INVESTIGATION OF CSF DYNAMICS AND COMPLIANCE FUNCTION

By

Rong-Wen Tain

A DISSERTATION

Submitted to the Faculty
of the University of Miami
in partial fulfillment of the requirements for
the degree of Doctor of Philosophy

Coral Gables, Florida

December 2012

UNIVERSITY OF MIAMI

A dissertation submitted in partial fulfillment of
the requirements for the degree of
Doctor of Philosophy

MATHEMATICAL MODELING OF CRANIOSPINAL HYDRODYNAMICS: INVESTIGATION OF CSF DYNAMICS AND COMPLIANCE FUNCTION

Rong-Wen Tain

Approved:

Noam Alperin, Ph.D. Professor of Radiology and Biomedical Engineering	M. Brian Blake, Ph.D. Dean of the Graduate School
Byron L. Lam, M.D. Professor of Ophthalmology	Ozcan Ozdamar, Ph.D. Professor Biomedical Engineering
Justin C. Sanchez, Ph.D. Associate Professor of Biomedical Engineering	Weizhao Zhao, Ph.D. Associate Professor of Biomedical Engineering
Mohammad Sabati, Ph.D. Assistant Professor of Radiology	

TAIN, RONG-WEN (Ph.D., Biomedical Engineering)
Mathematical Modeling of Craniospinal Hydrodynamics: Investigation of CSF Dynamics and Compliance Function (December 2012)

Abstract of a dissertation at the University of Miami.

Dissertation supervised by Professor Noam Alperin.
No. of pages in text. (108)

During each heart beat, the cerebrospinal fluid (CSF) flows back and forth between the cranium and spinal canal. This pulsatile flow is driven by the pulsatile blood flow to the cranial vault and is modulated by the biomechanical properties of the craniospinal system (e.g., intracranial and spinal canal compliances). Considerable effort has been made over the last eight decades, primarily using invasive techniques, to understand the dynamics of the CSF pulsation and the role of each of the system's sub-compartments in modulation of the CSF pulsation. Even with the significant technical advances in both invasive and non-invasive modalities over the recent years, there are still conflicting observations and interpretations regarding the role of the spinal canal compartment in regulating CSF volumes and pressures in the healthy and in several related neurological disorders such as idiopathic intracranial hypertension (IIH) and Chiari-malformations Type I.

Anatomically, it is expected that the mechanical compliance (the ability to accommodate additional volume without a large increase in pressure) of spinal canal compartment is larger than that of cranial compartment since the spinal canal is less confined by the spinal column bony structures compared to the cranial vault. Yet, reports by other groups suggest reversed cranio-spinal compliance distribution. This project employs novel noninvasive tools to quantify the craniospinal compliance distribution to

investigate the influence of spinal canal compliance on the CSF dynamics in healthy and in impaired CSF dynamics related pathologies. In vivo quantitative characterization of the subject-specific biomechanics is achieved by combining an MR imaging and a lumped parameter modeling. The model applied in this work is different from other modeling studies of craniospinal system in the manner it considers the influence of spinal canal compliance on the CSF flow dynamics. The model was validated by comparing the model derived results with invasive measurements based on CSF infusion. In addition, the reproducibility of estimated parameters was tested using repeated MR scans from a craniospinal flow phantom and from healthy subjects.

Application of this methodology to MRI data from healthy subjects and from patients with obesity-related idiopathic intracranial hypertension suggests, for the first time, a spinal canal involvement in the pathophysiology of IIH. The spinal canal compliance contribution to the overall craniospinal compliance is reduced in IIH compared to the healthy obese female subjects. In addition, modeling of the dynamic interplay between the cranial and spinal compliances explains the reason for the large pressure fluctuations documented in IIH. Furthermore, the modeling results even explain why obesity-related IIH and Chiari malformations occur at higher frequencies in females than in males.

DEDICATION

To my wife Chia-Hsuan, my best friend, my inspiration, my love.

ACKNOWLEDGMENTS

I don't wait for moods. You accomplish nothing if you do that. Your mind must know it has got to get down to work. —Pearl Buck

During years of my research career, with seemingly insurmountable task and besting chore I have experienced a very high quality of scientific training. I wish the work of my doctoral dissertation does not just show my scientific worth, but also enables further novel ideas to enhance our knowledge. Then it would stand to reason that this Ph.D. is really "worth it."

I would like to express my deepest gratitude to Dr. Noam Alperin not only for his precise and skilled mentorship, but also for his belief in me. His never-ending stream of ideas enriches me to the success of my work. I would like to thank Dr. Lam Byron for giving me the opportunity to work with idiopathic intracranial hypertension project. I would also like to thank my committee members Dr. Ozcan Ozdamar, Dr. Justin C. Sanchez, Dr. Weizhao Zhao and Dr. Mohammad Sabati for their encouraging words, thoughtful suggestions, constructive criticisms, and time.

I wish to thank Dr. Jung-Jiin Hsu for his unwavering help and support. To my colleagues and friends for sharing their enthusiasm and for comments on my work: Dr. Ahmet Bagci, Sang H Lee, Sudarshan Ranganathan, Pang-Yu Teng, and Michael Frisch.

I am, as always, indebted to my ever-loving wife Chia-Hsuan for the patience, understanding, encouragement, and inspiration. I would also like to thank my family. They are always supporting me with their best wishes.

Table of Contents

List of Figures

List of Tables

List of Abbreviations

ARMA	Autoregressive Moving Average
ART	Arterial Flow
BMI	Body Mass Index
COEF	Pearson's Correlation Coefficient
CR	Intracranial Compartment
CS	Cranio-Spinal System
CSC	Craniospinal Compliance
CSF	Cerebrospinal Fluid
FOV	Field of View
ICC	Intracranial Compliance
ICCI	Intracranial Compliance Index
ICP	Intracranial Pressure
ICVC	Maximal Intracranial Volume Change
IIH	Idiopathic Intracranial Hypertension
MIP	Maximum Intensity Projection
MRA	Magnetic Resonance Angiogram
MRV	Magnetic Resonance Venogram
PG	Pressure Gradient
PVI	Pressure-Volume Index
RSD	Relative Standard Deviation
SC	Spinal Canal Compartment
SCC	Spinal Canal Compliance
SCCC	Spinal Canal Compliance Contribution
SCCR	Spinal Canal Resistance Contribution
TE	Echo Time
TOF	Time of Flight
TR	Repetition Time
VEN	Venous Flow
VENC	Velocity Encoding
VFR	Volumetric Flow Rate

Chapter 1 Introduction

By definition, mechanical compliance is the ability of a compartment to accommodate additional volume without a large increase in pressure. Reduced craniospinal compliance and the resulted increased intracranial pressure (ICP) has been suggested to be associated with several related neurological disorders (e.g., idiopathic intracranial hypertension (Dhungana *et al.*, 2010), Chiari-malformation Type I (Alperin *et al.*, 2005b) and brain injuries (Deeren *et al.*, 2005)). The management of ICP is critical for preventing brain damage since it is required for maintaining an adequate cerebral perfusion pressure (>60 mmHg), and normal cerebral blood flow for intact neurological function (Schmidt *et al.*, 2011).

Clinical approaches to measure the overall craniospinal compliance (CSC) were presented in the late 20th century from the relationship between volumes and pressures using invasive injection or removal of fluid from the craniospinal system (Marmarou *et al.*, 1975; Löfgren and Zwetnow, 1973; Ekstedt, 1977). It has been shown that pressure (i.e., ICP) is a function of volume and compliance. Increased ICP is associated with reduced CSC. Over the past two decades, researchers focus on development of noninvasive approaches to measure intracranial compliance (ICC) (Alperin *et al.*, 2000; Egnor *et al.*, 2001; Wagshul *et al.*, 2006). However, the reliability and sensitivity of these noninvasive approaches have not been investigated. Furthermore, there are considerable differences between the different noninvasive approaches. Some of them are based on modeling of the craniospinal system, while others propose empirical

relationships between surrogate measures of the cerebrospinal fluid (CSF) flow dynamics and compliance. Finally, very few approaches account for the role of the spinal canal compartment contribution to the overall compliance of the craniospinal system.

The spinal canal and the cranial compartment are connected together. However, these two compartments are anatomically very different. The tough membrane that encloses the craniospinal system, the durra is less confined by bony structures than the cranium. Therefore the spinal canal compartment plays an important role in the overall regulation of ICP, especially in accommodating large changes such as the differences between upright and supine postures (Alperin *et al.*, 2005a).

Efforts have been made to characterize the contributions of each sub-compartment to the overall craniospinal system compliance (Löfgren *et al.*, 1973; Marmarou *et al.*, 1975; Magnaes, 1989; Wåhlin *et al.*, 2010; Tain *et al.*, 2011). However, results related to the distribution of craniospinal compliance (CSC) are inconsistent. Our group provided insight to the reasons for the conflicting results and was the first to demonstrate the role of the spinal canal compliance in a neurological disorder where ICP regulation is lost, i.e., idiopathic intracranial hypertension (IIH) (Tain *et al.*, 2011). This new insight may also explain elevated ICP reported in some astronauts following long duration exposure to microgravity (Alperin N, personal communication, 2012).

Mathematical modeling became an important investigational tool in the effort to better understand the craniospinal hydrodynamics. The first mathematical model of the CS hydrodynamics appeared in the literature some forty years ago (Agarwal *et al.*, 1969). These models usually employ electrical-circuit-analogue based on anatomical features of

CNS. An important example to the contribution of modeling to this field is the RC circuit model proposed by Marmarou et al to describe the dynamics of the CSF circulation, i.e., CSF formation and absorption rates (Marmarou *et al.*, 1978). This model helped explain relationships between craniospinal CSF volume, compliance and ICP. Since the introduction of MRI measurements of blood and CSF flows in the late 1980s, modeling work focused on understanding CSF pulsation dynamics (Alperin *et al.*, 1996; Yallapragada, 2003; Ambarki *et al.*, 2007).

This study employs modeling to further advance novel noninvasive methodology to measure the intracranial pressure and to quantify the craniospinal compliance distribution, which is critical for the overall understanding of the CSF flow dynamics in the healthy and disease states. This aim is achieved by combing MR-based measurements of cerebral blood and CSF flows to and from the craniospinal sub-compartments and a lumped parameter modeling approach (Tain and Alperin, 2009). The reliability and reproducibility of the model is reported in Chapter 3. Chapter 4 extends the discussion of reliability regarding the influence of cervical blood vessel compliances on the CS compliance measurements (Tain *et al.*, 2009). Chapter 5 describes the sensitivity of noninvasive methods for measurement of intracranial compliance (Tain and Alperin, 2009). Chapter 6 describes the method to determine compliance distribution of the craniospinal system (Tain *et al.*, 2011). Chapter 7 describes the CSF volume buffering function of intracranial and spinal compliance on ICP regulation that may advance future CSF study.

Chapter 2 Background

2.1 The Craniospinal System

The human craniospinal system includes the intracranial and spinal canal compartments. The contents of the system (i.e., brain tissue, spinal cord tissue, blood and CSF) are protected by the skull and vertebrate column. The meninges enclosing the CNS consist of dura matter, arachnoid matter and pia matter provide a hermetical enclosure for the CSF as shown in Figure 2-1. The meninges also provide a supporting framework for arteries, veins, and venous sinuses. The ventricles and subarachnoid space of the craniospinal system contains the CSF.

In healthy young adults, the average volume of the brain and spinal cord are approximately 1280 mL (Reite *et al.*, 2010) and 20 mL (Yanase *et al.*, 2006; Ko *et al.*, 2004), respectively. The reported average blood volumes in the cranium and in the spine are 4.5 mL/100 mL tissue (Gu *et al.*, 2006) and 4.3 mL/100 mL tissue (Lu *et al.*, 2008), respectively. Total intracranial CSF volume is 150 mL in average (Johanson *et al.*, 2008; Tsunoda *et al.*, 2000) including ventricular CSF volume of 23 mL (Reite *et al.*, 2010). Total CSF volumes in the spinal canal compartment measured from two healthy controls are 100 and 120 mL, respectively (Hogan *et al.*, 1996). Interestingly, based on very limited data, CSF volumes in the spinal canal compartment demonstrate large inter-individual variability(Lee *et al.*, 2001). In addition, the ratio of intracranial CSF volume to brain volume increases in aging (Wanifuchi *et al.*, 2002). Changes in CSF and blood

volumes distribution in the various sub-compartments are tightly related to the distribution of compliances within the craniospinal system.

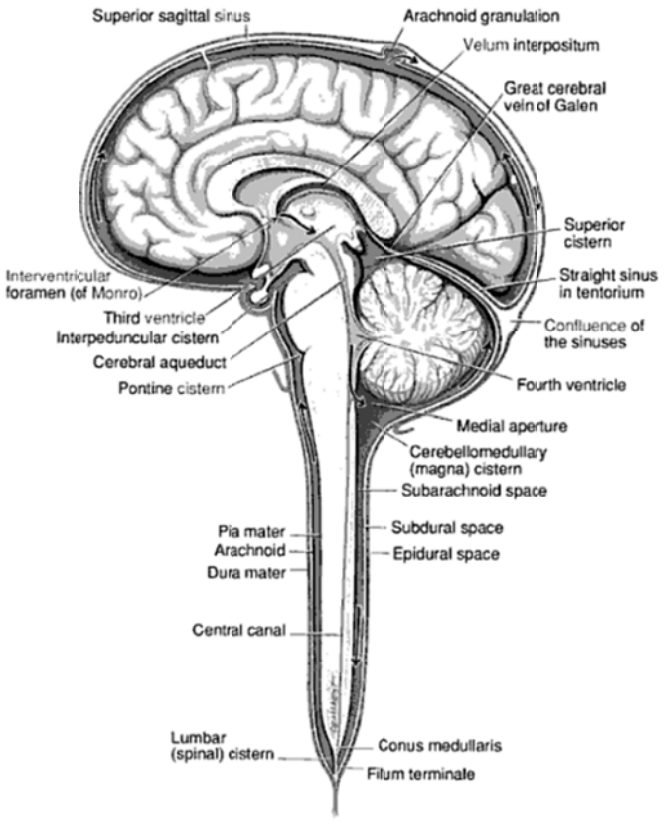

Figure 2-1: Diagram of human subarachnoid space surrounding the brain and spinal cord (Noback *et al.*, 2005).

2.2 The Blood Circulation through the Craniospinal System

The brain receives its blood supply from the heart mainly through 4 arteries, the two internal carotid arteries and two vertebral arteries (Noback *et al.*, 2005). These four arteries are interconnected with the Circle of Willis, an important anatomic vascular formation to provide backup circulation to the brain shown in Figure 2-2. Cerebral blood drainage can be separated into superficial and deep venous systems shown in Figure 2-3. The superficial cerebral veins are located on the surface of the cerebrum draining into the dural venous sinuses. The largest sinus, the superior sagittal sinus flows in the sagittal

plane under the midline of the cerebral vault. The superior sagittal sinus and the straight sinus drain into the transverse sinuses at the confluence of sinuses. The two transverse sinuses travel laterally and form the S-shaped sigmoid sinuses which then drain into the two internal jugular veins draining blood into the superior vena cava. The network of deep venous system is very complex. In general, the deep venous drainage is through the deep anastomotic veins to the region of the foramina of Monro. Blood is then drained into the internal cerebral veins, the Galenic system of veins and flows through the straight sinus.

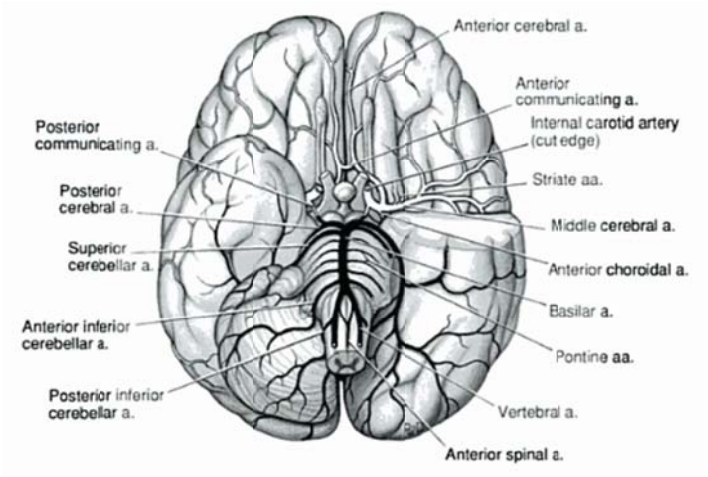

Figure 2-2: Major arterial blood supply to the brain (Noback *et al.*, 2005).

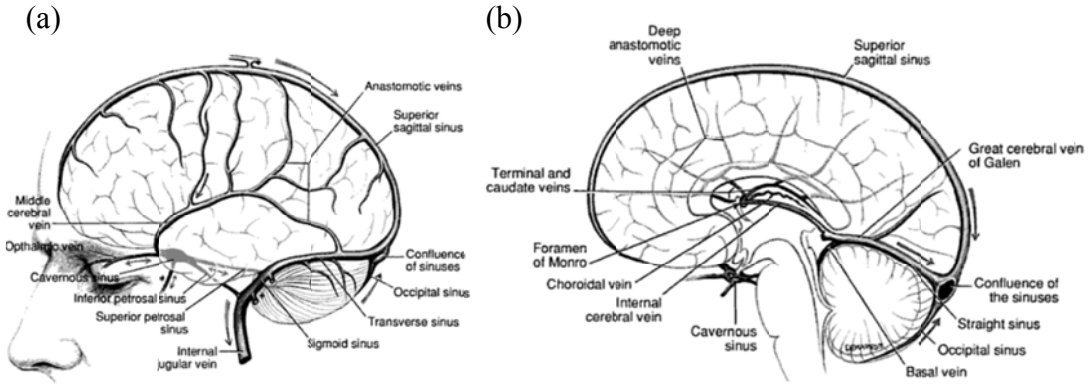

Figure 2-3: Venous drainage from the brain (a) lateral view of the brain; (b) medial view of the brain (Noback *et al.*, 2005).

The blood to spinal cord is supplied by the segmental spinal arteries that enter the intervertebral foramen shown in Figure 2-4a. The cervical spinal cord receive blood from the vertebral arteries (Fedorow *et al.*, 2010). The lower spinal (thoracic) cord received its blood supply from the intercostal artereis, which originate from the abdominal aorta. The venous system that drains the spinal cord is composed of several intercommunicating systems shown in Figure 2-4b. The radicular veins drain into the internal (or epidural) vertebral venous plexus and the occipital and basilar venous sinuses (Takahashi, 2010). These veins then enteres the intervertebral foramina to communicate with the vertebral veins, the intercostal veins, the lumbar veins, and the vena cava.

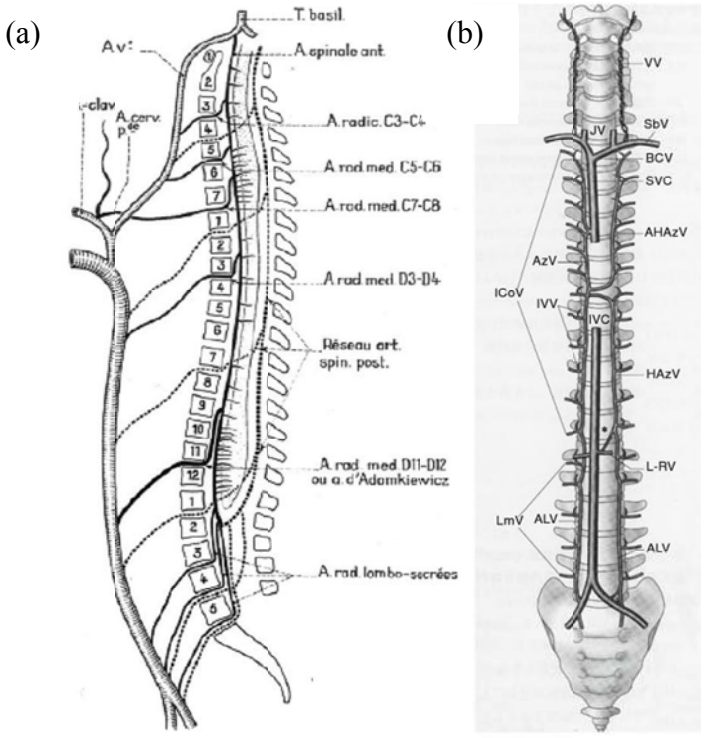

Figure 2-4: Diagrams of spinal cord blood supply (a) (Fedorow *et al.*, 2010) and venous drainage (b) (Takahashi, 2010). A. v, vertebral artery; A cerv p, deep cervical arteries; A s-clav, subclavian artery; T. basil, basilar artery; A. spinal ant., anterior spinal artery; A radic C3-C4, radicular artery at C3-C4; A rad. Med C5-C6, radicular artery at C5-C6; A rad. Med C7-C8, radicular artery at C7-C8; A rad. Med D3-D4, radicular artery at D3-D4; Reseau art. spin. post., posterior spinal artery; A rad. Med D11-D12, radicular artery at D11-D12; A rad lombo-sacrees, lumbosacral radicular arteries; VV, vertebral vein; JV, jugular vein; SVC, superior vena cava; ICoV, intercostals vein; LmV, lumbar vein; IVC, inferior vena cava.

2.3 Cerebrospinal Fluid

CSF is a transparent fluid with a density similar to that of water. It occupies the ventricular system and subarachnoid space around the brain and spinal cord. CSF is produced by the choroid plexus located in the lateral, third, and fourth ventricles (see Figure 2-1). Traditional view of the ***CSF circulation*** suggests that the CSF is formed from the lateral ventricles to the third ventricle and then the fourth ventricle. It then flows out of the ventricles to the subarachnoid space of the craniospinal system through the foramen of Magendie and Luschka. At the end, CSF is absorbed to the circulation system by entering the dural venous sinuses via the arachnoid granulations or villi (Noback *et al.*, 2005). Normally, the rate of CSF production and absorption is balanced in order to maintain constant CSF volume in the craniospinal system. In general the production rate in adult is about 500 ml/day or approximately 0.33 mL/min (Eklund *et al.*, 2007). Considering that the total CSF volume is about 250 ml (Johanson *et al.*, 2008; Tsunoda *et al.*, 2000; Hogan *et al.*, 1996), CSF will turn over about twice a day. Another type of CSF dynamics found in the craniospinal system is called cyclic ***CSF pulsation*** that is moving along with the craniospinal axis during each cardiac cycle. It is widely accepted that the CSF pulsation between the intracranial and spinal canal compartments is mainly due to the cyclic changes in ICP caused by the pulsatile blood flow and the resulting changes in intracranial volume during the cardiac cycle (Bhadelia *et al.*, 1997; Alperin *et al.*, 1996; Balédent *et al.*, 2001). Several studies suggest that only the cerebral arterial inflow is the driving force of the CSF pulsation (Balédent *et al.*, 2001; Egnor *et al.*, 2001), while other studies regards the difference between arterial inflow and the venous

outflow as the driving force for the CSF pulsation (Alperin *et al.*, 1996; Alperin *et al.*, 2000; Tain *et al.*, 2009).

2.4 Pressure-Volume Relationship

The relationship between the craniospinal volume and pressure has been the subject of many studies (Ryder *et al.*, 1953; Gilland, 1965; Shulman and Marmarou, 1971; Alperin *et al.*, 2000; Marmarou *et al.*, 1975; Katzman and Hussey, 1970; Ekstedt, 1977; Rekate, 2008). Ryder *et al.* were first to use infusion of fluid into the CSF space to characterize the pressure volume relationship (Ryder *et al.*, 1953). Similar technique were applied to study the pressure-volume curve in an isolated spinal canal compartment (Gilland, 1965). Six years later, Shulman and Marmarou proposed that the pressure and volume are related through a mono-exponential function (Shulman and Marmarou, 1971). This relationship is called the pressure-volume curve or the elastance curve (see Figure 2-5) and is described by the following equation

$$P = P_o e^{E_0 V} \tag{2-1}$$

where P_o is the initial pressure. E_o and V are the elastance coefficient constant and volume, respectively. An important finding from this mono-exponential relationship is linear relationship between the elastance (i.e., the inverse of compliance) and ICP. The mono-exponential relationship between ICP and intracranial volume is the basis for the MRI based method for derivation of ICP (Alperin *et al.*, 2000).

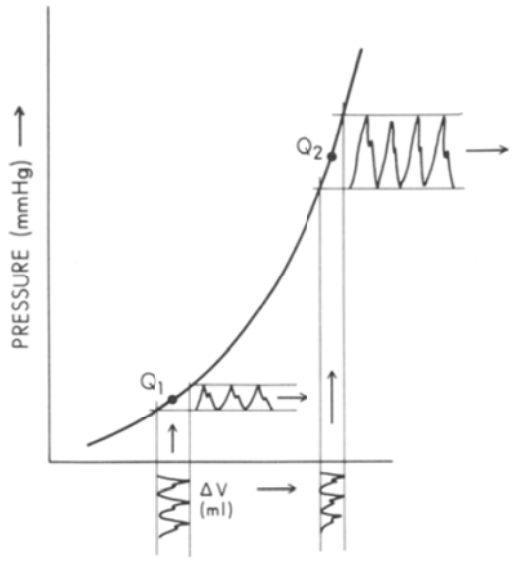

Figure 2-5: Pressure volume curve (Marmarou *et al.*, 1975).

2.5 CSF Infusion Test

Various invasive infusion methods are currently being used, more commonly in Europe, for research and for clinical evaluations of patients with CSF dynamics-related problems (e.g., normal pressure hydrocephalous (NPH) and idiopathic intracranial hypertension (IIH)). The most commonly used infusion methods include: a bolus injection, constant rate and constant pressure infusions. Infusion volumes and pressure recording are done simultaneously using two needles, which are inserted into the lumbar canal. With the bolus method, a single volume is quickly injected followed by a pressure recoding interval. The injections of fluid into CSF space are repeated with different incremental amounts (Marmarou *et al.*, 1975). The constant infusion method was proposed by Katzman and Hussey(Katzman and Hussey, 1970). With the constant infusion method, ICP reaches different steady states for different infusion rates. The injected rates and steady-state pressure are then used to derive compliance or CSF absorption resistance. The constant pressure method is an extension of the constant

volume infusion method (Ekstedt, 1977). In this method, six different steady levels of CSF pressure are achieved by various infusion rates.

A considerable limitation of these methods, besides being invasive, is the inconsistency of the measurements across the methods. It is very likely that the underlying cause of these inconsistencies is the fact that each method modulates the initial biomechanical state in a different manner which in turn, results with an altered biomechanical state. The discrepancy of compliance measurements using the bolus injection and the constant pressure infusion method has been recently reported (Wåhlin *et al.*, 2010). The MRI method proposed in this thesis utilizes the natural fluctuation of the system during the cardiac cycle for the compliance estimations and thus the measurement method does not interfere with the biomechanical state of the system.

2.6 Mechanical Properties of the Craniospinal System

CSF absorption rate, which is also termed absorption resistance, and a measure of the system compliance, e.g., a pressure volume index or PVI are the two main parameters of the craniospinal system determined using the various infusion tests.

Measurement of the CSF absorption resistance

Normally, CSF is absorbed by the arachnoid villi and flows into the superior sagittal sinus. The rate at which this absorption occurs is determined by the absorption resistance. An abnormal CSF absorption resistance has been proposed as the cause of several disorders such as hydrocephalus (Rekate, 2008).

With the bolus injection method, the resistance is calculated from the relaxation period of pressure after injections (Marmarou *et al.*, 1978). The constant rate and constant pressure infusion methods derive the absorption resistance from the infused volume and the difference of two corresponding steady state pressures (Katzman and Hussey, 1970). The reported range of normal CSF absorption resistance of 5 to 10 mmHg/(ml/min) (Eklund *et al.*, 2007). Elevated CSF absorption resistance of about 24 mmHg/(ml/min) and higher is sometimes found in idiopathic normal pressure hydrocephalus (Boon *et al.*, 1997).

Measurement of the craniospinal compliance

Compliance is defined as the ratio of the changes in volume and pressure. The craniospinal compliance determines the ability of craniospinal compartment to accommodate a large increase in volume (e.g., cerebral hemorrhages, tumors, brain swelling, impaired CSF absorption) without a large increase in pressure (i.e., ICP). Determination of compliance is important for diagnostic purposes, because it is altered by the pathophysiology of several CSF related disorders and it provides a prognostic value. The invasive bolus injection and the constant pressure infusion methods are commonly used for derivation of craniospinal system compliance at different mechanical states. Using the bolus injection method, a linear relationship was documented between the injected volume and the pressure response plotted in a semi-logarithmic scale (Marmarou *et al.*, 1975). The slope of the volume-log pressure curve is used to characterize craniospinal system compliance behavior and is termed the pressure-volume index (PVI). The PVI and its relationship to the compliance are described in the following equations

$$PVI = \frac{\Delta V}{\log_{10} \frac{P_p}{P_o}} \tag{2-2}$$

$$C = \frac{0.4343 * PVI}{P} \tag{2-3}$$

where P_0 is the initial pressure and P_p is the increased pressure due to the injected volume ΔV, C is the craniospinal compliance and P is the craniospinal pressure.

Measurements of the intracranial compliance using MRI

The intracranial compliance can be noninvasively estimated from the ratio of intracranial pressure and volume changes that occur naturally with each heart beat using MRI measurements of cerebral blood and CSF flows to and from the cranial vault (Alperin *et al.*, 2000). The change in the intracranial volume during each cardiac cycle is calculated from the net transcranial volumetric flow rates, i.e., the momentary difference in volumes of blood and CSF entering and leaving the cranial vault. The change in pressure is estimated from the CSF pressure gradient waveform, which is derived from the CSF outflow to and from of the brain by using the Navier-Stoke Equation (Urchuk and Plewes, 1994). The intracranial compliance index is then derived from the ratio of the maximal intracranial volume change and the maximal CSF pressure gradient change normalized by the CSF flow area (Alperin *et al.*, 2000).

Measurements of the spinal canal compliance

The spinal canal compliance influences the pulsation of ICP since it modulates the CSF volume that moves back and forth between the cranial and spinal canal compartments. Establishing the compliance contribution from the spinal canal compartment is thus important. However, CSF infusion-based determinations of the compliances of the individual sub-compartments of the craniospinal system provide conflicting results. A study of the craniospinal compliance distribution in six dogs using a constant infusion method suggested that the spinal canal compartment contributes larger compliance than the cranium (Löfgren *et al.*, 1973). Two years later, an almost opposite result of compliance distribution (cranium 62% vs. spinal canal 38%) was found in a cat study (Marmarou *et al.*, 1975). The compliance distribution was derived from individual compartment using bolus injection. Analogous to the cat experiment, patients with full cervical CSF blockage were used to study the compliance distribution (Magnaes, 1989). In contrast to Marmarou's findings, a larger spinal compliance (63%) was found when the patients were in the supine posture. In the upright position, the spinal canal compliance contribution reduced to 37% due to the shift of CSF volume from the cranium to the spinal canal. In a recent study, again conflicting results were found. A larger compliance contribution was measured from the intracranial compartments (an average of 63%) in supine elderly normal subjects (Wåhlin *et al.*, 2010). Our investigations summarized in Chapter 6 provide a detailed explanation for the possible sources of these conflicting results (Tain *et al.*, 2011). This work further determines the

craniospinal distribution in a similar cohort of healthy elderly subjects after addressing the limitation of the method proposed by Wåhlin *et al*. (Wåhlin *et al.*, 2010).

2.7 Summary

The CSF-related disorders such as hydrocephalus, idiopathic intracranial hypertension, and Chiari-malformation Type I are possibly associated with altered craniospinal system biomechanics (e.g., reduced compliance, high CSF absorption resistance, etc.). Currently, accepted approaches to characterize the system biomechanics are invasive and are often inconsistent. Therefore, application of well-established engineering principles, particularly the linear system theory and the MR techniques that enable noninvasive measurements of cerebral blood and CSF flow dynamics, to characterize the craniospinal system will potentially elucidate our limited understanding of the CSF related disorders as well as will provide a more accurate diagnostic tool leading to better management and treatment efficacy of this poorly understood domain.

Chapter 3 Lumped Parameter Model of Craniospinal System: Reliability and Reproducibility

3-1 Project Background

Lumped parameter modeling approach has been employed to characterize the intrinsic properties and behavior of the craniospinal system. Early modeling work described the relationship between cerebral blood flow circulations and CSF dynamics in the craniospinal system in terms of electrical analogous (Agarwal *et al.*, 1969). The hydraulic parameters of the circulation compartments including compliances and flow resistances were expressed by electrical capacitors and resistances, respectively. The system differential equations were used to simulate intracranial pressure dynamics and to explain potential causes, i.e., abnormal CSF absorption and reduced compliance, for several neurological disorders. Their work has since inspired numerous models of the CSF study (Takemae *et al.*, 1987; Rekate *et al.*, 1988; Lakin *et al.*, 2003; Stevens *et al.*, 2008). In contrast to the models focused on anatomical features of the craniospinal system, several researchers proposed models that emphasis on the mechanism of CSF reabsorption (Marmarou *et al.*, 1978; Fridén and Ekstedt, 1982; Bateman *et al.*, 2009). These types of models often combine CSF infusion methods (i.e., bolus injection and constant pressure infusion) to identify corresponding mechanical parameters of the system, i.e., compliance and CSF absorption resistance. The solution of the derived differential equations is then used to predict CSF pressure. However, it has been found that estimated parameters are influenced by the difference in CSF infusion paradigms (Sundström *et al.*, 2010; Wåhlin *et al.*, 2010).

Ursino has been the most prolific contributor to the ICP modeling literature (Ursino, 1988; Ursino *et al.*, 1995; Ursino *et al.*, 1996; Ursino *et al.*, 1997; Ursino and Lodi, 1998; Ursino *et al.*, 2000; Ursino and Giulioni, 2003). In general, his work focuses on the relationships between blood pressure, cerebral blood flow and intracranial pressure. Blood pressure is estimated indirectly from transcranial Doppler measurements of blood flow velocities in the middle cerebral arteries. In 1988, Ursino proposed a model relating ICP pulsations to the pulsatile cerebral blood volume within the intracranial space (Ursino, 1988). In the simulation of different craniospinal compliance, they found that the ICP pulsation is linearly proportional to the ICP. Ursino *et al.* further used this model to simulate ICP dynamics and compared with the pressure recorded from patients who underwent the bolus injection examination (Ursino *et al.*, 1995). They found that in some subjects, ICP dynamics do not return to the base line in a monotonic manner and thus proposed that is due to a varied CSF production rate. They further suggested that CSF production rate depends on capillary transmural pressure and blood flow. Ursino's later work further involved CO_2 reaction in cerebral vessels (Ursino and Lodi, 1998). In 2003, Ursino and Giulioni utilized the model to study the relationship between autoregulation and transcranial Doppler pulsatility (pulsatility index) (Ursino and Giulioni, 2003). They proposed a new autoregulation index that is related to arterial velocity amplitude, arterial pressure amplitude, and changes of cerebral perfusion pressure.

Once MRI methods for imaging of velocities became available (e.g., cine phase contrast), the measured blood and CSF flows (Marks *et al.*, 1992) were employed with modeling approaches to investigate the mechanism of changes in amplitude and phase of

flow dynamics and its association with altered mechanical properties of craniospinal system. Alperin *et al*. were the first to integrate subject-specific MRI-derived blood and CSF flow measurements with compartmental modeling (Alperin *et al.*, 1996). In this model, the arterial inflow and venous outflow were lumped together to become the net transcranial pulsatile blood flow that drives the CSF pulsations between the cranium and spinal canal. They further proposed a compartmental model of the craniospinal system that is characterized by an RC circuit, representing the intracranial compliance and the resistance to the craniospinal CSF flow. Later modeling by Egnor *et al.* proposed a theoretical RLC circuit model for the transmission of the arterial blood pressure to the CSF space (Egnor *et al.*, 2001). Their proposed theoretical model suggested that the CSF pressure and arterial blood pressure have a similar phase. A phase lag between the CSF and blood pressures then represents a reduction in compliance. Ambarki *et al.* proposed a comprehensive craniospinal model including arteries, veins, ventricular CSF space and extra ventricular CSF space (Ambarki *et al.*, 2007). Their model was able to simulate the phase relationship between blood and CSF flows. However, the input to this model was an artificial sinusoidal arterial pressure waveform. Other models were lacking because they neglected the spinal canal compartment (Wakeland and Goldstein, 2008).

In general, two types of mathematical models were proposed in the literature. The first type models assume literature reported values for some of the system components (Agarwal *et al.*, 1969; Ambarki *et al.*, 2007). However, the reliability of this approach is limited by assuming generic values for modeling subject-specific data due to the large biological variability. The reliability of the model-derived results depends on the validity

of the assumed values. The second type of modeling does not assume predetermined values for any of the system components (Alperin *et al.*, 1996; Yallapragada, 2003). The validity of these models depends on the ability to identify the system most relevant components for the system dynamics which is being investigated and measured. Our group in the modeling of craniospinal system was the first to employ the Bond Graph methodology (Gawthrop and Bevan, 2007). The Bond Graph approach utilizes the principles of energy and momentum conservation to guide the structure and the connections between system components that play a role in the overall system dynamics. Compared to the initial simple RC model proposed by Alperin *et al.* (Alperin *et al.*, 1996), the expended model includes the compliance and resistance characteristics of the spinal canal as well as the inertia of the CSF flow (Yallapragada, 2003).

Despite extensive research effort, modeling of the coupling between blood and CSF flows had only limited clinical impact so far. Incorporation of subject-specific modeling into clinical practice requires further investigations which demonstrate the validity and reproducibility of these models. Further, there is a clear need for a reliable modeling approach that can be integrated with subject-specific MRI measurements. The model proposed by Yallapragada and Alperin (Yallapragada, 2003) has several advantages and makes it a candidate for clinical translation. It does not assume predetermined values for specific components, it is practical because inputs and outputs for the system can be directly measured using MRI, and it is relatively robust and insensitive to noise. Previous simulation, where white noise was added to the MR

measures, demonstrated that the model converged to the same solution. This implies the identified circuit model can reproduce the desired flow and pressure dynamics.

The following section describes the additional validation work and investigation of various parameters on the overall robustness of the model. These include defining measures of the reliability of the model results. In addition, the model stability was tested with repeated MRI measurements obtained with a craniospinal flow phantom under well controlled conditions. These were then compared with repeated measurements obtained from healthy individuals.

The model of craniospinal system

The lumped parameter circuit model is based on two concepts, (i) simplified representation of the craniospinal system including the inlets and outlets of the system as shown in Figure 3-1 (Alperin *et al.*, 1996), (ii) the Bond Graph methodology to obtain the state-space equations of the system. The inlets and outlets of the cranial sub-compartment are the arterial blood inflow, the venous outflow, and the oscillatory CSF flow between the cranium and spinal canal. The input/output of the spinal canal compartment is the oscillatory CSF flow. This model assumes that the influence of the blood flow to the spinal cord on the craniospinal can be neglected due to the significantly smaller volumetric flow rates compared with flow rates to and from the cranium.

The Bond Graphs representation of the craniospinal system is shown in Figure 3-2. The input is the net transcranial blood flow, i.e., arterial inflow minus venous outflow (fav) and the output is the craniospinal CSF flow (fcsf). The intracranial impedance is

lumped into intracranial compliance (C1) and resistance (R1). C2 and R2 are for the spinal canal compliance and resistance, respectively. L2 represents the inertia momentum of CSF flow (output) between two compartments. p1 and p2 are the CSF pressures in the intracranial and spinal canal compartments. These components are connected by lines (power bonds). The power exchange occurs when the *effort (e)* and *flow (f)* flowing into or out of a port on each component. In hydraulic domain, the effort variable is the pressure and the flow variable represents the volumetric flow rate. The elements of the model are the mechanical properties of individual compartment. They are presented by the impedances (i.e., resistances and compliances). The momentum of CSF flow (system output) is represented by an inductance. The analogous RLC circuit of the Bond Graph model of the craniospinal system is shown in Figure 3-3 and its corresponding transfer function in s-domain (Laplace domain) is shown in Equation 3-1.

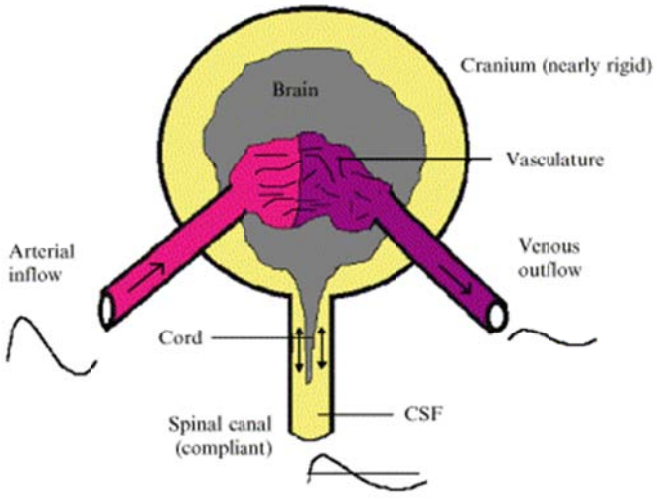

Figure 3-1: Compartmental model of craniospinal system (Alperin *et al.*, 1996).

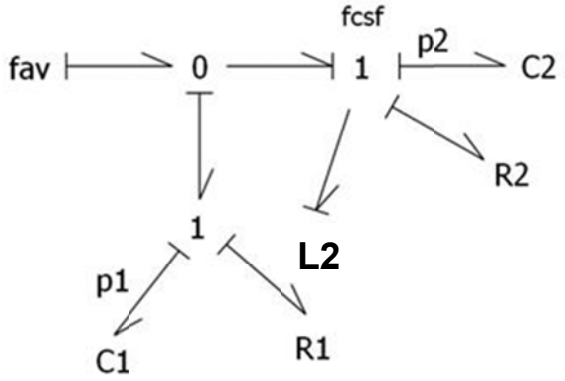

Figure 3-2: Bond Graph model of craniospinal system. The input is the net transcranial cerebral blood flow (fav) and the output is the craniospinal CSF flow (fcsf). The intracranial impedance is lumped into intracranial compliance (C1) and resistance (R1). C2 and R2 are for spinal canal compliance and resistance, respectively. L2 represents the inertia momentum of CSF flow (output). p1 and p2 are the CSF pressures in the intracranial and spinal canal compartments, respectively.

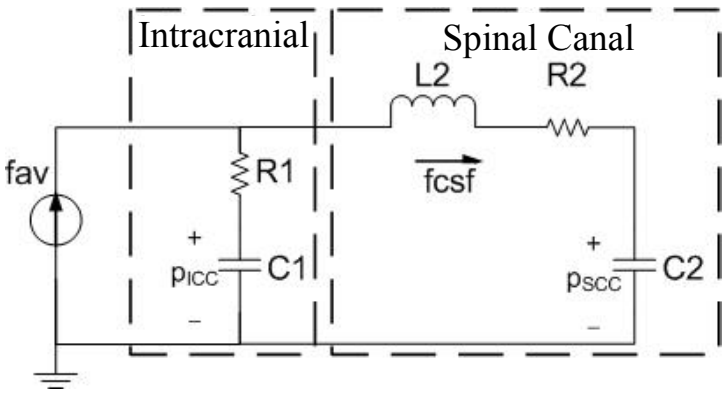

Figure 3-3: Analogous lumped parameter circuit model of the craniospinal system.

$$H(s)=\frac{F_{CSF}(s)}{F_{AV}(s)}=\frac{\frac{R1}{L2}s+\frac{1}{L2\cdot C1}}{s^2+\frac{1}{L2}(R1+R2)s+\frac{1}{L2}(\frac{1}{C1}+\frac{1}{C2})} \tag{3-1}$$

The natural frequency (ω_n) and damping ratio ($\xi_1+\xi_2$) of the system are then derived as following equations,

$$\omega_n=\sqrt{\frac{1}{L2}(\frac{1}{C1}+\frac{1}{C2})} \tag{3-2a}$$

$$\xi_1 = \frac{R1}{2\sqrt{L2(\frac{1}{C1}+\frac{1}{C2})}} \tag{3-2b}$$

$$\xi_2 = \frac{R2}{2\sqrt{L2(\frac{1}{C1}+\frac{1}{C2})}} \tag{3-2c}$$

The values of parameters can be calculated using either deterministic methods (e.g., autoregressive moving average method (ARMA)) or non-deterministic, iterative methods (e.g., Runge-Kutta method) (Ljung, 1999). Since the non-deterministic method requires initial values of system state variables such as p1 and p2 which require invasive pressure measurements, the system transfer function is obtained using ARMA constrained by the least square error method.

Estimation of the compliance and resistance distribution from subject-specific transfer function

The transfer function derived using the ARMA method does not yield the absolute values for R, L, and C but only a superposition of these parameters. These lumped parameters, however, can be used to quantify the distribution of compliance and resistance between the cranium and spinal canal. The contribution of spinal compliance (SCCC) and resistance (SCCR) to the overall craniospinal system can be derived using the relationship shown in Equations 3-3 a and 3-3 b, respectively**.**

$$SCCC(\%) = \frac{\frac{1}{L2 \cdot C1}}{\frac{1}{L2}(\frac{1}{C1}+\frac{1}{C2})} \times 100\% \tag{3-3a}$$

$$SCCR(\%) = \frac{(\frac{1}{L2}(R1+R2)) - \frac{R1}{L2}}{\frac{1}{L2}(R1+R2)} \times 100\% \quad (3\text{-}3b)$$

3-2 Sub-project I: Determination of Appropriate Goodness-of-Fit Measures

A measure of reliability is critical for the clinical utilization of the model. If the model-derived CSF flow waveform closely resembles the MR measured CSF waveform, it is reasonable to assume that the model is reliable. Two measures of "resembles" were assessed, 1) the fit which is the normalized Euclidean length of error described in Equation 3-4, and 2) the Pearson correlation coefficients between the model derived waveform and actual data (Equation 3-5).

$$fit = (1 - \frac{|f_{mea} - f_{sim}|}{|f_{mea} - \bar{f}_{mea}|}) * 100\% \quad (3\text{-}4)$$

$$Coef. = \frac{(f_{mea} - \bar{f}_{mea})(f_{sim} - \bar{f}_{sim})}{\sqrt{(f_{mea} - \bar{f}_{mea})^2}\sqrt{(f_{sim} - \bar{f}_{sim})^2}} \quad (3\text{-}5)$$

where f_{mea} and f_{sim} are the measured and simulated CSF flow waveforms, respectively.

One of the challenges with the use of goodness-of-fit measures is the need for reliable criteria to distinguish between "success" and "failure" of the model. Work toward establishing a reliable reference for a "successful" goodness-of-fit measure by comparing the modeling results with invasively obtained measures are described in this section. The modeling approach was used with MRI and invasive data that was recently used to investigate the cranio-spinal compliance distribution (Wåhlin *et al.*, 2010).

Wåhlin *et al.* proposed a semi-invasive method that utilizes MRI as well as the invasive pressure-volume test to quantify compartmental compliances in a group of healthy elderly subjects. For each individual, the volume changes of the intracranial and spinal canal compartments were derived from MR measurements of arterial blood and craniospinal CSF flows over one cardiac cycle. Wåhlin *et al.* model is different from our model as it neglects cerebral venous outflow dynamics. However, for the purpose of comparison with their invasively derived results, the venous outflow had to be eliminated from our model as well. The CSF pressure was recorded in the lumbar region as part of the constant pressure infusion test that these subjects have undergone. It is expected that a good agreement between the model estimate and the invasive measurement of compliance indicates "successful" modeling. Therefore, the comparison of the two independent approaches were used to determine the appropriate goodness-of-fit measures.

Measurement of the cranio-spinal compliance distribution using pressure-volume indices

The invasive CSF infusion methods such as the bolus injection and constant pressure infusion are currently accepted methods to estimate craniospinal compliance characteristics. These methods monitor changes of the CSF pressure with different patterns of injecting into or withdrawing CSF fluid from the craniospinal CSF space. The changes of volume and pressure are then associated with the elastance property of the craniospinal system. For example, using the constant pressure infusion method (Wåhlin *et al.*, 2010), the elastance coefficient can be defined as the pressure-volume index (PVI) shown in Equation 3-6,

$$PVI = \frac{\Delta V}{\log_{10}(\frac{\Delta P}{P} + 1)} \tag{3-6}$$

where ΔV is the volume change of a compartment, and ΔP is the pressure change in response to ΔV. P is the steady state pressure. For a given pressure value, PVI is proportional to craniospinal compliance (Marmarou *et al.*, 1975; Marmarou *et al.*, 1978) (Equation 2-3). In addition, studies reported that the total craniospinal compliance is sum of the intracranial and spinal canal compliances (Marmarou *et al.*, 1975; Löfgren and Zwetnow, 1973). This implies that the individual compartmental compliance can be derived by the ratio of the compartmental volume and pressure changes. In this study, the measurements of volumetric flows and CSF pressures from elderly healthy subjects were provided by Wåhlin's team. The ratio of ΔP and P were obtained invasively using the constant pressure infusion method, while ΔV was obtained using the MRI measurements of volumetric flow changes in the cranium and spinal canal.

MR based measurements of compartmental volume change

Compartmental volume change can be mathematically described by defining the input and output of the compartment. Wåhlin *et al.* suggested that the arterial inflow is buffered by the CSF and venous blood in the intracranial compartment and thus the inlet and outlet of the intracranial compartment are **the arterial inflow f_A , and craniospinal CSF flow f_{CSF} ,** respectively. The spinal canal compartment has a single inlet and outlet for the CSF flows from and back to the cranium. The mathematical expressions of the

volume changes of the cranio-spinal compartment (CS) and the two individual sub compartments (CR: intracranial, SC: spinal canal) are described in Equation 3-7.

$$\Delta\overline{V_{CS}}(i) = [f_A(i) - mean(f_A(i))] \cdot \Delta t \tag{3-7a}$$

$$\Delta\overline{V_{CR}}(i) = [f_A(i) - mean(f_A(i)) - f_{CSF}(i)] \cdot \Delta t \tag{3-7b}$$

$$\Delta V_{SC}(i) = f_{CSF}(i) \cdot \Delta t \tag{3-7c}$$

where i is the cardiac phase index sampled by time intervals of Δt. The maximal volume change of each compartment, which occurs in the systolic phase, is the peak to peak amplitude of volume change waveform. Equation 3-8 states that there is no change or accumulation of volume over the entire cardiac.

$$\sum_{\substack{cardiac\\cycle}} \Delta\overline{V_{CR}}(i) = \sum_{\substack{cardiac\\cycle}} [f_A(i) - mean(f_A(i)) - f_{CSF}(i)] \cdot \Delta t = 0 \tag{3-8}$$

Estimation of the spinal compliance contribution from the lumped parameter model

As described in Wåhlin's study, the input of the craniospinal system was the cerebral arterial inflow and the output was the craniospinal CSF flow. Thus the system transfer function in Equation 3-1 was modified and shown in Equation 3-9

$$H'(s) = \frac{F_{CSF}(s)}{F_A(s)} = \frac{\frac{R1'}{L2}s + \frac{1}{L2 \cdot C1'}}{s^2 + \frac{1}{L2}(R1'+R2)s + \frac{1}{L2}(\frac{1}{C1'} + \frac{1}{C2})} \tag{3-9}$$

where R1' is a lumped resistance and C1' is a lumped compliance that represent both venous system and CSF space to accommodate arterial flow in the intracranial compartment. The compliance contributed by the spinal canal compartment is calculated using Equation 3-10.

$$\overline{SCCC} = \frac{\frac{1}{\overline{L2 \cdot C1'}}}{\frac{1}{L2}\left(\frac{1}{C1'} + \frac{1}{C2}\right)} \times 100\% \tag{3-10}$$

Materials

MR images of blood and CSF flows and invasive CSF pressure recordings from 16 elderly subjects (3 Male and 13 Female, average age of 71±5 years) collected by Wåhlin *et al.*(Wåhlin *et al.*, 2010) was used for the comparison with the modeling results. MR velocity encoded phase contrast images were acquired with a 3T Achieva MR scanner. High velocity encoding of 70 cm/s was used for cerebral blood flow measurements and low velocity encoding of 7cm/s was used for CSF flow. Additional MR scan parameters were: TR=10~16ms, TE=6~11ms, FA=10~ 15 degrees, matrix= 160*160, slice thickness=6 mm. Transverse images were prescribed at the level between C2 and C3. The image segmentation for measuring cerebral blood and CSF flows was quantified by using the Pulsatility Based Segmentation (PUBS) method developed by Alperin and Lee (Alperin and Lee, 2003). Examples of MR images and flow measurements from a subject are shown in Figure 3-4. The elastance coefficient (PVI) for each individual was obtained using the invasive constant pressure infusion method. On average, the PVI of total craniospinal system was 9.5±2.4ml.

Results

The average volume change due to the pulsatile blood flow via cerebral arteries to the intracranial compartment during each cardiac cycle for all subjects was 2.1±0.5 ml. The maximal volume change of the intracranial and spinal canal compartments calculated using Equation 3-7 were 1.3±0.5 and 0.7±0.2 ml, respectively. Average PVIs for the intracranial and spinal canal compartments were 6.1±1.8 ml and 3.4±1.1 ml, respectively. Consequently, the spinal canal compliance contribution ($\overline{SCCC}$) is 36±8%.

The relationships between the modeling derived and the invasively obtained compliance distributions for all subjects is shown in Figure 3-5. A good agreement is demonstrated as evidence by the strong linear correlation between the two measures ($R=0.92$, $p<0.001$). On average, the difference of compliance distribution measurement between two methods was less than 5%. Further, there is no significant difference between the two measurements using the unpaired two tailed student t-test ($p>0.05$).

A comparison between the MRI measured and the model derived CSF flow waveform is shown in Figure 3-6. The measure of agreement between these two waveforms were fit=82% and correlation coefficient (COEF) of 0.98. The fit and COEF for each individual are shown in Figure 3-7a and b, respectively. Individual measurements of compliance distribution as well as the goodness-of-fit measures are summarized in Table 3-1. The fit and COEF for all subjects were 61±11% and 0.90±0.06, respectively.

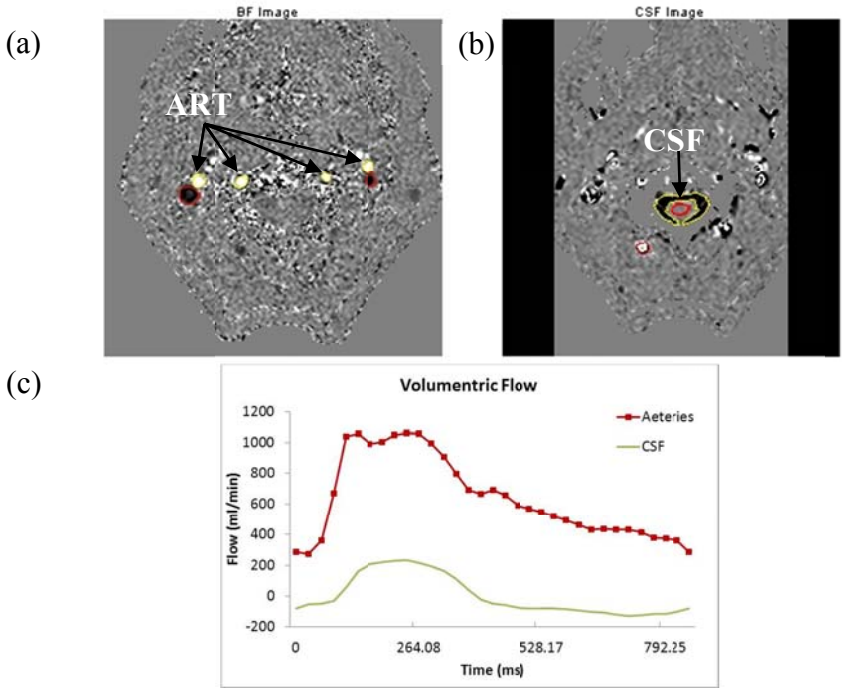

Figure 3-4: An example of velocity encoded MRI images of cerebral blood (a) and CSF (b) from one elderly subject for derivation of the blood and CSF flow waveforms (c). Flow in the cranial direction shown in white pixels and in caudal direction is black.

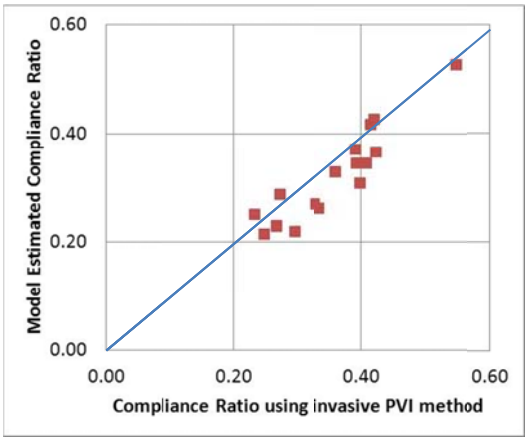

Figure 3-5: Spinal canal compliance contribution measured by the model (Y-axis) and by the PVI method (X-axis). The model-estimated compliance distribution is significantly correlated with the measurements obtained from the invasive PVI method (R=0.92, p<0.001).

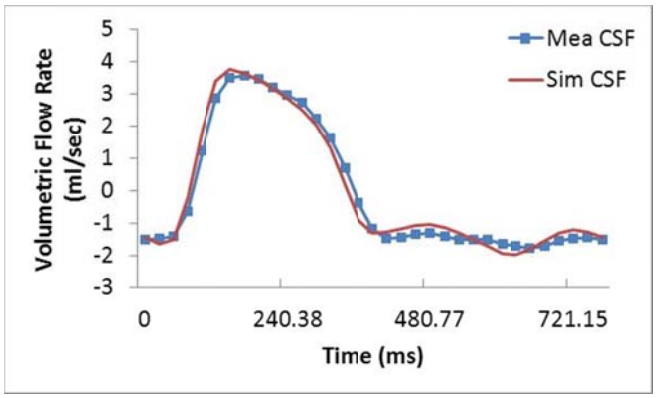

Figure 3-6: Measured and modeled CSF flow waveforms for an elderly subject. In this case, the fit is 82% and COEF is 0.98.

(a)

(b)

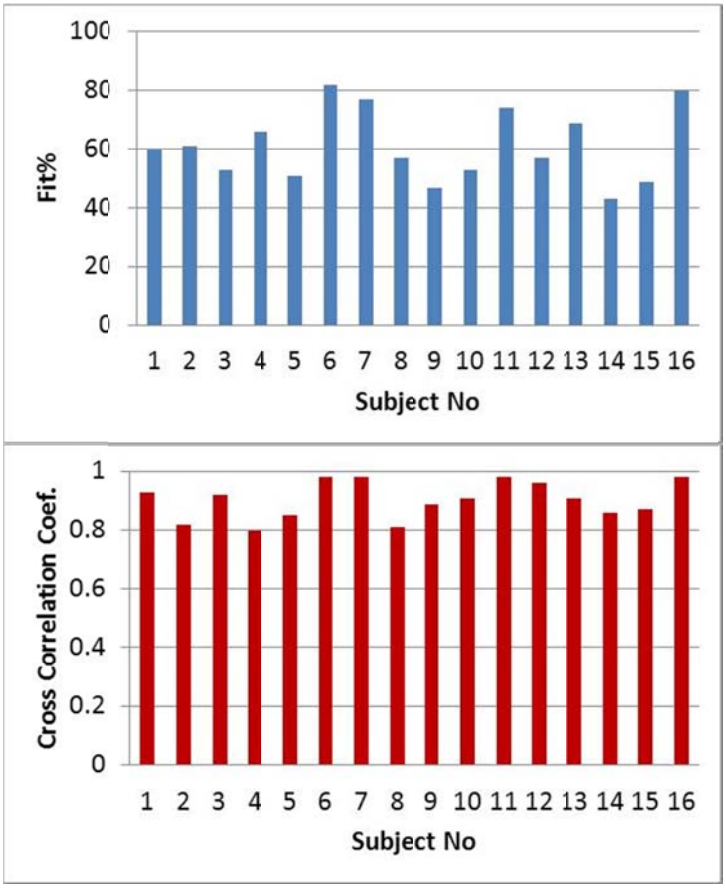

Figure 3-7: (a) Modeling fit and (b) cross correlation coefficients for all subjects.

Table 3-1: Measured parameters for individual subject includes MR measurements of the compartmental volume changes, model fit and cross correlation coefficients (COEF), and spinal canal compliance contribution (SCCC) derived from the PVI method and from the model.

Method	**MR-PVI**			**Model**			
Subject	**Vic (ml)**	**Vsc (ml)**	$\overline{SCCC}$ **(%)**	**fit (%)**	COEF	$\overline{SCCC}$ **(%)**	**diff (%)**
1	1.04	0.67	39	60	0.93	37	2
2	1.37	0.69	33	61	0.82	26	7
3	1.1	0.41	27	53	0.92	29	-2
4	1.01	0.74	42	66	0.8	37	5
5	1.35	0.76	36	51	0.85	33	3
6	0.96	0.68	41	82	0.98	42	-1
7	1.62	0.49	23	77	0.98	25	-2
8	1.08	0.7	39	57	0.81	34	5
9	0.96	0.66	41	47	0.89	35	6
10	2.32	0.97	29	53	0.91	22	7
11	0.63	0.76	55	74	0.98	53	2
12	1.53	1.01	40	57	0.96	31	9
13	2.01	0.73	27	69	0.91	23	4
14	1.95	0.64	25	43	0.86	22	3
15	1.17	0.57	33	49	0.87	27	6
16	1.31	0.95	42	80	0.98	43	-1
Mean	1.34	0.71	36	61.19	0.90	32	4
SD	0.45	0.16	8	12.22	0.06	9	3
p-Value						>0.05	

diff = MR-PVI SCCC(%) —Model SCCC(%)

Discussion

In this section, the modeled estimation of compliance distribution contributed by the intracranial and spinal canal compartments was compared with the recent reports using the semi-invasive method (Wåhlin *et al.*, 2010). The largest difference between the two methods was only 9% (Table 3-1), which demonstrates that the model provides a good estimate of the cranio-spinal compliance distribution ($\overline{SCCC}$: 36% using the PVI method vs. 32% using the model estimate). Even for cases with a lower fit (e.g., 51% fit

for subject 5), the model underestimates the distribution only by 3% (36% using the PVI method vs. 33% using the model). The fit was moderately correlated with the difference in compliance distribution between the two methods ($r = -0.53$, $p=0.03$). A stronger correlation may be expected with a greater sample size of subjects. The difference in compliance distribution between the two methods is plotted along with the fit (%), as shown in Figure 3-8.

The difference in compliance distribution between the two methods can be used to determine a threshold of goodness-of-fit measures for reliable measurement of compliance distribution using the modeling approach. In order to assure minimized error of the estimated mechanical properties using the modeling approach, a precision of 10% (±5%) measurement error between the model-based and the PVI-based compliance distribution is proposed. The measurement difference between the two methods for several levels of fit (%) is shown in Table 3-2. The proposed precision in estimation of compliance distribution is achieved when the fit exceeds 60%. In the group with fit over 60%, the minimal COEF was 0.8. Thus, the threshold of a minimum fit of 60% and minimum COEF of 0.8 is proposed to qualify a good estimation of system parameters using the modeling approach.

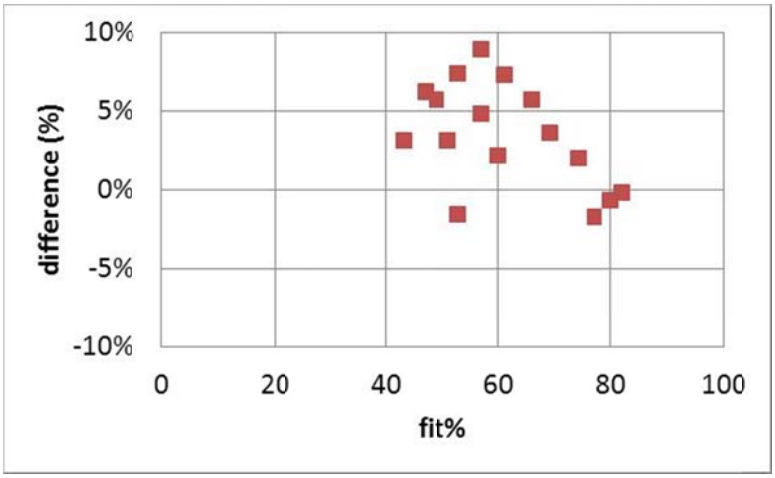

Figure 3-8: Measuring difference of craniospinal compliance distribution between the modeling approach and the invasive PVI method, which is plotted along with the model fit for all subjects.

Table 3-2: Measurement of the spinal canal compliance contribution (SCCC) at several levels of fit.

Fit (%)	COEF	# of subjects	MR-PVI SCCC(%)		Model SCCC(%)		diff%
			Mean	SD	Mean	SD	Mean (Range)
All	0.90±0.06	16	36	8	32	9	4 (-2~9)
>50%	0.91±0.07	13	37	8	33	9	3 (-2~9)
>60%	0.92±0.07	8	38	10	36	10	2 (-2~6)
>70%	0.98±0.00	4	40	13	41	11	-1 (-2~2)

diff% =MR-PVI SCCC — Model SCCC

Finally, Wåhlin *et al.* (2010) suggested that the cerebral venous system is part of intracranial "volume reservoir". However, from a system point of view the venous pulsatile flow should be taken into account as the outlet of the intracranial compartment and then be used for the calculation of intracranial volume change. Further investigation of the influence of pulsatile venous flow in estimation of volume change and craniospinal compliance is discussed in Chapter 4 and Chapter 6, respectively.

3-3 Sub-project II: Reproducibility of the Lumped Parameter Model

The reproducibility of the modeling approach in estimation of system parameters was evaluated by variance of the estimated system parameters using data from repeated MR scans on a craniospinal flow phantom and on healthy subjects.

The craniospinal flow phantom

A craniospinal flow phantom shown in Figure 3-9 (Alperin *et al.*, 2000) was constructed based on the compartmental model as shown in Figure 3-1. The phantom consists of a rigid container filled with water as the intracranial space, and a syringe attached with the rigid container as the spinal canal compartment. A small compliant closed outlet was connected to the container compartment to allow for a small volume change. A pump and a pulsatile valve was used to generate pulsatile flow into the phantom through the "arterial" opening, while the "venous" opening allowed the water to exit. A low friction syringe was used to simulate the pulsatility of CSF dynamics that communicates between the intracranial and spinal canal compartments. The phantom simulated two craniospinal conditions, (i) system with normal CSF communication that the plunger inside the syringe can move and (ii) system with no CSF communication by a fixed plunger. When using data derived from the system with a fixed plunger, the model approach is expected to derive a small spinal canal compliance.

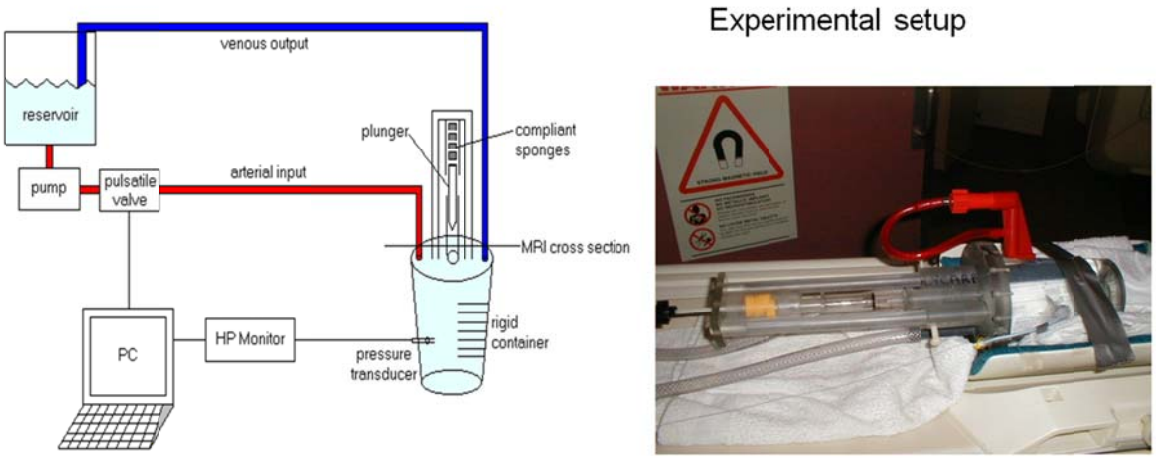

Figure 3-9: Diagram of the craniospinal phantom (Left) and a photo of the physical phantom (Right).

The lumped parameter model of craniospinal system

The lumped parameter craniospinal model that involves **arterial inflow, venous outflow and craniospinal CSF flow** shown in Figure 3-3 was used. For this study, successful modeling was considered when the fit exceeds 60% and the COEF exceeds 0.8.

MRI measurements of the compartmental volume change

The time-varying compartmental volume change waveforms are derived using the volumetric flow rates into and out of the specific compartment shown in Figure 3-1. The inlet and outlet of the cranial compartment are the arterial inflow f_A, venous outflow f_V, and craniospinal CSF flow f_{CSF}. The spinal canal compartment has a single inlet and outlet for the CSF flows from and back to the cranium. The mathematical expressions of the volume changes of the craniospinal compartment and the two individual sub compartments are described in Equation 3-11.

$$\Delta V_{CS}(i) = [f_A(i) - f_V(i)] \cdot \Delta t \qquad (3\text{-}11a)$$

$$\Delta V_{CR}(i) = [f_A(i) - f_V(i) - f_{CSF}(i)] \cdot \Delta t \quad \text{(3-11b)}$$

$$\Delta V_{SC}(i) = f_{CSF}(i) \cdot \Delta t \quad \text{(3-11c)}$$

where i is the cardiac phase index sampled by time intervals of Δt. The maximal volume change of each compartment, which occurs in the systolic phase, is the peak to peak amplitude of volume change waveform. Equation 3-12, which states that there is no change or accumulation of volume over the entire cardiac, is used to account for the small unmeasured venous outflow through secondary veins (Alperin *et al.*, 2000).

$$\sum_{\substack{cardiac \\ cycle}} \Delta V_{CR}(i) = \sum_{\substack{cardiac \\ cycle}} [f_A(i) - f_V(i) - f_{CSF}(i)] \cdot \Delta t = 0 \quad \text{(3-12)}$$

Materials

In the phantom experiment, cine phase contrast MR data was acquired by a 1.5T GE scanner. A high velocity-encoding (VENC) of 125 cm/s was used for measurements of the arterial inflow and venous outflow, while a low VENC of 6 cm/s was used for measurement of the CSF flow. Other MRI scan parameters included TR=21 ms, TE=6.6ms, FA= 25 degree, FOV=14 cm. An example of high and low VENC MR images and the obtained flow waveforms from the phantom are shown in Figure 3-10 (with free syringe). MR images and flow measurements for the phantom with a restricted syringe are shown in Figure 3-11.

MR images from healthy volunteers were acquired using a 3T scanner (Siemens Medical Solutions, Germany). Six subjects (29±14 years, 1 male and 5 female) were

provided informed consents. The MRI brain protocol included anatomical imaging and two additional retrospectively gated velocity encoded cine phase contrast scans for quantitation of blood and CSF flows to and from the cranium. Blood flow was imaged using high velocity encoding (VENC) of 70 cm/sec. The CSF flow was imaged using a lower VENC of 7 cm/s. Other imaging parameters include field of view of 14 cm, slice thickness of 5–6 mm, acquisition matrix of 256x160, shortest repetition (repetition time is defined based on Siemens convention) and echo times (43–52 ms and 7–10 ms), and flip angle of 20 degrees. The image locations were at the C2 level. Total arterial inflow to the cranium was derived by summation of flows through the internal carotid and vertebral arteries. Venous outflow was obtained by summation of the volumetric flow rates through the internal jugular veins, and through the three main secondary channels when present (e.g., epidural, vertebral, and deep cervical veins). Venous flow through the secondary channels was obtained from the low VENC images. Images were reconstructed into 32 cardiac phases using the same projected heart rate for both the blood and CSF flows. An example of high and low velocity encoded MR phase contrast images and the obtained arterial, venous and CSF flow waveforms of one cardiac cycle from a healthy subjects is shown in Figure 3-12.

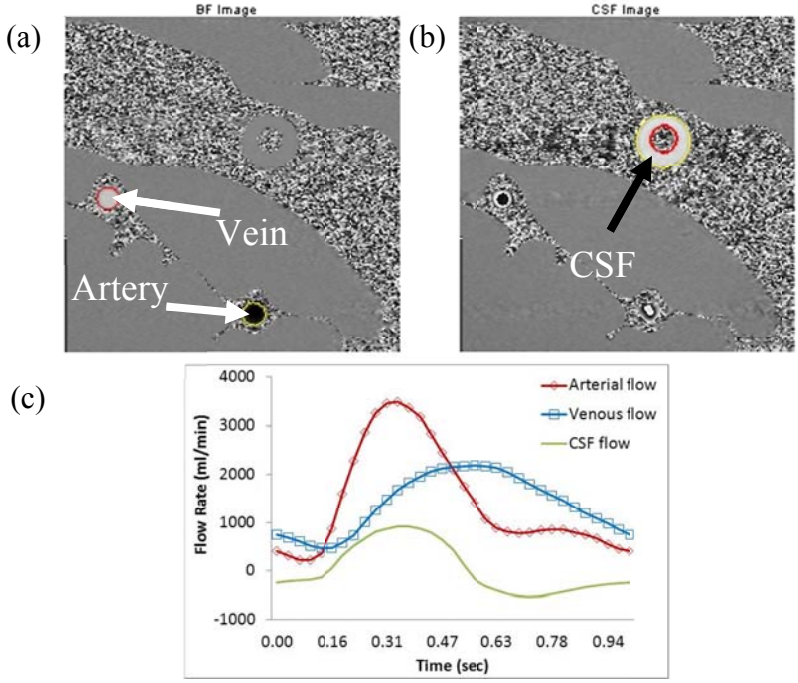

Figure 3-10: An example of velocity encoded MRI images of simulated blood (a) and CSF (b) using craniospinal phantom with a free syringe. The derivation of the blood and CSF flow waveforms is in (c).

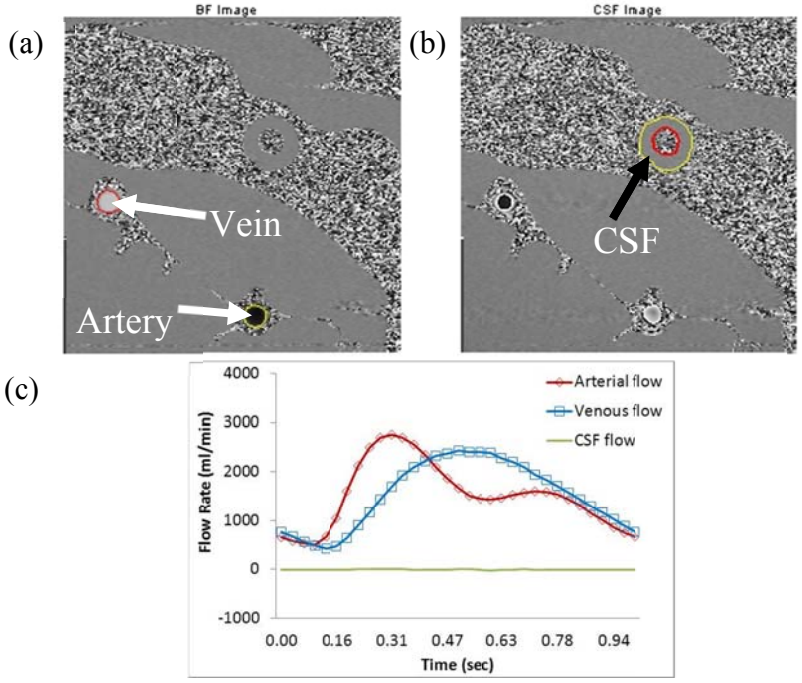

Figure 3-11: An example of velocity encoded MRI images of simulated blood (a) and CSF (b) using craniospinal phantom with a fixed syringe. The derivation of the blood and CSF flow waveforms is in (c).

Results

For the phantom study, the goodness-of-fit of all phantom data were 71±21% and 0.94±0.09, respectively. Large variance of fit was caused by the much lower fit for modeling the system dynamics with restricted syringe. The lower fit is expected because the modeling procedure is difficult to fit almost "no-flow" dynamics. Examples of simulated CSF flows for the two-condition phantom studies are shown in Figure 3-13. By excluding the result for simulating the "restricted" state, the goodness-of-fit were 83±7% and 0.99±0.00, respectively. Regarding to the flow measurements, the relative standard deviation (RSD) of measurements of total cerebral blood flows via the arteries (ART) and veins (VEN) were less than 7%. The RSDs of maximal volume change in the intracranial and spinal canal compartments were less than 12%. In contrast, the variances of estimated model parameters were similar to the variances of flow measurements. For the system with the free syringe, the RSDs of the damping ratio and nature frequency were less than 12%. The variances of compliance distribution estimated by the model were within the variances of blood flow and individual volume change (RSD <8%). For the phantom with a fixed syringe, large variances of the estimated damping ration and nature frequency were found (Table 3-3). However, small variations in estimation of compliance and resistance distributions were observed (RSD < 5%). The lumped parameters estimated from measured flows are summarized in Table 3-3.

Regarding the modeling results using data from health subjects, the average and SD of fit and COEF were 78±3% and 0.96±0.04, respectively. The variances of cerebral blood flow in the arteries and veins were within 10%. On average, the RSD of ΔV_{CR} was

over 15% and that of ΔV_{SC} was about 10%. Large variance in the compartmental volumetric flow may cause large variance in estimation of system parameters (ω_n and ($\xi_1 + \xi_2$)) as well as the compliance distribution (SCCC) and resistance distribution (SCCR). The measured parameters are listed in Table 3-4.

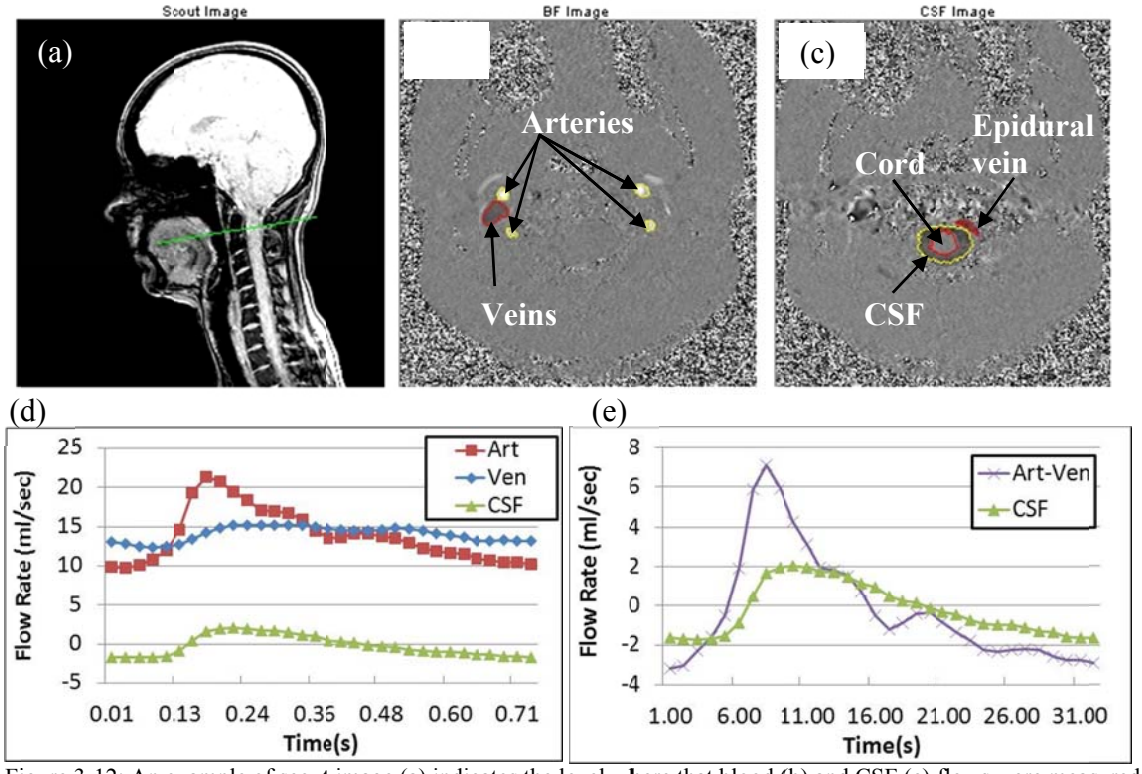

Figure 3-12: An example of scout image (a) indicates the level where that blood (b) and CSF (c) flows were measured. The derived blood and CSF flow waveforms is shown in (d). The CSF is plotted again with the net transcranial blood flow in (e).

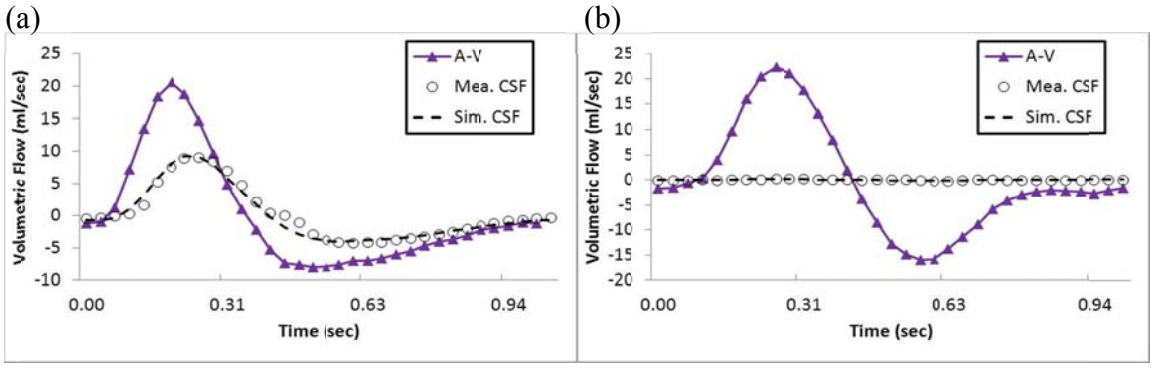

Figure 3-13: Measured flows and modeled CSF flow waveform of the phantom (a) with a free syringe and (b) with a fixed syringe.

Table 3-3: Measurements obtained from repeated MR scans on the craniospinal phantom.

Expt # (MR scans)		MR Measurements				Lumped Parameters			
		ART (ml/min)	VEN (ml/min)	ΔV_{CR} (ml)	ΔV_{SC} (ml)	ω_n	$\xi_1+\xi_2$	SCCC (%)	SCCR (%)
Free syringe #1 (4)	Mean	1494	1454	3.71	3.56	14.9	1.08	63	60
	SD	35	47	0.17	0.45	0.9	0.11	4	2
	RSD (%)	2	3	4	12	6	10	6	3
Free syringe #2 (4)	Mean	1102	1064	2.06	1.41	31.7	0.94	49	83
	SD	82	23	0.20	0.09	0.7	0.05	4	3
	RSD (%)	7	2	10	6	2	6	8	4
Restricted syringe (3)	Mean	1556	1559	4.24	0.02	33.9	0.88	1	99
	SD	20	10	0.07	0.01	2.6	0.37	0	1
	RSD (%)	1	1	2	50	8	42	0	1

Table 3-4: Measurements obtained from repeated MR scans on six healthy subjects.

Subject # (MR scans)		MR Measurements				Lumped Parameters			
		ART (mL/min)	VEN (mL/min)	ΔV_{CR} (mL)	ΔV_{SC} (mL)	ω_n	$\xi_1+\xi_2$	SCCC (%)	SCCR (%)
1 (5)	Mean	818	679	0.55	0.53	24.8	1.30	74	78
	SD	56	65	0.11	0.02	12.3	0.19	6	13
	RSD(%)	6	9	20	4	49	14	8	16
2 (4)	Mean	810	558	0.64	0.47	34.6	1.27	48	76
	SD	35	43	0.13	0.07	13.7	0.05	9	8
	RSD(%)	4	8	20	15	40	4	19	10
3 (3)	Mean	884	653	0.60	0.52	42.5	1.39	57	71
	SD	65	22	0.09	0.08	14.4	0.07	2	1
	RSD(%)	7	3	15	14	34	5	4	2
4 (3)	Mean	912	659	0.56	0.83	32.7	1.30	64	55
	SD	61	34	0.12	0.12	10.1	0.09	5	7
	RSD(%)	7	5	20	15	31	7	7	13
5 (4)	Mean	1006	695	0.61	0.84	23.5	1.50	74	55
	SD	34	34	0.02	0.05	3.8	0.11	5	8
	RSD(%)	3	5	3	6	16	7	7	15
6 (3)	Mean	770	717	0.65	0.44	22.5	1.48	73	72
	SD	70	40	0.21	0.03	9.8	0.20	5	3
	RSD(%)	9	6	31	6	44	14	7	4

Discussion

In this section, the robustness and repeatability of the modeling method for estimation of subject specific craniospinal system were demonstrated. The ARMA method is capable of detecting changes in the mechanical properties of the craniospinal flow phantom. The variance for compliance and resistance distribution was similar to the variance for the input and output flow measurements (Table 3-3). As expected, the estimated spinal compliance was very small and spinal resistance was very large for the phantom with a restricted syringe (Table 3-3). These results strongly support the validity of the model and its ability to characterize the system biomechanical state.

In contrast to the phantom experiments where there is very low variability between each cardiac cycle, the human brain hemodynamics has an inherent physiological variability. Therefore, the hemodynamic and hydrodynamic variability influence the variability of the estimated system parameters. Results showed that the variance for blood flow measurements obtained in the cerebral arteries and veins due to the physiologic variability is on the order of 10%. This is in agreement with previously reported variance of 7.1% derived from three repeated MRI scans in 15 healthy subjects (Spilt *et al.*, 2002). However, the variance for the measurements of compartmental volume change was slightly larger than that of flow measurements. On average, the RSD of the maximal volume change was 18% for the intracranial compartment and 10% for the spinal canal compartment. This may indicate possible changes in the biomechanical parameter of craniospinal system during MRI studies. As expected, the variances of system natural frequency (ω_n) and damping ratio ($\xi_1 + \xi_2$) as well as the compliance and

resistance distributions were significantly larger in the healthy subjects than that in the phantom experiments.

3-4 Summary

This study confirmed the reliability and reproducibility of the proposed modeling approach for characterization of the craniospinal system. A reliable measurement of system properties is achieved when both measures of quality of fit exceeds 60% and 0.8, respectively. The reproducibility of this approach was tested using data from repeated MR scans on a flow phantom and on healthy subjects. When data acquired from subjects, larger variability due to physiological variation is expected. This causes slightly large variances in the estimation of compliance and resistance distributions.

Chapter 4 Influence of the Compliance of the Neck Arteries and Veins on the Measurement of Intracranial Volume Change by Phase-Contrast MRI

4-1 Project Background

Reliable determination of volume change of a given compartment is critical for derivation of compliance measures. The MRI method for measurement of the intracranial compliance and pressure estimates the volume change during the cardiac cycle by accounting for the volumetric flow rates that enter and leave the cranium, namely the arterial inflow, venous outflow and craniospinal CSF flow (Alperin *et al.*, 2000; Dhoondia and Alperin, 2003; Miyati *et al.*, 2007). It is a challenging measurement since this is a small volume, on the order of a fraction of one mL, derived from the difference between much larger volumes. Ideally, the measurement location should be as close as possible to the boundaries of the cranium. However, due to anatomical and practical constraints, arterial inflow and venous outflow measurements are obtained at locations slightly distal to the cranial vault inlets. Since the arteries and veins leading and draining blood from the brain are not rigid pipes, it is important to quantify the influence of the measurement locations on the reliability of the intracranial volume change and compliance measurements. This is especially important as other groups who attempted to reproduce these measurements did not consider this effect and used measurement locations that are even more distal to the cranium inlet (Balédent *et al.*, 2004; Marshall *et al.*, 2008).

Reliable measurement of maximal intracranial volume change (ICVC) requires careful consideration of the scanning protocol and utilization of the cine phase contrast

MR technique. It has been previously shown that a synchronized measurement of the CSF and blood flows considerably reduced measurement variability, from 18% (Alperin *et al.*, 2000) to about 10% (Dhoondia and Alperin, 2003), because it eliminates erroneous time delays when the CSF and blood flows are sampled at different heart rates. A synchronous measurement of blood and CSF flow rates can be achieved using a single scan with interleaved dual velocity encoding (VENC) phase contrast technique (Dhoondia and Alperin, 2003). Large measurement variability in the ICVC, over 30%, has been reported with unsynchronized sampling of the blood and CSF flows and a distal location (at the level of C3) (Marshall *et al.*, 2008).

This study determines the influence of the level at which the arterial inflow and venous outflow are measured on the calculation of the ICVC (Tain *et al.*, 2009). The influence of the location at which the CSF is measured will be considered in a separate report. From review of the literature, it seems that different groups choose different levels above the carotid bifurcation for the measurement of the total cerebral blood flow. The two most common locations are an upper level that intersects the v2 segment of the vertebral arteries (upper C2 just before the vertebral veins turn to enter the skull base) (Alperin *et al.*, 1996; Alperin *et al.*, 2000; Dhoondia and Alperin, 2003; Glick *et al.*, 2006; Miyati *et al.*, 2007) and a lower location, further away from the skull base, typically below C2 (Balédent *et al.*, 2004; Marshall *et al.*, 2008). Due to the pulsatile nature of the arterial and venous flows, and due to the finite compliance of the vessel segment between these two levels, the shape of the volumetric flow waveform can be different between the two locations with the same total volumetric flow. Therefore, it is expected that the location of the measurement may influence the calculation of the

intracranial volume change. The degree by which the pulsatility of the arterial and venous blood flows influences these measurements were investigated in order to account for this influence for improved reliability of direct measurement of ICVC, intracranial compliance and pressure measurements using MRI.

4-2 Materials and Methods

MRI data sets from 9 subjects (37±14 years, 4 male and 5 female) who underwent measurements of intracranial compliance and pressure using MRICP program (Alperin *et al.*, 2000) were analyzed. All subjects signed an informed consent approved by the intentional review board. Each data set included two retrospectively gated high velocity encoded cine phase contrast scans (70 cm/sec) for measurements of the total cerebral blood flow and a third cine PC scan with low VENC (7 cm/sec) at the upper C2 level for measurement of the cranio-spinal oscillatory CSF flow volume. Other imaging parameters include FOV of 14cm, slice thickness of 6 mm, acquisition matrix of 256x160, minimal TR and TE of 12 and 7ms, respectively, and flip angle of 20 degrees. The two high VENC scans were placed one at an upper location (upper C2 level) and the second at a lower level (lower C2-upper C3). The average distance between these two levels was 21.6±7.3 mm. Images were reconstructed into 32 cardiac phases using the same projected heart rate for both locations. A short 2D TOF MRA scan covering the upper cervical spine was used as a scout for guiding the selection of the upper and lower locations. The imaging planes were selected at orientations that are as perpendicular as possible to the main 4 arteries leading blood to the brain (internal carotid and vertebral

arteries), and internal jugular veins (IJV). Examples of coronal MIP MRA and MRV with the 2 locations are shown in Figure 4-1.

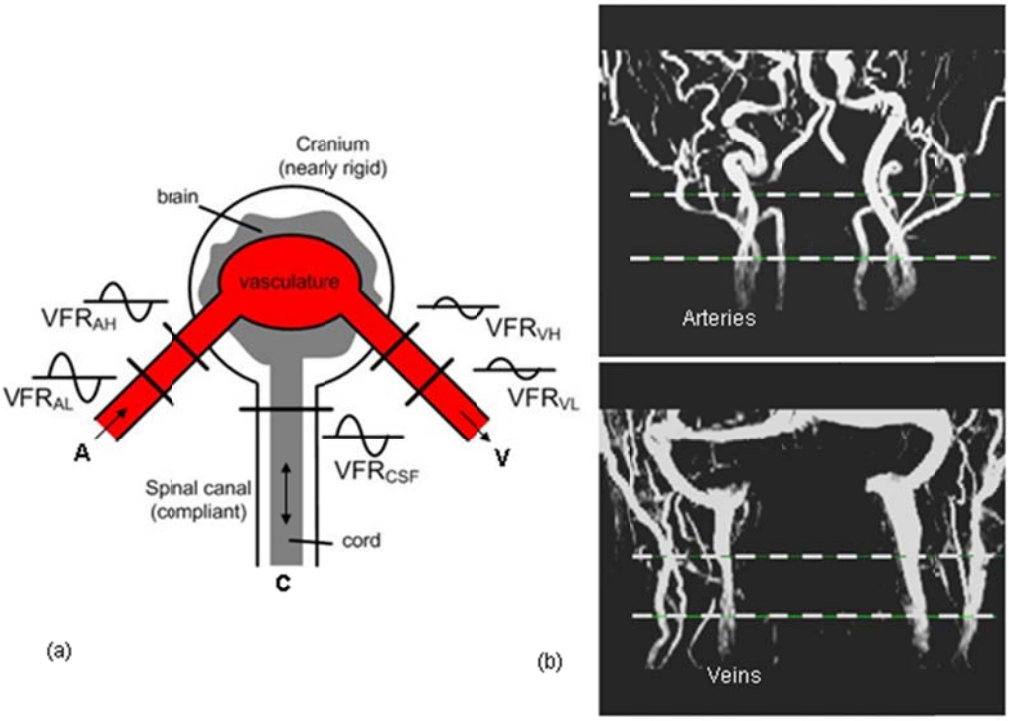

Figure 4-1: (a) The compartmental model of the craniospinal system demonstrating the measurement of intracranial volume changes from the differences between volumetric arterial inflow (A), venous outflow (V), and CSF flow (C) rates. The level at which the blood inflow and outflow is imaged can influence the measurement of intracranial volume change. (b) Coronal MIP MRA (top) and MRV (bottom) with the 2 locations used for the blood flows measurements are indicated by the dashed line (Tain *et al.*, 2009).

The intracranial volume (ICV) change waveform was calculated following a previously described method (Alperin *et al.*, 2000). Briefly, the transcranial volumetric flow rate (VFR) waveform is first obtained for each time point of the cardiac cycle by subtracting the venous and CSF outflow rates from the arterial inflow rate. Then the ICV change is derived by integration of the transcranial flow rate with respect to time as shown in Equation 4-1,

$$ICV(T) = \sum_{i=0}^{T} [VFR_{ART}(i) - VFR_{VEN}(i) - VFR_{CSF}(i)] \cdot \Delta t, \qquad 0 \le T \le RR \tag{4-1}$$

where VFR_{ART}, VFR_{VEN}, and VFR_{CSF} are the arterial, venous, and CSF volumetric flow rates, respectively, and RR is the period of one cardiac cycle.

The maximal volume change occurring in the arterial and venous vessel segments that are bound by the upper and lower imaging planes were calculated to assess their influence on the derivation of the ICV change measurements, respectively. The individual segment volume change waveform was calculated by subtracting the outlet flow rates from the inlet flow rates for each time point and then integrating the net volumetric flow rate with respect to time, as described in Equations 4-2 and 4-3,

$$dVFR(i) = VFR_I(i) - VFR_O(i) \tag{4-2}$$

$$\Delta VC(i) = dVFR(i) \cdot \Delta t \tag{4-3}$$

where VFR_I and VFR_O are measured inlet and outlet volumetric flow rates, respectively. $dVFR$ and ΔVC are the net volumetric flow rate between in-outlet flows and the segment volume change, respectively. Prior to the calculation of the volume change, a constant value (dc) was either added or subtracted to maintain volume conservation over the cardiac cycle as described in Equations 4-4 and 4-5,

$$dc = \frac{\sum_{i=1}^{N} (VFR_I(i) - VFR_O(i))}{N} \tag{4-4}$$

$$CVFR(i) = VFR(i) + dc \tag{4-5}$$

where $\boldsymbol{CVFR}$ represents the dc-corrected volumetric flow rate. In addition, the maximal intracranial volume change was calculated using the arterial and venous flow waveforms derived from the upper and lower locations, separately, with the same CSF flow waveform.

Paired *t*-test was used to determine if there was a statistically significant difference between the two ICVC measurements. The influence of the degree of the pulsatility of the arterial and venous flows on the ICVC measurement was assessed from the relationship between the peak-to-peak amplitude of arterial and venous flows and the ratio of the upper and lower measurements of ICVC. In addition, for each individual arterial and venous vessel segments, the peak-to-peak amplitude of the net volumetric flow was calculated and compared with the maximal volume change of that segment. Linear regression was then used to identify correlations between pulsation levels and volume changes.

4-3 Results

In all nine data sets, the ICVC measurement obtained using the upper location was smaller than the one obtained with the lower location. The respective mean ICVC were 0.51 vs. 0.71 mL. The difference was statistically significant with $p<0.05$. The mean ratio of the lower vs. upper measurements was 1.39±0.32 (mean±SD). Examples of volumetric flow rate waveforms in left internal carotid arterial and jugular vein obtained using the upper and lower imaging planes from one subject are shown in Figure 4-2. The measured volumetric flow waveforms are shown in Figure 4-2a and d. For each vessel, the waveforms from the upper (◯) and lower (+) locations are shown in the same graph.

The net volumetric flow rates for these vessels are shown in Figures 4-2b and e respectively, and the volume change for the vessel segments bounds by the upper and lower imaging planes are shown in Figures 4-2c and f, respectively. As can be seen, the arterial waveforms at the upper and lower locations are very similar and therefore the volume change in the arterial vessel segments are small as shown in Figure 4-2c. On the other hand, the venous flow is much less similar between the upper and lower location resulting with a larger volume changes in the venous vessel segments as can be seen in Figure 4-2f.

The average pulse amplitude (peak-to-peak value) of the arterial and venous volumetric flows is summarized in Table 4-1. In general, the arterial pulse amplitude was similar at the two levels (mean ratio of 1.04), while the venous pulsatility was larger at the lower location (mean ratio of 1.3). The individual segments and the combined arterial and venous segments maximal volume change are listed in Table 4-1. The maximal volume change of the venous side is almost twice that of the arterial side, 0.39±0.25 mL vs. 0.21±0.1 mL. Thus these findings suggest that the influence from venous side on the ICVC measurements is considerably larger than the arterial side.

Large differences in the venous lumen area were found between the upper and lower location of the jugular veins. On average, at the lower location, the lumen area was larger and the mean velocity was slower compared with the upper location, by 60% and 30%, respectively. Mean and SD of lumen areas and velocities at the two levels are listed in Table 4-1. An example of velocity and magnitude images from upper and lower location is shown in Figure 4-3. These images also demonstrated that the flow velocities

during the cardiac cycle are more uniform in the upper location compared with the lower location (Figure 4-3 top).

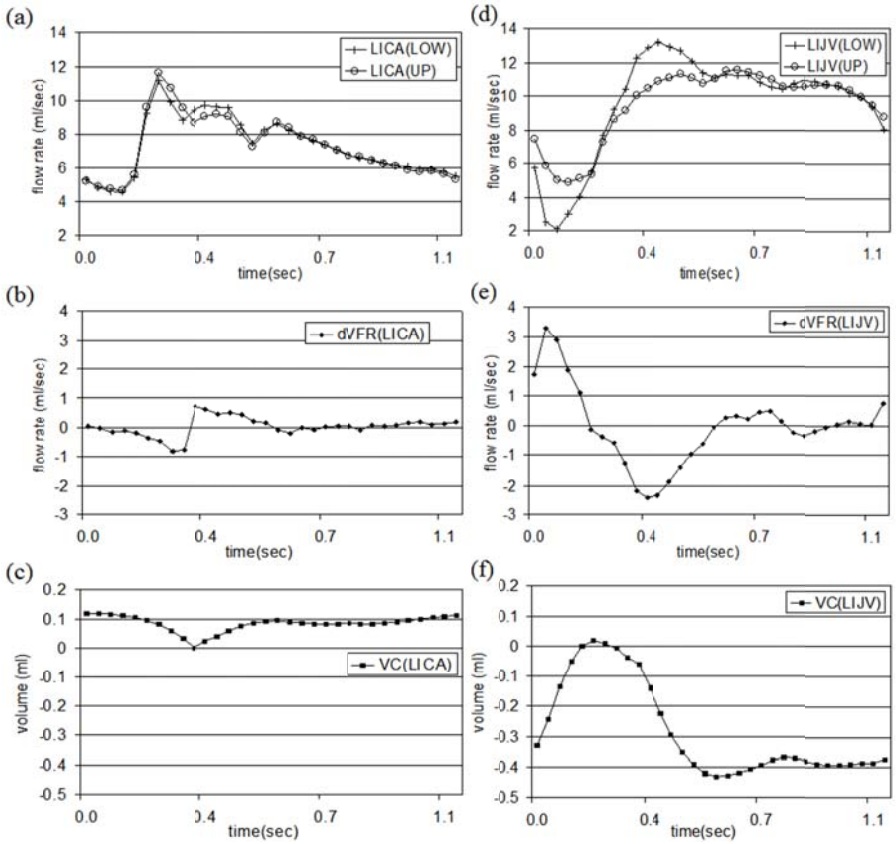

Figure 4-2: An illustration of the blood flow dynamics in left carotid arteries (left column) and left internal jugular vein (right column) measured at upper and lower location from one subject. The measured flow waveforms are shown in (a) and (d) respectively. (b) and (e) are the flow differences derived from (a) and (d) respectively. The volume change waveform in (c) and (f) are derived from the integration of the waveforms in (b) and (e) over a cardiac cycle (Tain *et al.*, 2009).

Table 4-1: Blood flow parameters obtained from the upper and lower image planes (Tain *et al.*, 2009).

		Peak to peak volume change (ml)	Peak to peak VFR (ml/sec)		Mean velocity (cm/sec)		Lumen area (cm^2)	
		Intracranial compartment	Arteries	Veins	RIJV	LIJV	RIJV	LIJV
MRI plane location	Lower	0.71	11.99	7.43	14.0	12.1	0.47	0.32
	Upper	0.59	11.64	5.64	20.2	18.5	0.32	0.20
Ratio (L/U)	Mean	1.39	1.04	1.30	0.71	0.69	1.49	1.72
	SD	0.32	0.100	0.45	0.20	0.34	0.36	0.65

Note: RIJV, LIJV=Right, left internal jugular vein.

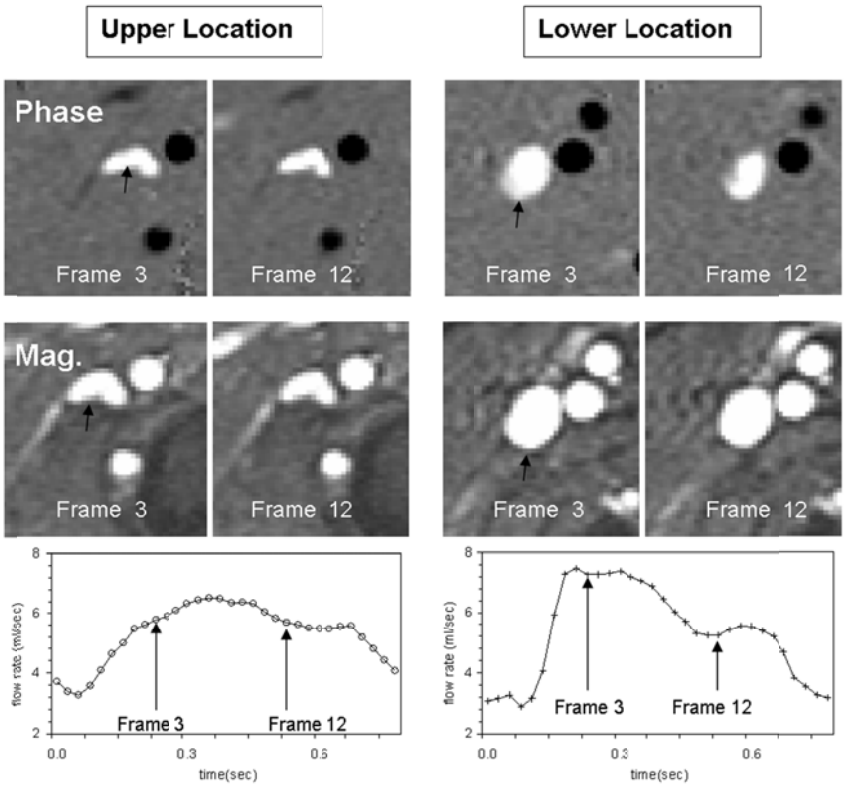

Figure 4-3: An example of phase (top) and magnitude (middle) images from the upper (left) and lower (right) locations showing the velocity and the lumen of the right internal jugular vein (black arrow). Two cardiac frames are shown to demonstrate changes in velocities across the lumen. The flow velocities are more uniform during the cardiac cycle in the upper location. The corresponding volumetric flow rate waveforms at both locations are shown at the bottom. As can be seen, the flow at the lower location is more pulsatile.

Finally, the relationship between the ratio of the lower vs. upper maximal ICV change and arterial and venous pulsatility were assessed by linear regression. The most significant correlations were found with the pulsatility of the net venous flow ($R^2 = 0.77$, $p<0.05$) and the flow at the lower level ($R^2 = 0.59$, $p<0.05$) shown in Figure 4-4. As expected, the higher the venous pulsatility, the larger the expected difference in the ICV change measurements between the two different locations.

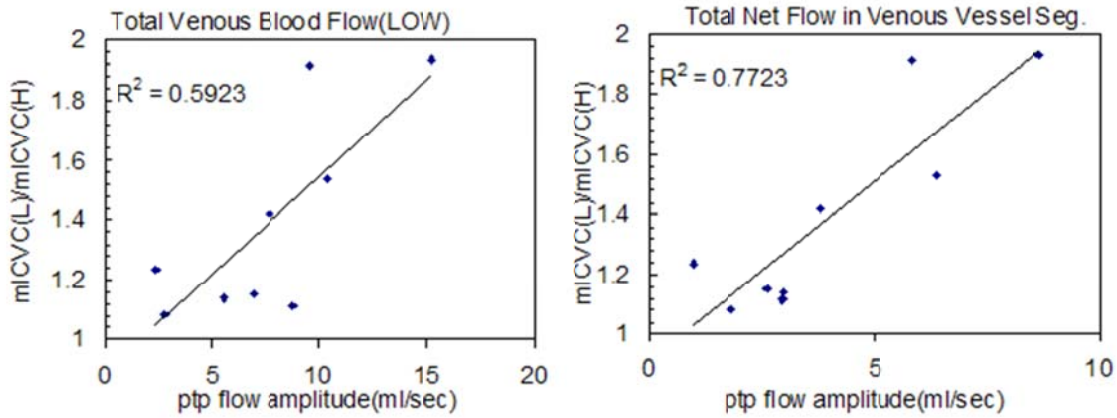

Figure 4-4: Linear relation of the ratio of maximal ICV change with respect to the peak-to-peak (ptp) flow amplitude of venous flow measured at the lower location (left), and to the peak-to-peak flow amplitude of the flows in the venous vessel segments (right).

4-4 Discussion

This study demonstrates that the location along the vessel at which the arterial inflow and venous outflow are imaged influences the measurement of intracranial volume change during the cardiac cycle is a predictive way. Consistently, a larger ICV change is obtained when the lower location is used as compared when the upper location is used. This is expected because the additional volume of the included vessels segments is "added" to the intracranial volume. The mean ratio of the lower vs. upper measurements of the nine data sets was 1.39. Therefore, the intracranial compliances measured using the location that is on average lower by 2 cm from the more optimal location (just below the skull base) are expected to be overestimated by an average of about 40%.

Changes in venous pulsatility along the cerebral drainage pathway have been previously reported by Kim et al (Kim *et al.*, 2007). They proposed a lamped parameter model to predict the extra-cranial venous outflow dynamics based on measured arterial inflow, CSF flow and venous flow in the sagittal and straight sinuses, and validated their

prediction that intracranial venous pulsatility is lower than the extra-cranial, i.e., pulsatility in the jugular veins just below the skull base. The increase pulsatility in the upper jugular veins may be in part due to additional drainage from the petrosal sinus (Beards *et al.*, 1998). The current report points to variation in venous pulsatility between two locations along the same vein with no major branch drainage in between these locations. Thus this further emphasizes the importance of selecting an extra cranial location close to the skull base for the most reliable estimates of the ICVC. This study also demonstrates that the measurement of ICVC is very sensitive to the dynamic of the waveforms (timing of onset and magnitude of the pulse amplitude), especially of the venous outflow, which contributed the most to the larger ICVC obtained using a level that is about 2-3 cm furthers away from the skull base.

Two causes potentially explain the larger effect of the venous influence of the ICVC measurement than the arterial influence. The arterial pulse wave velocity measured at the carotid arteries is on the order of 5-10 m/sec (Kobayashi *et al.*, 2004). Therefore, the time delay between the systolic onsets at the inlet and outlet that are 2 cm apart would be on the order of about 4 msec or less. This short delay is well below the temporal resolution of the MR measurement, as can be seen in Figures 4-2a and d. The systolic onsets of the upper and lower waveforms, in both the right and left internal carotid arteries, occur at approximately the same time and therefore, the net arterial flow waveform is relatively flat as seen in Figure 4-2b. The large influence of the venous outflow is related to the more complex venous flow due to changes in flow pattern between the upper and lower location of the internal jugular veins. The venous flow in

the upper location is more uniform across the lumen during the cardiac cycle compared with the lower location. Furthermore, since the internal jugular vein lumen area is smaller at the higher location, the flow velocity is faster. Therefore, due to the Venturi effect, the fluid pressure is lower at the upper portion of the vein, which explains the partial collapse of the vein at this level compared with the lower level as can be seem in Figure 4-3. The link between pulsatility and the magnitude of the ICVC obtained using imaging plane at difference locations along the vessel segment is demonstrated from the relationship between the ratio of the lower to upper ICVC as a function the peak-to-peak amplitude of the net (R^2 of 0.77, $p<0.05$) and lower location (R^2 of 0.59, $p<0.05$) venous outflow shown in Figure 4-4. This clearly implies that the measurement of the venous outflow should be obtained at the level reported in the initial publications of the ICVC method (Alperin *et al.*, 2000; Glick *et al.*, 2006), i.e., close to the skull base to minimize the influences of the compliance and collapsibility of the arteries and veins, respectively. These findings explain the larger values of ICVC and larger measurement variability reported in a recent investigation of factors affecting the reproducibility of the intracranial volume change measurement by MRI (Kim *et al.*, 2007).

In conclusion, measuring cerebral blood and CSF flows using PC-MRI at a level close to the skull base (C1-C2) to minimize the influence of the compliance of arteries and the collapsibility of veins is suggested for a reliable measurement of ICVC.

Chapter 5 Noninvasive Intracranial Compliance from MRI-Based Measurements of Transcranial Blood and CSF Flows: Indirect vs. Direct Approach

5-1 Project Background

Intracranial compliance (ICC) can be altered by different diseases (e.g., hydrocephalus and Chiari-malformations), and thus measurement of ICC is important both for our understanding of the biomechanical behavior of the craniospinal system and for diagnostic purposes. Invasive ICC measurements have led to the important discovery that ICP is a mono-exponential function of intracranial volume (ICV) thus ICC is inversely related to ICP. The same group has also demonstrated the importance of ICC in the prognosis of head trauma (Maset *et al.*, 1987). However, the volume-pressure response test is not commonly performed in clinical practice because of the increased risk associated with an invasive test, and due to the additional loading of the already compromised intracranial compartment. Therefore, developing a noninvasive method to measure ICC is highly warranted.

The development of MRI techniques for imaging of dynamic motion provides a noninvasive mean for measuring the blood and CSF flows in the craniospinal system. Several investigators attempted to estimate ICC from these MRI measurements either using an indirect relationship between measured parameters and ICC (Balédent *et al.*, 2004; Egnor *et al.*, 2001; Miyati *et al.*, 2003; Wagshul *et al.*, 2006) or directly by measuring the ratio of the changes in volume (dV) and pressure (dP) occurring during the cardiac cycle (Alperin *et al.*, 2000). The direct approach is the noninvasive analogous to

the invasive volume-pressure response test. The dV is derived from the momentary differences between volumes of blood and CSF that flows into and out of the intracranial vault during each cardiac cycle, and the dP (pulse pressure) is derived from CSF pressure gradient waveform, which in turn, is obtained using the Navier-Stoke relationship (Urchuk and Plewes, 1994; Alperin *et al.*, 2000; Loth *et al.*, 2001). This derivation is based on the technique proposed by Urchuk and Plewes who demonstrated in flow phantom an accuracy of better than 8% of the derived non-steady pressure gradients waveforms (Urchuk and Plewes, 1994).

The indirect methods to estimate ICC include measures based on phase-lag analysis and modeling-based approaches. The phase-lag method focuses on the phase shift between CSF and cerebral blood volumetric flows (Balédent *et al.*, 2004; Wagshul *et al.*, 2006). Balédent *et al.* studied the timing of peak systolic cervical CSF flows relative to the arterial inflow in healthy volunteers and in patients with communication hydrocephalus (Balédent *et al.*, 2004). They found that in hydrocephalus patients, the delay between these peaks is shorter than in healthy subjects and suggested that it is due to lower ICC in hydrocephalus. Wagshul *et al.* measured a small mean phase shift of the first harmonic component of the measured blood and CSF waveforms in healthy subjects and therefore concluded that this is consistent with no phase shift between these two waveforms (Wagshul *et al.*, 2006). They also concluded that the phase of CSF flow provides a measure of local changes in compliance.

A lumped parameter model based approach of the craniospinal compartments was proposed by several groups to assess phase and amplitude relationships between

pressures and/or volumetric flows, and biomechanical properties such as the intracranial compliance (Agarwal *et al.*, 1969; Alperin *et al.*, 1996; Ambarki *et al.*, 2007; Chu *et al.*, 1998; Egnor *et al.*, 2001; Guinane, 1972; Yallapragada, 2003; Yallapragada and Alperin, 2004). Egnor *et al.* proposed an RLC model where the arterial inflow and cervical CSF flow are in resonance, and this resonance is required for a smooth capillary blood flow (Egnor *et al.*, 2001). Their model further explained the phase lag of the ICP pulse with respect to the arterial pulse occurs with decreased intracranial compliance. Makki *et al.* used this phase lag to estimate the compliance in a phantom experiment using similar RLC model (Makki *et al.*, 2007). A more recent study by Ambarki *et al.*, presents a detailed lumped parameter model that includes additional intracranial sub compartments. Amplitude and phases of measured volumetric blood and CSF flow waveforms were compared with the model-derived values with good correspondence (Ambarki *et al.*, 2007). Although findings from these studies suggest that phase lag between CSF and cerebral blood flows, and/or amplitudes of these waveforms might be a useful indicator to assess ICC, it is not clear whether there is a predetermined relationship between these parameters and ICC. In this work, the effect of **a change** in ICC on the phase and amplitude of the cranio-spinal CSF flow, and on the direct measure of ICC, the ICC index derived from the blood and CSF flow waveforms, is assessed to address this question.

The lumped parameter model (Figure 3-3) utilized in this work is to study the effect of changes in ICC on the relationship between arterial, venous, and CSF flow waveforms to determine if the arterial-CSF flows phase relationship is a reliable estimate

of ICC. The arterial, venous and CSF volumetric flow waveforms were obtained with velocity-encoding phase contrast MRI scans. The lumped parameters of the initial state of the craniospinal model are first obtained by minimizing the difference between the measured and the model estimated CSF flow waveforms. A change in ICC is then introduced into the model to generate a new CSF flow waveform from which we quantify the effect of the altered compliance on arteriovenous -CSF phase lag, CSF volumetric flow amplitude, maximal intracranial volume change, and CSF pressure gradient. The last two parameters are used to derive the ICC index (Alperin *et al.*, 2000). In addition, the effect of ICC on the magnitude and phase responses of the system transfer function are also characterized using Bode plots (e.g., semi-logarithmic plots of gain (in dB) and phase as a function of frequency with a logarithmic frequency axis) to assess the phase and amplitude changes within the relevant frequency range. A preliminary version of this work has been presented at the 2008 SPIE Medical Imaging conference (Tain and Alperin, 2008).

5-2 Methods and Materials

MRI measurements of transcranial arterial, venous and CSF flow

Arterial inflow, venous outflow, and cranio-spinal CSF pulsatile volumetric flow waveforms were obtained using MRI flow data from five healthy volunteers with no known history of neurological problems (4 males and 1 females, 32±7 years) and two patients with elevated ICP (2 females, 15 and 16 years). All subjects signed an informed consent approved by the intentional review board. Data was acquired with a 1.5T or 3T MRI scanner (GE healthcare, Milwaukee, WI) using retrospectively gated velocity-

encoded cine phase-contrast technique (Alperin *et al.*, 2005b). A high velocity-encoding (VENC of 70-90 cm/s) scan was used for measurements of the arterial inflow through the internal carotids and vertebral arteries, and the venous outflow through the internal jugular veins. A low VENC scan (VENC of 7 cm/sec) was used for measurement of the CSF flow in the upper cervical spinal canal and venous outflow through secondary veins such as epidural and vertebral veins. Other MRI scan parameters were similar as described in Chapter 4. The total volumetric arterial inflow was calculated by summation of the volumetric flow through the individual internal carotid and vertebral arteries, and the venous outflow was calculated by summation of the flow through the jugular veins and secondary veins such as epidural, vertebral and deep cervical veins. The change in the intracranial volume during the cardiac cycle (ICVC) was calculated from the net volumetric flow rates as described in Equation 3-11b using the constraint defined in Equation 3-12 for scaling the measured venous outflow to match the total arterial inflow. The CSF pressure gradient (PG) waveform was derived from the CSF flow data using the method proposed by Urchuk and Plewes which utilizes the Navier-Stoke relationship between pressure gradient, and temporal and spatial derivatives of the fluid velocity for incompressible fluid in a rigid tube (Urchuk and Plewes, 1994). In the upper cervical spine, the convective acceleration and viscosity terms are considerably smaller than the inertia term (Loth *et al.*, 2001). In addition, the upper cervical spinal canal is relatively straight with a relatively unchanged cross sectional area, thus contribution of mass divergence is small. The pressure gradients waveform is therefore approximated using a time derivative of the CSF flow waveform. It has been previously shown that the resulted measurement variability of the maximal pressure gradient change is approximately 8%

(Alperin *et al.*, 2000). The intracranial compliance index (ICCI) was then derived from the ratio of the maximal intracranial volume change and the maximal pressure gradient change normalized for the CSF flow area (Alperin *et al.*, 2000).

Model simulation of CSF flows with several intracranial compliance states

The lumped-parameter electrical circuit model that is analogous to the cranio-spinal system was used to simulate CSF flow dynamics (Figure 3-3). To study the effect of compliance, the first step was to modify the estimated transfer function. A change in the intracranial compliance (C1) was achieved by modifying the transfer function as shown in Equation 5-6, where $\boldsymbol{m}$ is the factor by which C1 is changed. Parameters were then calculated for both decreased and increased compliances relative to the natural compliance state by changing the value of $\boldsymbol{m}$ from 0.05 to 2.8 in steps of 0.1. A 2.8 fold was selected based on previous publication that demonstrates an average 2.8 fold increase in the intracranial compliance from the supine to the upright posture (Alperin *et al.*, 2005a).

$$\overline{\boldsymbol{H}(\boldsymbol{s})} = \frac{\dfrac{\boldsymbol{R}1}{\boldsymbol{L}2}\boldsymbol{s} + \dfrac{1}{\boldsymbol{L}2 \cdot \boldsymbol{m} \cdot \boldsymbol{C}1}}{\boldsymbol{s}^2 + \dfrac{1}{\boldsymbol{L}2}(\boldsymbol{R}1 + \boldsymbol{R}2)\boldsymbol{s} + \dfrac{\boldsymbol{m} \cdot \boldsymbol{C}1 + \boldsymbol{C}2}{\boldsymbol{L}2 \cdot \boldsymbol{m} \cdot \boldsymbol{C}1 \cdot \boldsymbol{C}2}} \tag{5-6}$$

Flow amplitude and phase analysis

The effect of the change in compliance was characterized by several measures. The first measure was derived from the simulated CSF waveforms. The relative change in the peak amplitude of the CSF waveform and the time lag between the CSF and the

transcranial blood flow waveforms for each modified compliance states were calculated. The time lag was obtained by using cross-correlation function. The direct estimate of compliance, the ICC index, was calculated for each compliance state for comparison. In addition, the Bode plots of the craniospinal system model were generated for each state of ICC. The magnitude attenuation and phase angle at the first harmonics of heart rate were then recorded from these plots.

5-3 Results

An example of measured and model-derived CSF flow waveform from one of the healthy subjects is shown in Figure 5-1. The fit and cross correlation coefficient (COEF) that quantifies the goodness of the solution for this example were 90% and 0.99, respectively. This quality is typical for all cases as the mean and SD for all seven subjects were 82±6% and 0.99±0.01. The model derived CSF flow waveforms for increased and decreased compliance states are shown in Figure 5-2a and b, respectively. These waveforms have similar shapes but the peak-to-peak amplitude decreases with increase in compliance as expected. Note that no obvious phase change is notable. Furthermore, when the compliance was very small (0.05xC1), the shape of CSF flow waveform approached that of the net transcranial blood flow waveform (A-V).

Average relative change in amplitude of the CSF waveform and the time lag between the CSF and the A-V waveforms for a sample of 6 compliance states over the range of 0.05 to 2.8 of the initial state are summarized in Table 5-1. In the case of decreasing C1 (ICC), the peak-to-peak amplitude of CSF waveform (ptp CSF) and the maximum PG (ptp PG) increased, but the ICVC decreased. The decrease in ICVC is

expected as more CSF is flowing out of the cranium during the systolic phase of the cardiac cycle. The reverse occurred when compliance increased ptp CSF and ptp PG decreased and the ICVC increased as expected. The ICCI, the ratio of ICVC and ptp PG, demonstrated the largest changes and followed most closely the trend of changes in ICC among all calculated parameters. In contrast, the phase lag was the least affected by the change in compliance. The phase difference was on the order or less than one sampling time period for temporal resolution of 32 frames per cardiac cycle.

Figure 5-3 shows Bode plot of the craniospinal system derived from the measured A-V and CSF flow waveforms. The craniospinal system behaves as a low pass filter, with monotonically decreasing magnitude and increasing phase lag as a function of frequency. The corresponding plots for the 6 compliance states are shown in Figure 5-4. At 7 rad/sec about, the 1st harmonics of heart rate (the subject's heart beat is 66 bpm), both the magnitude and phase were being affected. The average and SD of magnitude and phase angle at the 1st harmonics obtained for the 5 healthy subjects at each of the 6 compliance states are shown in Figure 5-5. These figures demonstrate a different behavior of amplitude and phase angle. The amplitude attenuation increases monotonically with increased compliance as expected. The phase angle, however, did not show a monotonous change and further, the differences were relatively small and within the range of inter-subject variability. This suggests that the phase angle is considerable less sensitive to a change in compliance compared with the amplitude attenuation as demonstrated in Table 5-1.

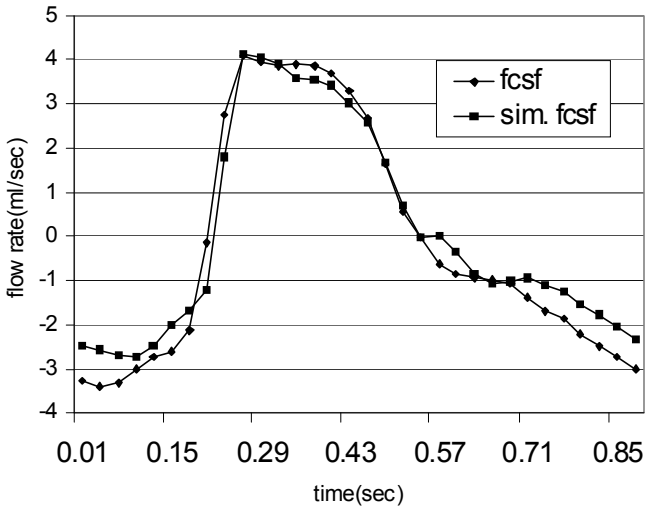

Figure 5-1: An example of the MRI-based measured (**f**csf) and the model-derived (sim. **f**csf) CSF flow waveforms. The goodness of fit in this example is 90% and 0.99 (Tain and Alperin, 2009).

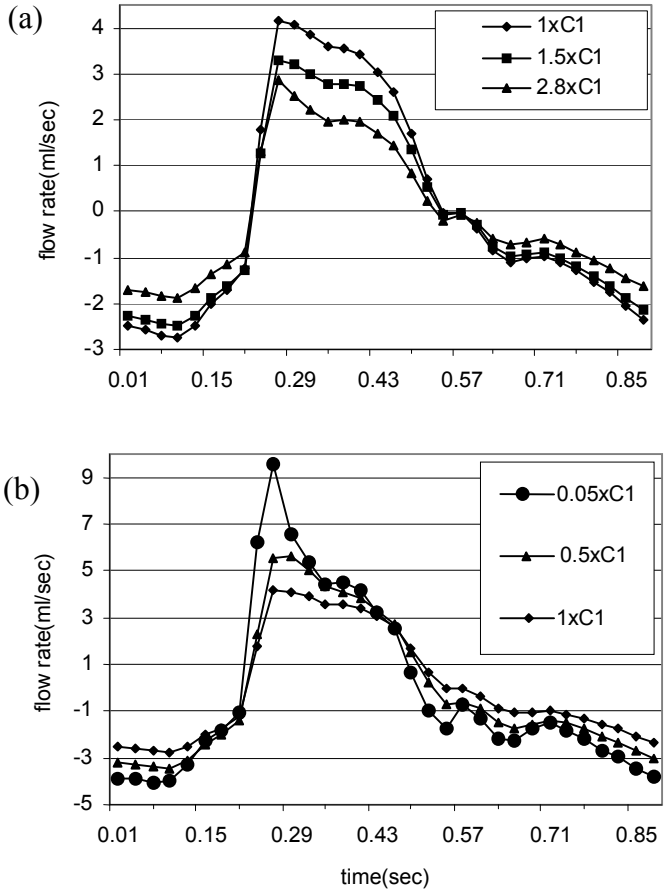

Figure 5-2: Simulated CSF waveforms for increased (a) and decreased (b) ICC states. No significant phase shift is observed with changes in ICC. The changes in amplitude are considerably larger (Tain and Alperin, 2009).

Table 5-1: Average values of relative change in the indirect and direct measures of ICC at 6 different compliance states derived from five healthy subjects (Tain and Alperin, 2009).

	ptp CSF flow (%)	ptp PG (%)	ptp ICVC (%)	ICC Index (%)	Phase lag (% of one period)	Phase lag (ms)
0.05 x ICC	95.10	149.20	-59.40	-82.09	3.13	31
0.50 x ICC	28.12	52.64	-25.29	-49.49	1.34	13
1.00 x ICC	-	-	-	-	-	-
1.50 x ICC	-14.62	-17.07	2.52	24.52	0.45	4
2.00 x ICC	-22.16	-23.17	9.07	42.30	0.89	9
2.80 x ICC	-28.83	-28.21	15.83	65.68	1.79	18

The reference point is the unchanged compliance state (1.00xC1).

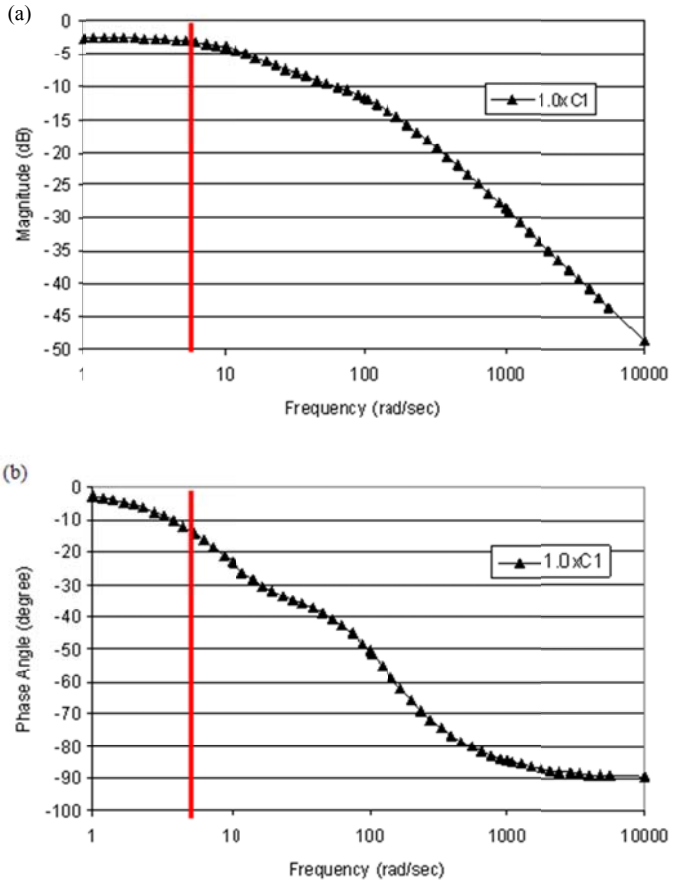

Figure 5-3: An example of magnitude (a) and phase (b) responses of modeled craniospinal system of a healthy subject. The vertical line marks the frequency of the first harmonics of the subject's heart rate (Tain *et al.*, 2009).

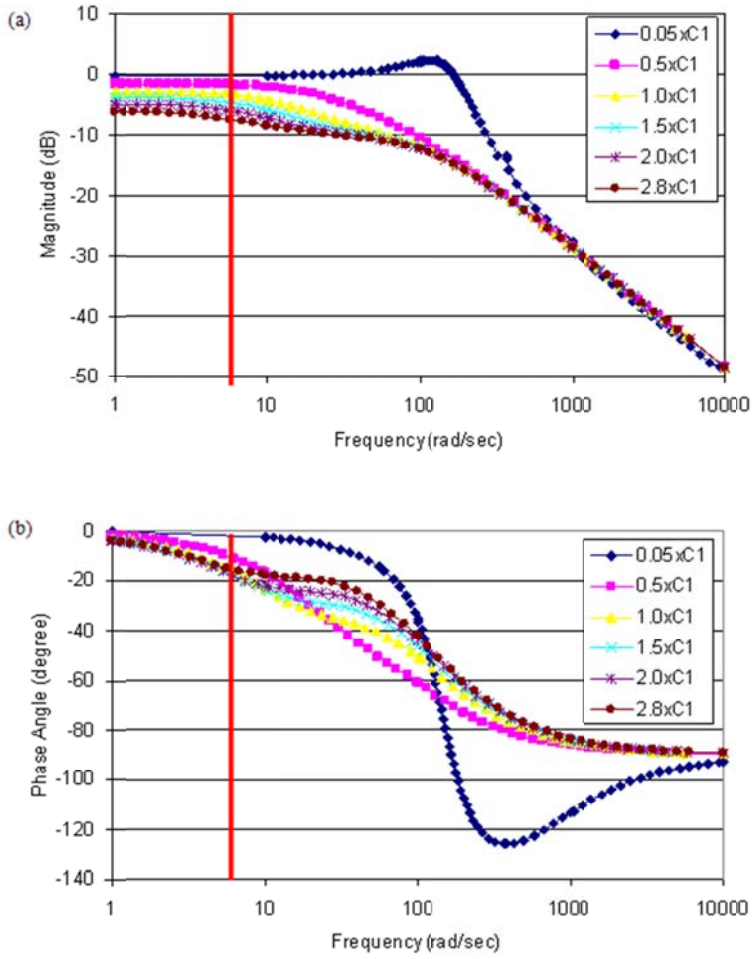

Figure 5-4: Magnitude (a) and phase (b) responses of the same modeled craniospinal system calculated at six different compliance states. At the first harmonics of the subject's heart rate frequency, the magnitude decreases monotonically with an increase in compliance. The change in the phase angle is not monotonic with respect to the compliance and relatively smaller (Tain *et al.*, 2009).

The relationship between the modeled intracranial compliance state and the direct measure of compliance - the ICC index was calculated and plotted for a subject with normal ICP (i.e., normal ICC) and for a subject with an elevated ICP (lower ICC). The relationship between the ICC index and the relative compliance for these two subjects are shown in Figures 5-6 and 5-7, respectively. At the reduced compliance states (elevated ICP), the ICCI followed the changes in ICC approximately in a linear manner. At the increased compliance state (below normal ICP), the ICCI deviated from the linear relationship and saturates as the compliance increases. Interestingly, for the subject with

elevated ICP the ICCI saturated much less and follows a linear relationship over the entire range.

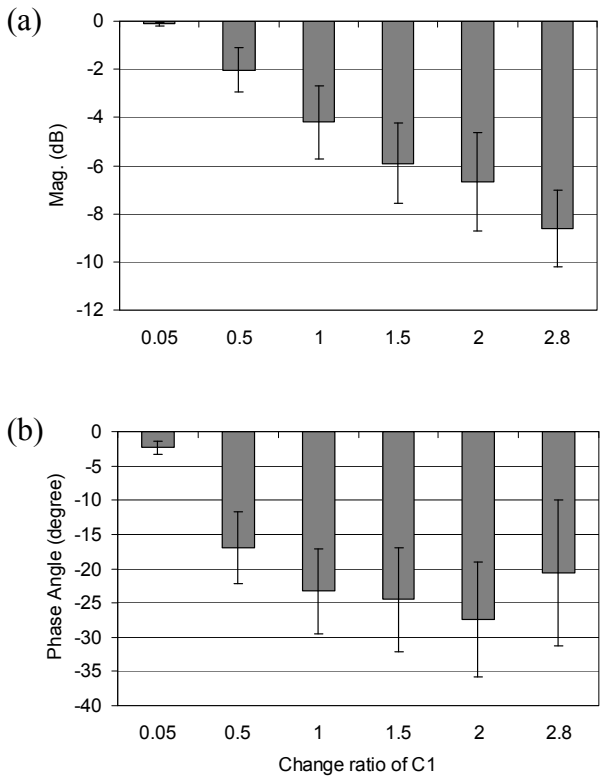

Figure 5-5: Mean and SD values of the magnitude (a) and phase angle (b) from all the healthy subjects at the 1st harmonics of the subjects' heart rate. The magnitude response decreases monotonically with increasing compliance. The relative sensitivity of the phase angle to a change in compliance is smaller than that of the decrease in magnitude (Tain and Alperin, 2009).

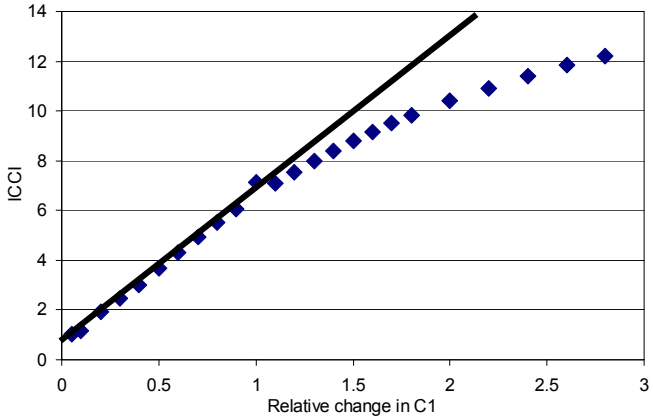

Figure 5-6: A plot of the ICC index vs. a relative change in ICC derived for a healthy subject with normal intracranial compliance and pressure. In low and normal compliance states (elevated and normal pressure) the relationship is linear. The curves start saturate in the increased compliance states (at low ICP) (Tain and Alperin, 2009).

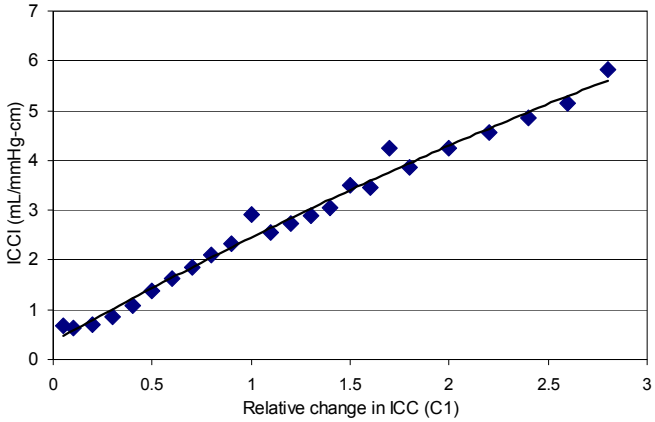

Figure 5-7: A plot of the ICC index vs. a relative change in ICC derived for a subject with elevated intracranial pressure (low compliance). The relationship between ICCI and a relative change in ICC is linear over the entire compliance states (Tain and Alperin, 2009).

5-4 Discussion

The clinical importance of ICC motivated an effort by several groups to establish a noninvasive measure of this parameter. Recent effort focused on using MRI measurements of blood and CSF flows for estimation of ICC utilizing the fact that these are coupled and the ICC modulates the CSF flow. This study compared and assessed the sensitivity of several measures that have been previously proposed as estimates of ICC. These measures included an indirect measure of compliance such as the phase lag between the blood and CSF flows previously suggested as a marker for ICC (Balédent *et al.*, 2004; Egnor *et al.*, 2001; Miyati *et al.*, 2003; Wagshul *et al.*, 2006) and a direct measure of compliance, the ICC index, which is defined as the ratio of the systolic volume and pressure changes that occur naturally with each heart beat (Alperin *et al.*, 2000). The assessment was performed using in vivo dynamic MRI measurements from healthy subjects (normal ICC) and subjects with elevated ICP (reduced ICC) and a compartmental model of the craniospinal system to simulate the effect of a change in ICC

on the CSF flow for a given blood flow input. This model was chosen because it is able to successfully predict measured CSF flow waveforms obtained by MRI in humans.

Phase lag is a natural choice for estimation of compliance because a change in electrical capacitance is often associated with a change in the phase between the input and output of the 1st order RC circuit. Several investigators indeed demonstrated different mean phase differences between the CSF and the arterial inflow waveforms in healthy and in hydrocephalic subjects and suggested that this is due to differences in intracranial compliances (Balédent *et al.*, 2004; Miyati *et al.*, 2003; Wagshul *et al.*, 2006). However the selectivity of the phase lag to **a known change in ICC** cannot be estimated from these results. This work utilized a lumped-parameter model that was shown to be able to "explain" actual flow measurements (Ambarki *et al.*, 2007; Yallapragada, 2003) to generate a **known change in ICC**. The model was used in conjunction with actual blood and CSF flow measurements to increase the reliability of the analyses. The similarity between the predicted and measured CSF waveforms and the consistency across the different subjects (a mean of 80% goodness fit) support the validity of the chosen model.

The derived simulated CSF waveforms for increased compliance states (Figure 5-2a) and for reduced compliance states (Figure 5-2b) revealed that the dominant change was in the amplitude and not in the phase. These findings provide the initial evidence that measures of ICC based on amplitude would be considerable more sensitive than those based on phase lag. Table 5-1 lists the relative change from the initial compliance state, in percentage, in the amplitudes of the CSF flow, the CSF pressure gradient, maximal change in intracranial volume, and the ICCI. The change in phase is listed in time (msec)

and in relative percentage of one cardiac cycle. From comparison between the phase and the amplitude measures it is obvious that the phase is considerably less sensitive to changes in ICC than the amplitude. The alternative way to analyze the relationship between compliance and the time delay is from the measures of cranio-spinal system's spectrum response via the Bode plot. The frequency response is a representation of the system's response to sinusoidal inputs at varying frequencies. The mean and SD of the magnitude and phase difference at the fundamental frequency of heart rate obtained from the normal subjects (Figures 5-5a and b, respectively) clearly show a monotonic change in the magnitude response with increased ICC while the change in the phase lag was not monotonic and was also associated with larger relative SD. These further support the advantage of amplitude over phase based ICC measures as seen in Figure 5-2. Further, the change in the phase lag was on the order of only 10 degrees for a change in ICC from 0.5 to 1.0 and less than 5 degrees for a change from 1.0 to 1.5. This translates to 30 and 15 milliseconds, respectively, which is approximately the limit of the temporal resolution of the MRI sampling rate of the flow data. Therefore, current temporal resolution is insufficient for detection of change in ICC that corresponds to a less than 10-degree change in phase.

Among the amplitude measures, a change in ICC affects the parameters with different proportions. For the reduced compliance states, the largest change occurred in the pressure gradient waveform while for the increased compliance state, the largest change occurs in the ICCI. However, only the ICCI demonstrated the most linear proportional change with respect to a change in ICC, thereby providing the most reliable quantitative estimate for the ICC. The sensitivity of ICC index with respect to the change

in ICC can be further assessed from two examples shown in Figures 5-6 (normal compliance) and 5-7 (low compliance). For the subject with the normal compliance, the ICCI was approximately linearly correlated with the ICC for the normal and reduced ICC range and starts to saturate as ICC increases. For the subject with the elevated ICP (reduced compliance), there is considerably less saturation. There are two possible reasons for the saturation that occurs with increasing compliance. First, the model parameters estimation procedure does not provide estimates of the individual parameters (i.e., C1, R1, C2, R2 and L2), but instead it provides the natural frequency and the damping ratio of the system (Equation 3-2). Therefore, the simulation of the increased compliance state could not be derived by direct modification of the C1 (ICC) value alone and therefore changes in the CSF waveforms that could occur due to changes in R or I are not accounted for in the simulation. The second possible reason could be the effect of the spinal compliance (C2) on the CSF flow, which is not accounted for in the calculation of the ICC index. The direct approach assumes that the spinal canal compliance is larger than the intracranial compliance. In the clinical relevant range of normal or reduced ICC (normal or elevated ICP), these simulations demonstrate a liner relationship between the ICC and the ICC index.

5-5 Summary

The pulsatile flow of CSF between the cranium and the spinal canal with every heartbeat is driven by the pulsatile blood flow to and from the cranium and is largely modulated by the intracranial mechanical compliance. MRI now provides noninvasive measurements of volumetric blood and CSF flows to and from the cranium. Several

approaches were proposed to derive noninvasive estimates of ICC from these measurements. The sensitivity of the different estimates of ICC to a change in ICC is studied and quantified in this work. The main finding of this work is that amplitude based measures of compliance are considerably more sensitive to changes in ICC than phase lag based measures. Furthermore, among the amplitude-based measures, the ratio of the maximal (systolic) intracranial volume and pressure changes, e.g., the ICC index, is the most reliable estimate of ICC over a wide range of different ICC states.

Chapter 6 Craniospinal Compliance Distribution in the Healthy and Disease States

6-1 Project Background

In vertebrates, the overall cranio-spinal compliance is determined by the sum of the individual compliances of the cranial and spinal canal compartments (Löfgren *et al.*, 1973; Marmarou *et al.*, 1975). Given that both compartments contribute to regulation of intracranial pressure (ICP), it is important to be able to determine how the overall cranio-spinal canal compliance is distributed to understand the role of the spinal canal compartment in ICP regulation, especially since the overall compliance changes with posture (Magnaes, 1989; Alperin *et al.*, 2005a), with a change in ICP (Marmarou *et al.*, 1975), and with different pathologies (Maset *et al.*, 1987; Miyati *et al.*, 2007).

From anatomical consideration, it is expected that in the supine posture, when hydrostatic pressure is similar in the cranium and spinal canal, the spinal canal (SC) contribution to the total cranio-spinal (CS) compliance is larger than the cranial (CR) compartment contribution because the dura in the spinal canal, especially in the lumbar region and dural sac, is less confined by bony structures compared with the cranial vault. Over the last several decades different methods were proposed for estimation of the CS compliance (Löfgren and Zwetnow, 1973; Marmarou *et al.*, 1975; Mann *et al.*, 1978; Shapiro *et al.*, 1980; Avezaat and van Eijndhoven, 1986; Magnaes, 1989; Czosnyka *et al.*, 1990; Raabe *et al.*, 1999; Wåhlin *et al.*, 2010). These methods rely on infusion of fluids into the cerebrospinal fluid (CSF) spaces and recording the change in CSF pressure under different infusion paradigms. Yet, infusion based approaches for estimation of the

cranio-spinal compliance distribution provided disparate results (Löfgren and Zwetnow, 1973; Marmarou *et al.*, 1975; Magnaes, 1989; Wåhlin *et al.*, 2010).

Using a constant rate infusion method in dogs, Löfgren and Zwetnow found that the cranial contribution is smaller than the spinal canal contribution (Löfgren and Zwetnow, 1973). Using a bolus injection method in cats, Marmarou *et al*. revealed a mono-exponential relationship between intracranial pressure and volume (Marmarou *et al.*, 1975). The linear slope in a semi-logarithm scale of the derived pressure-volume curve was termed pressure-volume index (PVI). PVI is the factor by which pressure and elastance (e.g., inverse of compliance) are linearly related. In contrast to previous findings using the constant infusion method, they reported a larger compliance contribution from the cranial compartment, 68% vs. 32 % for the spinal canal. Fourteen years later, Magnaes applied the bolus method to estimate individual cranial and spinal compliances in patients with CSF blockage at the cervical level (Magnaes, 1989). They found that the cranial compartment contribution is smaller, about 37% of the total compliance. A third infusion method, a constant pressure infusion, applies a variable infusion rate to achieve several different constant pressure states (Ekstedt, 1977). This approach utilizes the natural pressure pulsation to determine the PVI from the linear relationship between the amplitude of the pulsation and mean pressure (Avezaat and van Eijndhoven, 1986). A constant pressure infusion test in conjunction with MRI measurements of blood and CSF flows to and between the cranio-spinal compartments was recently proposed by Wåhlin *et al*. to estimate the CS compliance distribution in supine aged healthy subjects, without the need to physically isolate the two compartments

(Wåhlin *et al.*, 2010). In contrast to earlier report, that approach suggests a larger cranial contribution, 65%, vs. 35% from the spinal canal.

This study employs the lumped parameter methodology to investigate potential sources for the inconsistency of the craniospinal compliance distribution found in literature. This work further proposes and evaluates the robustness of a new noninvasive approach for estimation of the craniospinal compliance and resistance distributions. The investigation is done using MRI data obtained from elderly healthy subjects similar to the population used in the Wåhlin's study (Wåhlin *et al.*, 2010). In addition, the potential clinical relevance of this method is demonstrated by assessing the cranio-spinal compliance distribution in newly diagnosed obese female patients with idiopathic intracranial hypertension (IIH). Cranio-spinal compliance distribution measurements are used to test the hypothesis that IIH in obese females is associated with reduced spinal canal compliance contribution due to increased abdominal pressure, which in turns, contributes to the elevated ICP.

6-2 Methods

Compliance and resistance distributions within the cranio-spinal system

The relative spinal canal compartment contribution to the global craniospinal resistance and compliance (to CSF flow) can be estimated from the system transfer function shown in Equations 3-3a and 3-3b. In the literature, the compliance distribution was estimated based on derivation of the PVI for each compartment (Marmarou *et al.*, 1975). With the invasive approach, the two sub-compartments are isolated and the PVI of each sub-compartment is assessed using the infusion test. The reliability of the transfer

function based approach was assessed by comparing the compliance distribution ratio calculated directly from the transfer function (Equation 3-3a) with the PVI derived distribution as well as by comparing two simulated conditions, "communicating" and "isolated" cranio-spinal sub-compartments, which simulated the invasive approach for derivation of the compliance distribution. The isolation of the compartment enabled estimation of its contribution to the overall compliance independently of the other compartment. Compartmental isolation was achieved by increasing R1 or R2 values until the maximal volume change in the "isolated" compartment was less than 0.05 ml.

Estimation of cranio-spinal compliance using pressure-volume indices (PVI)

The derivation of the PVI (Equation 3-6) requires estimation of the compartmental volume change (ΔV) and the relative pressure change ($\frac{\Delta P}{P}$). These parameters was obtained using the MRI measurements of volumetric arterial inflow and venous outflow to and from the cranium, and CSF flow between the cranium and the spinal canal (Alperin *et al.*, 2000). The pressure pulsation (ΔP) in each of the sub-compartments was then derived from the lumped parameter model based on the compliance-flow relationship shown in Equation 6-1,

$$\Delta P(i) = \frac{1}{C_x} f_x(i) \cdot \Delta t \qquad (6\text{-}1)$$

where f_x and C_x are the net volumetric flow rate and compliance of each sub-compartment, respectively. While the model enables the derivation of the pressure change it does not provide an absolute mean pressure (P). However, since subjects were

scanned in the supine posture, the mean pressure in each of the sub-compartment was assumed to be the same. This assumption was previously confirmed with invasive pressure measurement (Lenfeldt *et al.*, 2007). The cranio-spinal compliance distribution was then obtained from the ratio of the individual PVI of each sub-compartment.

MRI measurements of the compartmental volume change

The time-varying compartmental volume change waveforms are derived using the volumetric flow rates into and out of the specific compartment shown in Figure 3-1. The inlet and outlet of the cranial compartment are the arterial inflow f_A, venous outflow f_V, and craniospinal CSF flow f_{CSF}. The spinal canal compartment has a single inlet and outlet for the CSF flow from and back to the cranium. The mathematical expressions of the volume changes of the cranio-spinal compartment and the two individual sub compartments are described in Equation 6-2.

$$\Delta V_{CS}(i) = [f_A(i) - f_V(i)] \cdot \Delta t \tag{6-2a}$$

$$\Delta V_{CR}(i) = [f_A(i) - f_V(i) - f_{CSF}(i)] \cdot \Delta t \tag{6-2b}$$

$$\Delta V_{SC}(i) = f_{CSF}(i) \cdot \Delta t \tag{6-2c}$$

where i is the cardiac phase index sampled by time intervals of Δt. The maximal volume change of each compartment, which occurs in the systolic phase, is the peak to peak amplitude of volume change waveform. Equation 6-3, which states that there is no change or accumulation of volume over the entire cardiac, is used to account for the small unmeasured venous outflow through secondary veins (Alperin *et al.*, 2000).

$$\sum_{\substack{cardiac\\cycle}} \Delta V_{CR}(i) = \sum_{\substack{cardiac\\cycle}} [f_A(i) - f_V(i) - f_{CSF}(i)] \cdot \Delta t = 0 \qquad (6\text{-}3)$$

6-3 Materials

The study was approved by the IRB and all subjects provided informed consent. MR images were acquired from two different cohorts of subjects. Data from **7** aged healthy subjects (mean age 64 ±10 years) were used to test the consistency of the derivation of cranio-spinal compliance distribution. Elderly adults were studied to enable comparison with literature results (Wåhlin *et al.*, 2010). Eight newly diagnosed female IIH patients (BMI of 35±7 kg/m^2, mean age of 28±9 years) and 9 healthy female subjects (BMI of 36±3 kg/m^2, mean age of 32±9 years) were studied to assess the role of cranio-spinal compliance contribution in IIH. The diagnosis of IIH was made based on modified Dandy criteria and confirmed by lumbar puncture (opening preserve ranged from 26 to 41 cm water). Presented symptoms include mild to severe headache, and mild to moderate papilledema (grading range was mostly 2 and 3).

MRI scans of the IIH and control subjects were performed using a 1.5T scanner and of the aged healthy subject using a 3T scanner (Siemens Medical Solution, Germany). The MRI brain protocol included anatomical imaging and two additional retrospectively gated velocity encoded cine phase contrast scans for quantitation of blood and CSF flows to and from the cranium (Alperin *et al.*, 2000). MR scan parameters were similar as described in Chapter 4. Images were reconstructed into 32 cardiac phases using the same projected heart rate for both the blood and CSF flows.

6-4 Results

For the 7 elderly healthy subjects, the fit and COEF were 77±5% and 0.90±0.11, respectively. The computed contribution of the spinal canal to the overall cranio-spinal compliance obtained using the transfer functions was 69±16%. This value is consistent with values derived using the PVI calculation for the communicating state, 68±13%, (Table 6-1A), and the isolated state 66±13% (Table 6-1B).

Table 6-1: Compliance distribution using PVI calculation under two conditions: (A) Communicating compartments and (B) Isolated compartments (Tain *et al.*, 2011).

	CR	SC	$\frac{SC}{CR+SC}$(%)
(A)			
PVI_{comm} (ml)	11.69±3.30	34.43±28.23	68±13%
ΔV (mL)	0.81±0.24	0.86±0.29	–
ΔP (mmHg)	1.29±0.34	0.79±0.59	–
(B)			
PVI_{iso} (mL)	12.74±3.31	32.94±24.54	66±13%
ΔV (mL)	1.51±0.45	1.47±0.42	–
ΔP (mmHg)	2.41±0.84	1.44±1.12	–

In contrast to the similar PVI values obtained for the "communicating" and the "isolated" states, the maximal volume change is different between the two states as expected (Table 6-1). In the communicating state, the average maximal volume change in the cranial and spinal sub-compartments were 0.81 and 0.86 mL, respectively. Yet, a smaller pulse pressure was obtained in the spinal canal, the sub-compartment with the larger compliance, as expected for a compartment with the larger compliance (Table 6-1A). Similar behavior was seen in the "isolated" state, except that the respective volume changes, 1.51 and 1.47 mL, as well as the resulting pulse pressure, 2.41 and 1.44 mmHg, are much larger. Again, this was expected, because only one sub-compartment at a time is "functioning" to accommodate the pulsatile volumetric blood flow.

For obese female controls the goodness-of-fit were 76±8% and 0.92±0.07, and were 82±5% and 0.99±0.01 for IIH. In controls, the spinal canal compartment contributed larger compliance (SCCC) and resistance (SCCR) than the intracranial compartment. The SCCC and SCCR were 76±11% and 63±14%, respectively. For IIH patient the SCCC and SCCR were 60±13% and 60±15%, respectively. The spinal compliance contribution in IIH was significantly lower than the normal obese controls ($p<0.05$).

6-5 Discussion

Previously reported invasive measurements of the cranio-spinal compliance distribution provide conflicting observations regarding the contribution of the spinal canal to the overall cranio-spinal compliance. From anatomical consideration, it is expected that the spinal canal contribution is larger than the cranial contribution due to the dura being less confined by the bony structures, especially in the lumbar region, and because CSF can expand into the dural sleeve of the nerve root (Hogan *et al.*, 1996). MRI provides a noninvasive means to estimate volumetric flow rates into and out of the cranio-spinal system and its individual sub compartments (Alperin *et al.*, 2006; Miyati *et al.*, 2007). This capability was employed in the current study in combination with lumped-parameter modeling (Tain and Alperin, 2009) to noninvasively estimate the cranio-spinal compliance distribution. The reliability of this approach is demonstrated by the consistency of the compliance distribution values obtained using the subject-specific transfer function and direct estimation based on the ratio of the volume change and pulse pressure during the cardiac cycle. The obtained values of the spinal canal contribution are 69 and 68%, respectively. In addition, similar spinal canal compliance contributions are

obtained when the contribution is estimated under a simulated isolated state, 66%, which is analogous for the invasive approach for quantitation of the compliance distribution. The similar value supports the consistency of the derivation and the validity of the approach. All the 3 approaches yield a larger spinal canal compliance contribution compared to the cranial sub-compartment, as expected from anatomical consideration. The derived value of about 2:1 (SC:CR) compliance distribution is in good agreement with previous observation of spinal canal contribution of 63% in elderly humans (Magnaes, 1989).

In contrast, Wåhlin *et al.* found that the cranial compliance is larger than the spinal canal compliance, 65% versus 35%, respectively (Wåhlin *et al.*, 2010). Their novel approach combined for the first time MRI flow measurements with invasive infusion measurements to derive the relative compliance contribution of each compartment. CSF and blood flows were used to obtain the volumetric changes and the invasive constant pressure infusion method was used to estimate the ratio of pulse pressure and mean pressure. Further experiments in this study expand on Wåhlin's work with two major differences; first, the actual venous outflow is used to calculate the volume change while their approach assumed a constant venous outflow. The second difference is the usage of the lumped parameter modeling in conjunction with the MRI flow measurements to estimate the pulse pressure magnitude in each compartment, instead of the infusion test. The influence of the venous outflow dynamics on the derivation of the compliance distribution was demonstrated by calculating the maximal volume changes in the cranial and spinal sub-compartments twice, once using actual venous outflow and once using a constant, non-pulsatile venous outflow. Differences in the calculated volume change

waveforms due to the venous outflow contribution obtain in one of the subjects are demonstrated in Figure 6-1.

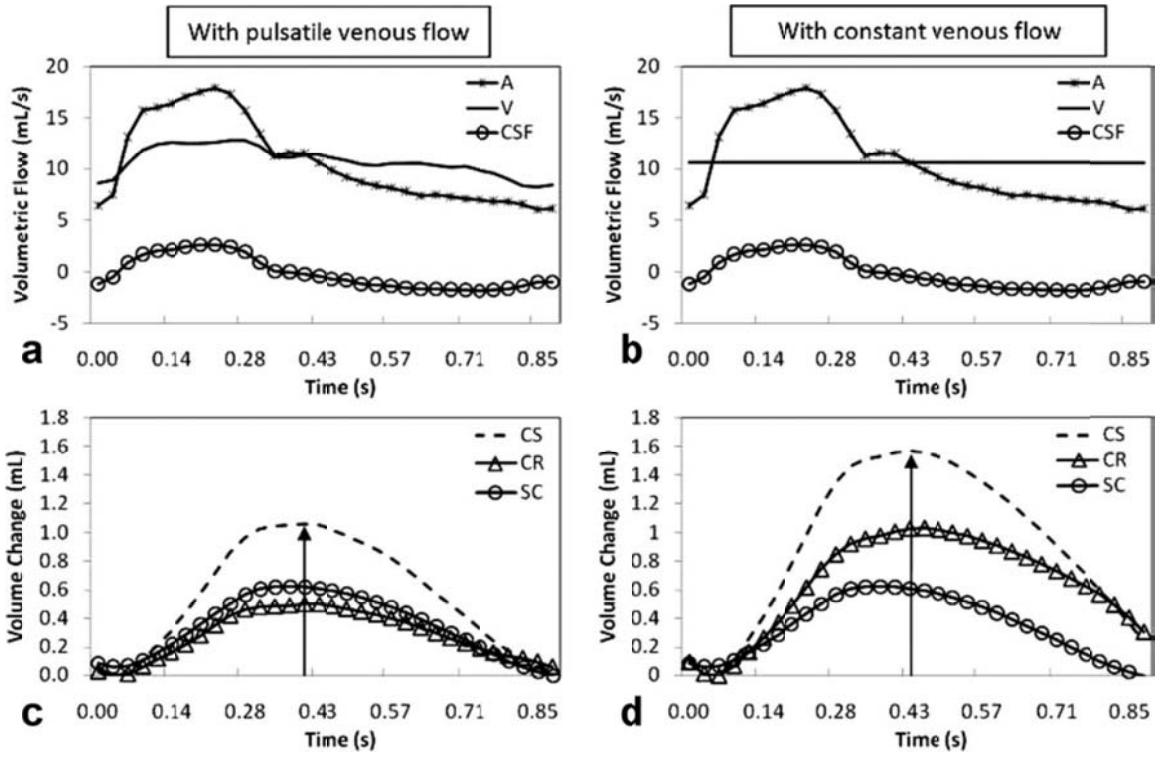

Figure 6-1: The influence of venous flow dynamics on the derivation of the volume change waveforms. Examples of arterial, venous, and CSF flow waveforms from one of the subjects used for derivation of the volume change waveforms are shown in (a) Actual venous outflow is replaced with constant venous outflow in (b) Corresponding cranio-spinal, cranial, and spinal compartmental volume change waveforms are shown in (c) and (d). A larger peak-to-peak volume change is observed in the cranial compartment when a non-pulsatile venous dynamics is used (d) (Tain *et al.*, 2011).

The volume change during the cardiac cycle in each of the sub-compartment and the global craniospinal volume change are shown for an actual venous outflow and for an assumed constant venous outflow. The average maximal volume change values from the seven subjects are summarized in Table 6-2. The venous outflow affects the derivation of the volume change in the cranial sub-compartment and therefore of the overall craniospinal compartment (Table 6-2). With constant venous flow, the average maximal volume change in the cranial compartment was larger by 51%. A larger volume change suggests a larger compliance, thus the overestimating of the cranial compliance. The

volume change in the spinal canal compartment is unaffected by the cerebral venous outflow.

This observation is further validated by the derivation of the average spinal canal compliance using constant and actual venous outflow. The results, which are summarized in Table 6-3, demonstrate that the average spinal canal compliance contribution increases from 40% to 49% when actual venous outflow is accounted for. This value was still smaller than the value of 69% obtained using our method. A second factor that contributed to the overestimation of the cranial compliance is assumed similar pulse pressure amplitude in both the cranial and the spinal canal sub-compartments. The invasive method used by Wåhlin *et al*. measures the pulse pressure in the spinal canal and the same value is assumed in the cranium. This assumption contrasts reports documenting higher pulse pressure in the cranium (Lindgren and Rinder, 1969; Eide and Brean, 2006). The lumped-parameter model used in our approach allows to estimation of the pulse pressure in each compartment individually.

A potential clinical usefulness of determining cranio-spinal compliance distribution is demonstrated in the application of the method toward elucidating the pathophysiology of neurological disorders associated with altered ICP. IIH is associated with periods of considerably elevated CSF pressure and it is commonly occurring in obese females (Dhungana *et al.*, 2010). A statistically significant smaller spinal canal compliance contribution was found in our homogenous cohort of IIH patients compared with healthy female of similar age and BMI, 60±13% versus 76±11%, respectively. Reduced compliance in the spinal compartment, which normally provides the majority of

the craniospinal compliance, is therefore a likely contributor for the increased ICP in IIH. IIH is believed to be associated with impaired CSF absorption (Karahalios *et al.*, 1996). Impaired absorption is likely to increase CSF volume, which in conjunction with reduced compliance buffering would result in elevated ICP. The association between IIH and obesity further support the involvement of the spinal canal compartment in IIH. MR imaging of the spinal CSF spaces demonstrated that obesity is associated with reduced CSF cross-sectional area explained by inward displacement of the foramen contents caused by increased abdominal pressure (Hogan *et al.*, 1996). Lee et al further demonstrates that lumbar CSF volume can be reduced by increasing abdominal pressure (Lee *et al.*, 2001). These observations point to a potential mechanism that causes reduced spinal canal compliance in IIH, i.e., an increased abdominal pressure limits the expansion of the spinal canal CSF spaces.

Table 6-2: Compartmental Volume Change (ΔV) Obtained With Pulsatile and Constant Venous Outflow (Tain *et al.*, 2011).

	ΔV (mL)		
Compartment	With pulsatile venous flow	With constant venous flow	Difference (%)
CS	1.16±0.41	1.54±0.48	37±27%
CR	0.66±0.19	0.98±0.28	51±39%
SC	0.67±0.33	0.67±0.33	–

Table 6-3: Compartmental PVI Derived Using a Constant and Pulsatile Venous Outflow (Tain *et al.*, 2011).

	CS	CR	SC	$\frac{SC}{CR+SC}$ (%)
PVI_C (mL)	7.36±2.28	4.42±1.38	2.94±1.05	40±6%
PVI_P (mL)	5.48±1.95	2.97±0.94	2.94±1.05	49±7%

C = constant venous outflow; P = pulsatile venous outflow.

Chapter 7 Dynamic Coupling between the Intracranial and Spinal Canal Compartments

7-1 Project Background

The spinal canal compliance (SCC) modulates the amount of CSF that enters the spinal canal compartment from the cranium within each cardiac cycle, (e.g., in response to the systolic increase in cerebral blood volume), and the relative CSF volume distribution between the compartments (e.g., in response to intracranial CSF accumulation due to impaired CSF absorption). The spinal canal is thus a volume reservoir that plays an important role in regulation of ICP. For example, reduced spinal canal compliance leads to disproportional CSF accumulation in the cranium, which is likely the cause of loss of ICP regulation in IIH (e.g., IIH is associated with large fluctuations in ICP) (Alperin *et al.*, 2012). Regardless of the importance of the interplay between ICP and the craniospinal compliance distribution for the understanding of the craniospinal hydrodynamics, the cranio-spinal hydrodynamic coupling has not been well investigated. Even less is known about the craniospinal compliances' redistribution that occurs between considerably different hydrodynamic states such as supine and upright postures (Magnaes, 1989; Alperin *et al.*, 2005a). The complexity of craniospinal system arises from the fact that the compliances are non-linear functions of both the volume and the pressure.

As described in Chapter 6, it is our recent work that elucidated, for the first time, the reasons for the conflicting reports regarding which sub-compartment dominates the overall craniospinal compliance in the supine posture (Wåhlin *et al.*, 2010). In this

chapter, the lumped parameters modeling is utilized to explore the behavior of this complex system by investigation of the dependency of the pressure and volume changes within the individual sub-compartments over a wide range of compliances states. Model-derived simulations of the craniospinal CSF pulsation at different compliance states are used to study the function of spinal canal compartment in regulation of ICP. Current investigations expand the modeling approach described in Chapter 5 by manipulating compliances of each sub compartment individually, where previously only the ratio between C1 and C2 was manipulated. In addition, the sate space equations were derived to estimate the pressure behaviors at each sub compartment. These modeling were then applied to data obtained from three cohorts, healthy males, healthy obese females, and patients with obesity related IIH.

7-2 Materials

A total of 26 MR data sets from three cohorts, 9 healthy male (age of 31±8 years), 9 obese healthy female (age of 32±9 years), and 8 newly diagnosis obese IIH patients (age of 28±8 years) were randomly selected from data acquired in the previous study. The obese healthy females with similar age and BMI were used as controls for the obesity-related IIH patients.

7-3 Methods

MR measurements of the cerebral blood and craniospinal CSF flows over one cardiac cycle were used for estimation of the subject-specific transfer function of the craniospinal system (Chapter 3). The discrete transfer function is shown in Equation 7-1.

$$H(z)=\frac{F_{CSF}(z)}{F_{AV}(z)}=\frac{m_1 z+m_0}{z^2+n_1 z+n_0} \tag{7-1}$$

The system transfer function was then used to simulate the hydrodynamics of the intracranial and spinal canal compartments for different conditions and combinations of compliances.

Computer simulation of the compartmental pressure and volume dynamics

The volume and pressure change dynamics in the intracranial and spinal canal compartments were simulated using the lumped parameter circuit model. First of all, the system transfer function (Equation 7-1) was transformed to the state space equations shown in Equation 7-2,

$$\begin{cases}\begin{bmatrix} f_{CSF}(n+1) \\ p_1(n+1)-p_2(n+1)\end{bmatrix}=\begin{bmatrix}-n_1 & 1\\ -n_0 & 0\end{bmatrix}\begin{bmatrix} f_{CSF}(n) \\ p_1(n)-p_2(n)\end{bmatrix}+\begin{bmatrix} m_1 \\ m_0\end{bmatrix}f_{AV}(n)\\ f_{CSF}(n)=\begin{bmatrix}1 & 0\end{bmatrix}\begin{bmatrix} f_{CSF}(n) \\ p_1(n)-p_2(n)\end{bmatrix}\end{cases} \tag{7-2}$$

where p is compartmental pressure, m and n are the discrete transfer function coefficients from Equation 7-1, and f is the trans-compartmental volumetric flow rate. The zero-order hold method was used to convert the discrete-time parameters to the continuous-time parameters using the following equations.

$$\begin{bmatrix} -n_1 & 1 \\ -n_0 & 0 \end{bmatrix} = 1 + \mathbf{F}T \Rightarrow \mathbf{F}T = \begin{bmatrix} -n_1 - 1 & 1 \\ -n_0 & -1 \end{bmatrix} \Rightarrow \mathbf{F} = \begin{bmatrix} \frac{-n_1 - 1}{T} & \frac{1}{T} \\ \frac{-n_0}{T} & \frac{-1}{T} \end{bmatrix}$$

$$\begin{bmatrix} m_1 \\ m_0 \end{bmatrix} = T\mathbf{G} \Rightarrow \mathbf{G} = \begin{bmatrix} \frac{m_1}{T} \\ \frac{m_0}{T} \end{bmatrix} \tag{7-3}$$

where F and G are the state space parameters in continuous time domain, and T is the sampling interval. Then the continuous-time transfer function can be derived by the following equation.

$$H(s) = H(s\boldsymbol{I} - \boldsymbol{F})^{-1}\boldsymbol{G} = \frac{\frac{m_0}{T}s + \frac{1}{T^2}(m_0 + m_1)}{s^2 + \frac{n_1 + 2}{T}s + \frac{1}{T^2}(n_1 + n_0 + 1)} \tag{7-4}$$

where I is the identity matrix. The state variables with different compliance states were then calculated by using the following state space equations.

$$\begin{cases} \begin{bmatrix} dp_1 \\ df_{csf} \\ dp_2 \end{bmatrix} = \begin{bmatrix} 0 & -\frac{(m_0 + m_1)}{T^2}\frac{1}{\alpha} & 0 \\ 1 & -\frac{n_1 + 2}{T} & -1 \\ 0 & (\frac{-1}{T^2}((m_0 + m_1) - (n_1 + n_0 + 1)))\frac{1}{\beta} & 0 \end{bmatrix} \begin{bmatrix} p_1 \\ f_{csf} \\ p_2 \end{bmatrix} + \begin{bmatrix} \frac{(m_0 + m_1)}{T^2}\frac{1}{\alpha} \\ \frac{m_0}{T} \\ 0 \end{bmatrix} f_{av} \\ f_{csf} = \begin{bmatrix} 0 & 1 & 0 \end{bmatrix} \begin{bmatrix} p_1 \\ f_{csf} \\ p_2 \end{bmatrix} \end{cases} \tag{7-5}$$

where α and β are the scaling factors for the intracranial and spinal canal compliances, respectively. Both factors were set from 0.1 to 2 with step of 0.1. The compliance range

was defined based on findings that the intracranial compliance in the upright posture is about 2.8 folds larger than in the supine posture (Alperin *et al.*, 2005a).

Volume change of the intracranial and spinal canal compartments

The compartmental volume change waveform was derived from the integration of measured compartmental volumetric flow waveform over one cardiac cycle (Equation 6-2).

7-4 Results

In general, the changes in the cranial and spinal volume and pressure pulsation amplitudes with respect to changes in the cranial and spinal compliance distribution follow similar trends for all subjects, as expected. The differences between the cohorts however, are mainly related to the rate at which changes occur and the interval at which they occur. Examples of the simulated volume and pressure changes with respect to the changes in the intracranial compliance (C1) while the spinal compliance (C2) is fixed, changes in C2 while C1 is fixed, and changes in the total compliance (C1+C2) while the ratio C1/C2 is unchanged using the MRI data obtained from a healthy subject are shown in Figure 7-1. With increasing C1 and total craniospinal compliance (TC), the maximal intracranial volume change (dV1) increases, and the ICP pulsation (dP1) decreases. In contrast, when increasing spinal canal compliance (C2), the CSF flow to spinal canal compartment is increased resulting with increased volume change (dV2). As a consequence, the volume and pressure changes in the intracranial compartment are decreased. The volume and pressure simulations with different compliance for the three

cohorts are shown in the following pages. For each cohort, the mean value is presented by solid line and the standard error of the mean is presented by error bar.

Influence of the intracranial compliance in the compartmental volume and pressure changes

When comparing healthy male to obese female subjects, the intracranial volume change (dV1) was larger in the male subjects compared with the obese female subjects (Figure 7-2). This is also true for the volume change of spinal canal compartment (dV2). However, this difference was not statistically significant due to large inter-individual variability. The mean cranial and spinal volume changes of the IIH cohort was between the mean values of the other two cohorts. The pressure changes are shown in Figure 7-3. In contrast to the volume changes, the cranial and spinal pressure changes were significantly higher in the IIH group compared to the healthy cohorts. This is in agreement with clinical data of spinal canal invasive pressure recordings obtained from IIH patients undergoing lumbar puncture. An example of pressure recording for a non-IIH and an IIH patients demonstrating higher pressure fluctuation in IIH is shown in Figure 7-4.

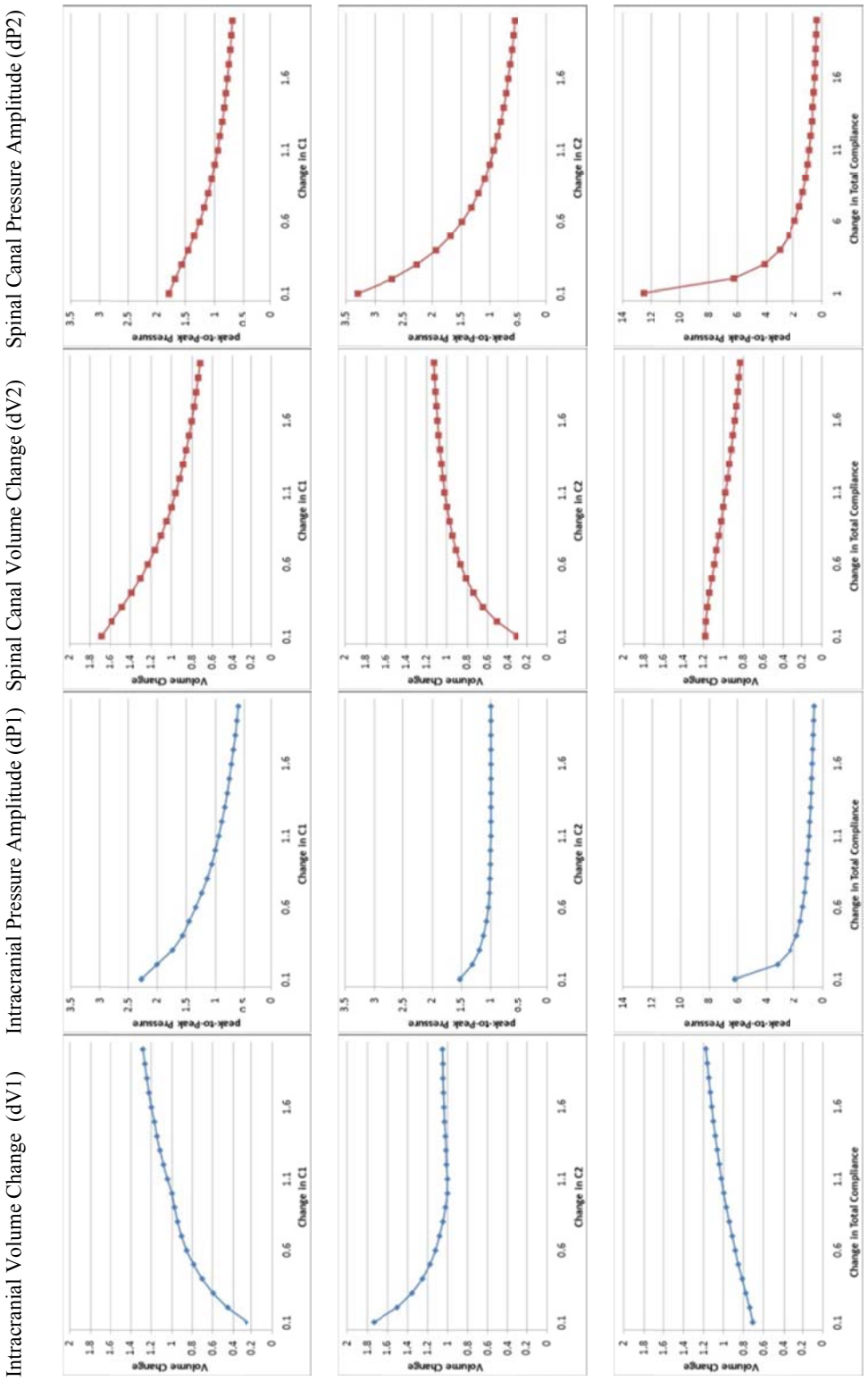

Figure 7-1: Simulation of compartmental volume and pressure change with different intracranial and spinal compliance states.

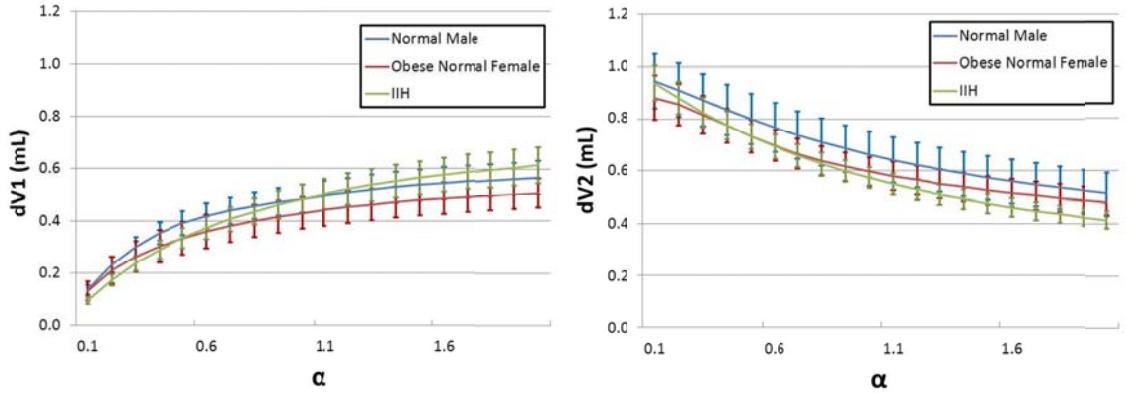

Figure 7-2: Simulated compartmental volume changes for different intracranial compliance states.

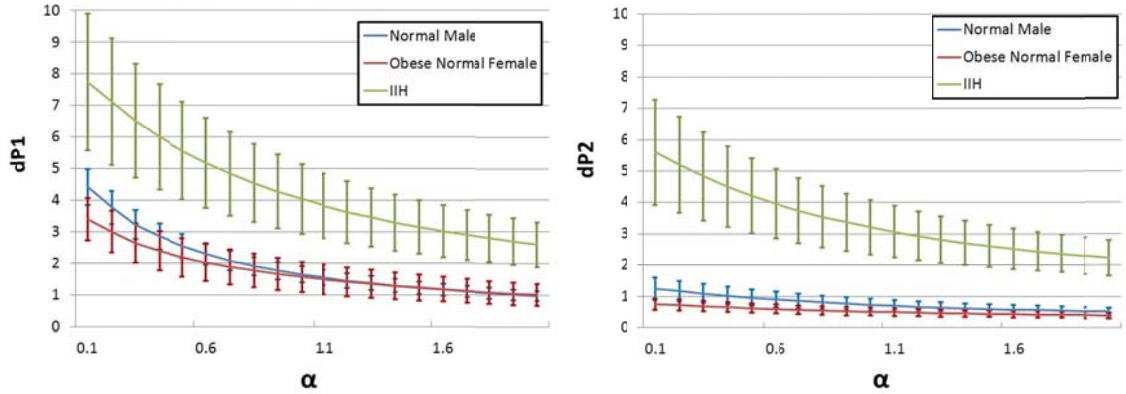

Figure 7-3: Simulated compartmental pressure amplitudes for different intracranial compliance states.

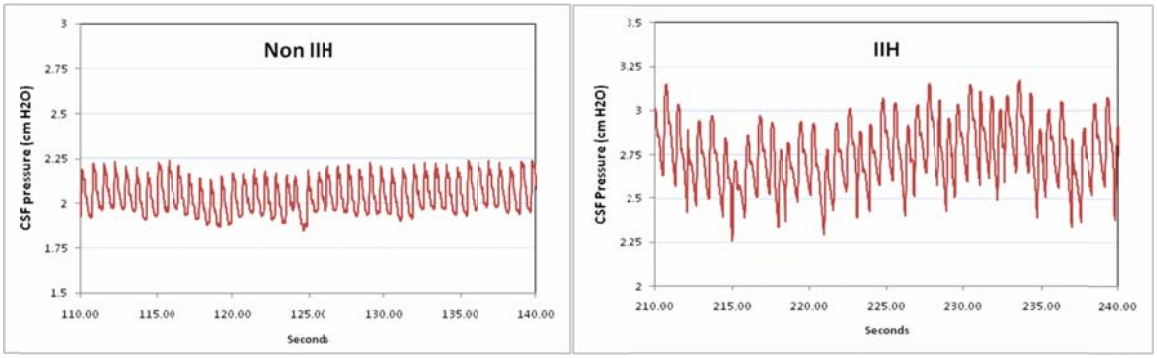

Figure 7-4: CSF pressure recordings from the lumbar region demonstrating increased pressure pulsation in IIH. Data provided by Dr. Göran Kindåker from the Institution of neurology, Academic hospital in Uppsala, Sweden.

Influence of the spinal canal compliance in the compartmental volume and pressure changes

Figures 7-5 to 7-6 demonstrate the changes in the volume and pressure with respect to increasing spinal canal compliance. As expected, the trends for the volume change in each compartment were reversed compared with changes associated with increase in the intracranial compliance. The pressure pulsation of two compartments in IIH was again larger than in the normal male and obese female subjects (Figure 7-6). An unpaired two tailed t-test at 95% confidence interval showed that the peak-to-peak pressure of both compartments in IIH is significantly larger than the peak-to-peak pressure in normal subjects ($p<0.05$).

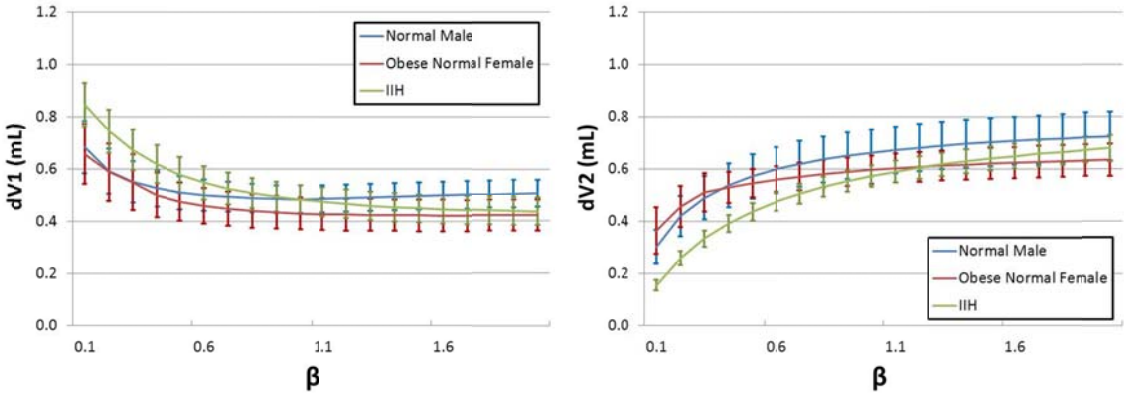

Figure 7-5: Simulated compartmental volume changes for different spinal canal compliance states.

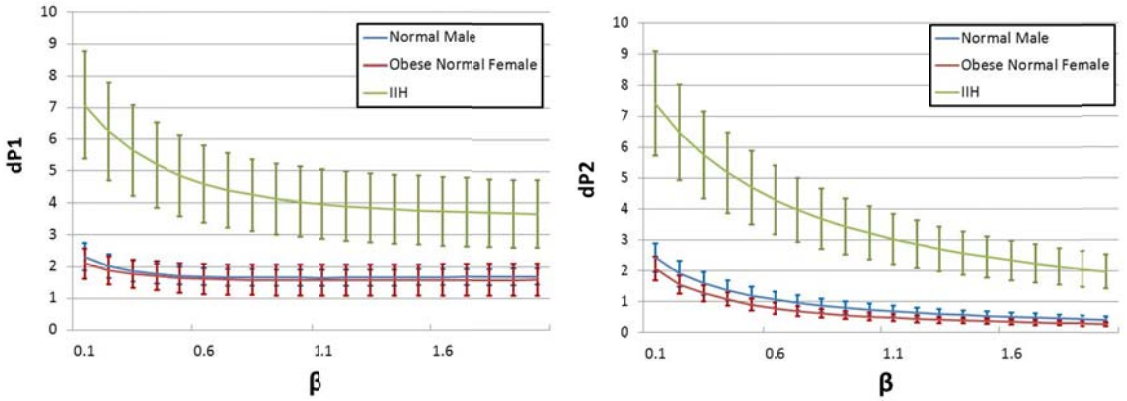

Figure 7-6: Simulated compartmental pressure amplitudes (peak-to-peak) for different spinal canal compliance states.

Influence of the total compliance in the compartmental volume and pressure changes

The effect of a change in total craniospinal compliance on the volume and pressure change dynamics is similar to that of a change only of the intracranial compliance. When total compliance increases, intracranial volume change is increased and spinal canal volume change is decreased (Figure 7-7). For the peak-to-peak compartmental pressure, the IIH patients again have larger pressure pulsation than the normal controls (Figure 7-8).

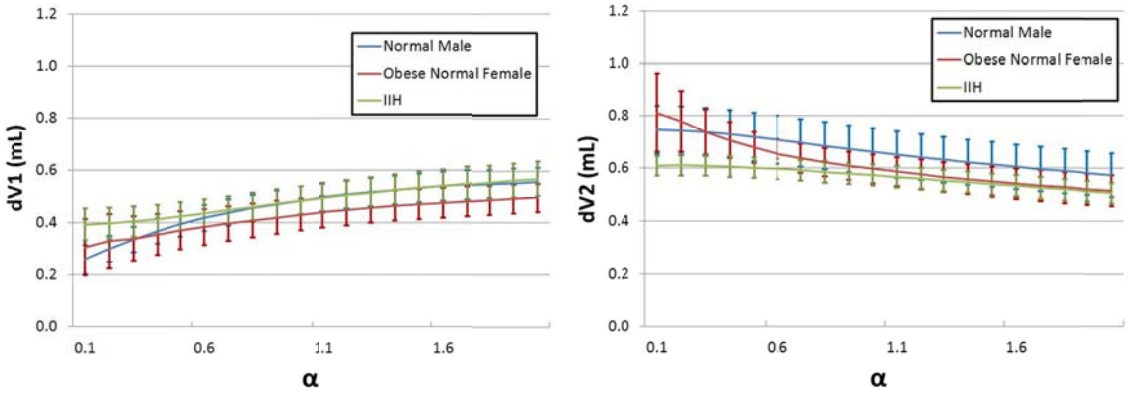

Figure 7-7: Simulated compartmental volume changes for different total craniospinal compliance states.

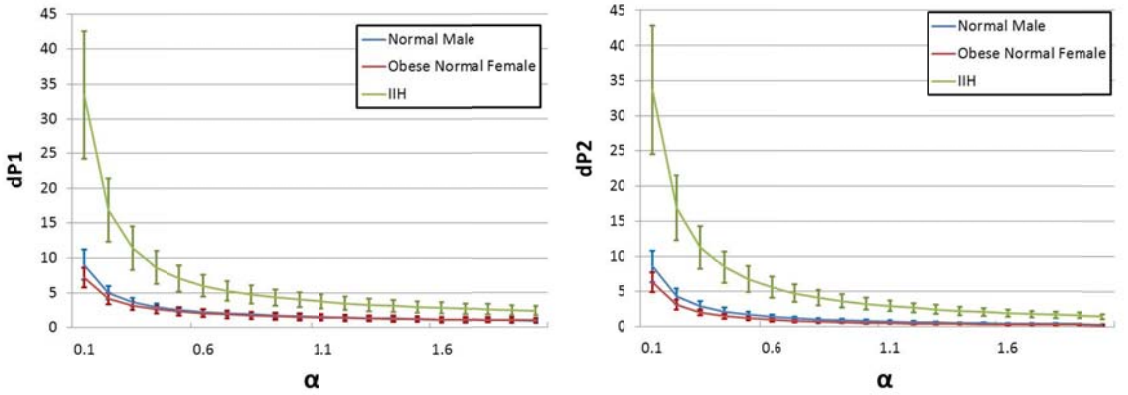

Figure 7-8: Simulated compartmental pressure amplitudes (peak-to-peak) for different total craniospinal compliance states.

7-5 Discussion

The dependency of the volume and pressure pulsation in the craniospinal sub-compartments with respect to a change in the total compliance and in its relative cranio-spinal distribution for three cohorts has been studied by modeling simulations. Overall, the model predictions are in agreement with findings in invasive clinical recording. The model simulations further demonstrate that the peak-to-peak compartmental pressure indeed increase as expected with reduced compartmental compliance. The simulations further demonstrate that the reduced spinal canal compliance (SCC or C2) is associated with increased spinal canal pressure pulsation as found in IIH. Furthermore, the model simulation can be used to assess stability of the craniospinal system as discussed in the following section.

Function of the spinal canal compartment in the regulation of ICP

The elastic spinal dural sac acts as a reservoir for CSF in response to intracranial volume changes during each cardiac cycle. This property is impaired if the SCC is reduced. The consequence of reduced SCC is an overall reduced system compliance and an increase in ICP. In 1973, Löfgren and Zwetnow applied pressure-volume (PV) test in dogs (Löfgren and Zwetnow, 1973). The individual compartments' PV curves were obtained from isolated intracranial and spinal canal compartments. The spinal PV curve demonstrated a slower rate of pressure increase with increasing volume confirming the fact that the spinal canal dominates the regulation of ICP. This concept can be supported by modeling simulations of changes in SCC as shown in Figure 7-9. In the figures, volume and pressure simulations for different SCCs were normalized by the value of the

initial system state. The solid line is the mean value for each cohort and the error bar represents standard error of the mean. In healthy male subjects, the magnitude of the intracranial pressure change (dP1) is nearly constant with respect to changes in SCC across wide range of compliance (from 0.4 to 2). The magnitude of the dP1 in the female subjects demonstrates a shorter interval where of unchanging pulse pressure (from 0.9 to 2) suggesting a smaller spinal canal compliance buffering. This may explain the fact that some CSF related disorders associated with compliance such as Chiari-malformation type I occurs at a significantly higher frequency in females compared with male subjects. The range of a stable dP1 is further reduced in IIH (1.6 to 2), indicating the least spinal canal compliance buffering.

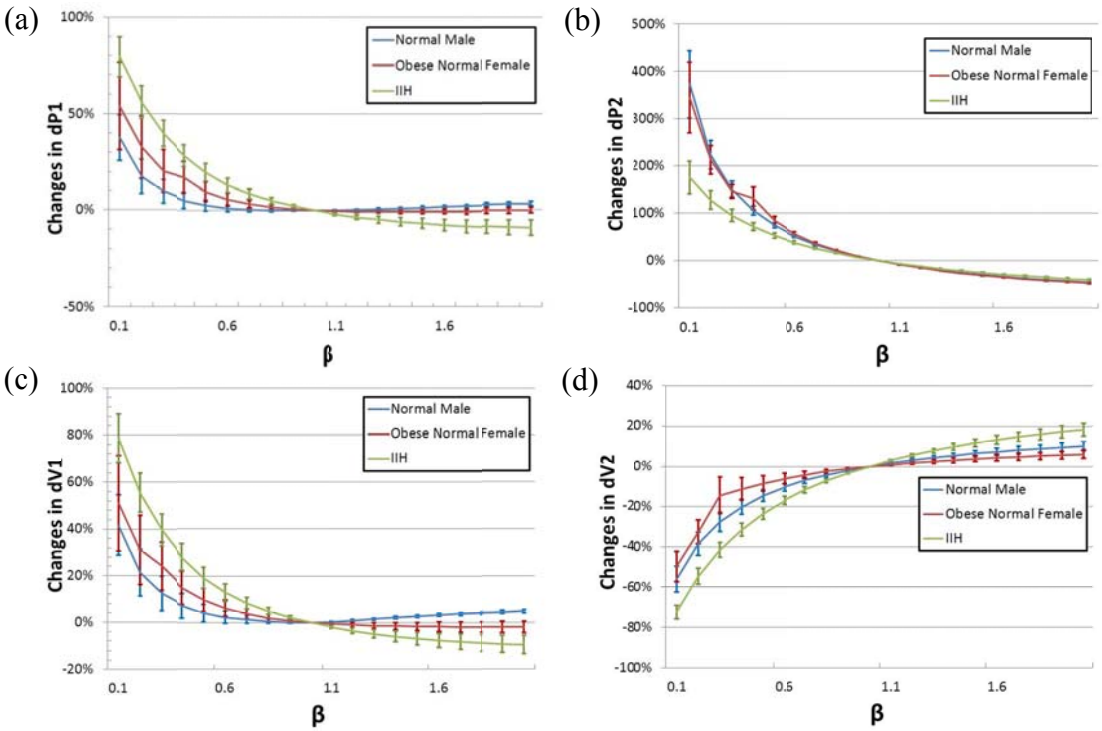

Figure 7-9: Normalized volume and pressure pulsation changes in the intracranial compartment simulated with different spinal canal compliances.

Model simulation in assessing craniospinal stability

The work summarized in the previous chapter provides the compliance characteristics leading to the elevated ICP in IIH. An earlier study of long term ICP monitoring in IIH revealed vary large fluctuation in the ICP (4-30mmHg) during a period of 24 hours (Gücer and Viernstein, 1978). The simulations presented in this chapter enable comparison of the craniospinal hydrodynamic stability between the three cohorts. Simulation examples from three subjects (one normal male, one obese normal female, and one IIH patient) are shown using 3-D surface plots (Figure 7-10). The value of the simulated pressures was normalized by the minimal pressure value over the entire sub-compartmental compliances states. The pressure of the initial craniospinal compliance state is marked by a white dot. As shown in Figure 7-10, a similar behavior is seen for the healthy male and female subjects. The dark blue corresponds to regions where dP1 is not significantly influenced by changes in intracranial (ICC) and spinal canal compliance (SCC). When both ICC and SCC are very small, dP1 increases significantly as shown in dark red color. In IIH, the initial craniospinal compliance state is near the boundary of dark blue region, which means that the patient's craniospinal system no longer provides "enough CSF space buffering".

There are several limitations for this modeling simulation. In the current simulation the input to the model, i.e., the arterial and venous blood flow, is kept fixed for all conditions. However, it is likely that the cerebral autoregulation blood flow will be effected by changes in ICP to maintain the perfusion pressure (Balestreri *et al.*, 2006). This feedback mechanism is not considered in the modeling simulations. A second

limitation is due to the fact that the lumped parameter modeling does not allow for derivation of the values of the individual system components (e.g., R, L, and C). Therefore, further investigation can help to understand the relationship between the estimated absolute values of the “circuit equivalent voltage” and the hydrodynamics equivalent for the pressure pulsation.

7-6 Summary

The spinal canal compartment provides a volume reserve for ICP regulation. In this study, simulations of CSF flow dynamics at different spinal canal compliance states were used to characterize the coupling between the system sub-compartments. The simulation provides insight into the pathophysiology of obesity-related IIH and is able to explain the chronically elevated ICP, the higher spinal canal cardiac related CSF pressure pulsation, and the large non-cardiac related fluctuation in ICP.

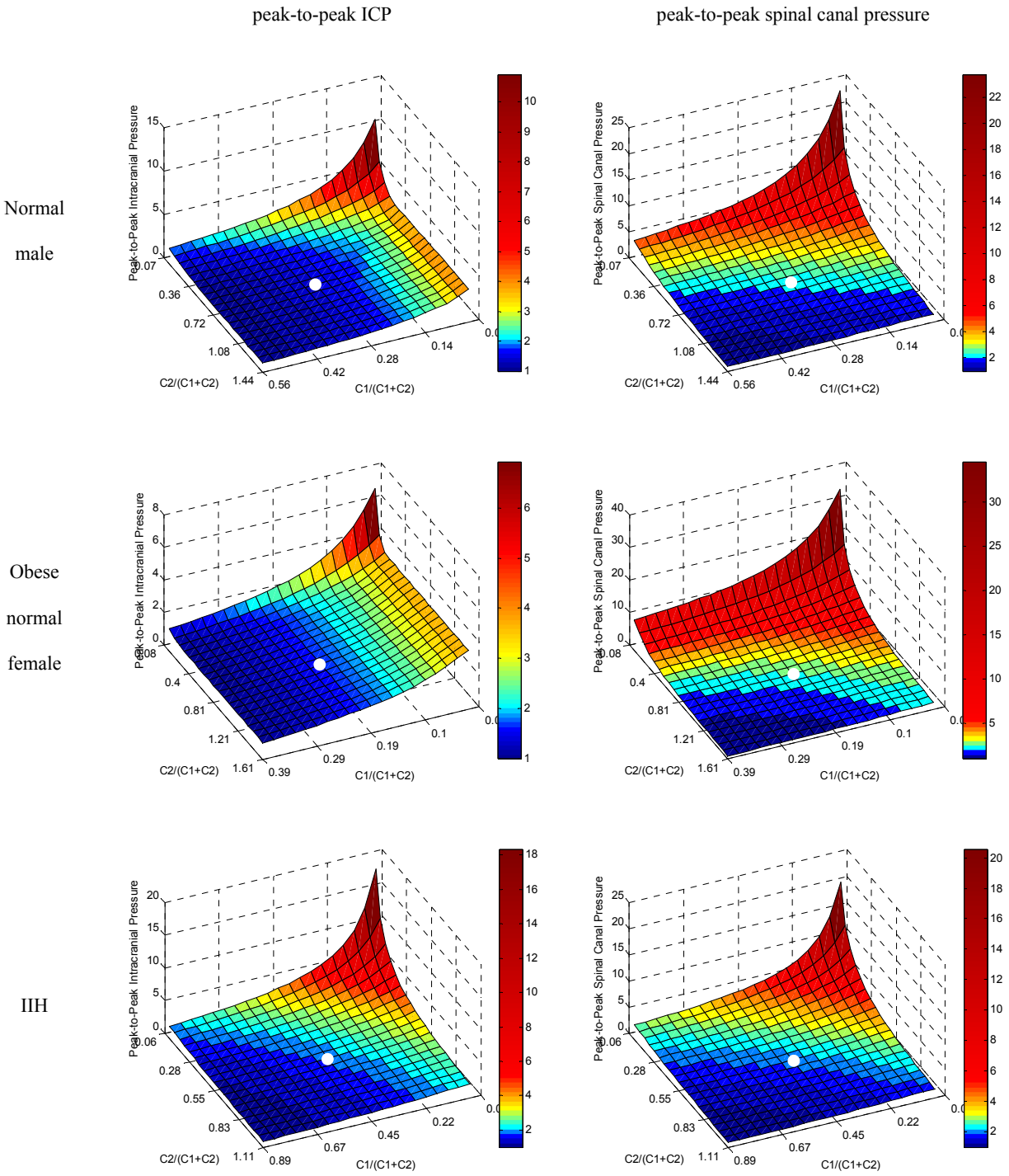

Figure 7-10: 3D surface plots of compartmental pressure changes simulated from the modeled craniospinal system with different intracranial and spinal canal compliances. The white dot in the plot indicates the value of initial system condition.

References

Agarwal G., Berman B., Stark L. (1969) A lumped parameter model of the cerebrospinal fluid system. *IEEE Trans Biomed Eng,* **16**, 45-53.

Alperin N., Lee S. (2003) PUBS: pulsatility-based segmentation of lumens conducting non-steady flow. *Magn Reson Med,* **49**, 934-944.

Alperin N., Lee S., Loth F., Raksin P., Lichtor T. (2000) MR-Intracranial pressure (ICP): a method to measure intracranial elastance and pressure noninvasively by means of MR imaging: baboon and human study. *Radiology,* **217**, 877-885.

Alperin N., Lee S., Sivaramakrishnan A., Hushek S. (2005a) Quantifying the effect of posture on intracranial physiology in humans by MRI flow studies. *J Magn Reson Imaging,* **22**, 591-596.

Alperin N., Mazda M., Lichtor T., Lee S. H. (2006) From Cerebrospinal Fluid Pulsation to Noninvasive Intracranial Compliance and Pressure Measured by MRI Flow Studies. *Current Medical Imaging Reviews,* **2**, 117-130.

Alperin N., Ranganathan S., Bagci A. M., Adams D. J., Ertl-Wagner B., Saraf-Lavi E., Sklar E. M., Lam B. L. (2012) MRI Evidence of Impaired CSF Homeostasis in Obesity-Associated Idiopathic Intracranial Hypertension. *AJNR Am J Neuroradiol*.

Alperin N., Sivaramakrishnan A., Lichtor T. (2005b) Magnetic resonance imaging-based measurements of cerebrospinal fluid and blood flow as indicators of intracranial compliance in patients with Chiari malformation. *J Neurosurg,* **103**, 46-52.

Alperin N., Vikingstad E., Gomez-Anson B., Levin D. (1996) Hemodynamically independent analysis of cerebrospinal fluid and brain motion observed with dynamic phase contrast MRI. *Magn Reson Med,* **35**, 741-754.

Ambarki K., Baledent O., Kongolo G., Bouzerar R., Fall S., Meyer M. (2007) A new lumped-parameter model of cerebrospinal hydrodynamics during the cardiac cycle in healthy volunteers. *IEEE Trans Biomed Eng,* **54**, 483-491.

Avezaat C., van Eijndhoven J. (1986) Clinical observations on the relationship between cerebrospinal fluid pulse pressure and intracranial pressure. *Acta Neurochir (Wien),* **79**, 13-29.

Balestreri M., Czosnyka M., Hutchinson P., Steiner L. A., Hiler M., Smielewski P., Pickard J. D. (2006) Impact of intracranial pressure and cerebral perfusion pressure on severe disability and mortality after head injury. *Neurocrit Care,* **4**, 8-13.

Balédent O., Gondry-Jouet C., Meyer M., De Marco G., Le Gars D., Henry-Feugeas M., Idy-Peretti I. (2004) Relationship between cerebrospinal fluid and blood dynamics in healthy volunteers and patients with communicating hydrocephalus. *Invest Radiol,* **39**, 45-55.

Balédent O., Henry-Feugeas M., Idy-Peretti I. (2001) Cerebrospinal fluid dynamics and relation with blood flow: a magnetic resonance study with semiautomated cerebrospinal fluid segmentation. *Invest Radiol,* **36**, 368-377.

Bateman G., Stevens S., Stimpson J. (2009) A mathematical model of idiopathic intracranial hypertension incorporating increased arterial inflow and variable venous outflow collapsibility. *J Neurosurg,* **110**, 446-456.

Beards S. C., Yule S., Kassner A., Jackson A. (1998) Anatomical variation of cerebral venous drainage: the theoretical effect on jugular bulb blood samples. *Anaesthesia,* **53**, 627-633.

Bhadelia R., Bogdan A., Kaplan R., Wolpert S. (1997) Cerebrospinal fluid pulsation amplitude and its quantitative relationship to cerebral blood flow pulsations: a phase-contrast MR flow imaging study. *Neuroradiology,* **39**, 258-264.

Boon A., Tans J., Delwel E., Egeler-Peerdeman S., Hanlo P., Wurzer H., Avezaat C., de Jong D., Gooskens R., Hermans J. (1997) Dutch normal-pressure hydrocephalus study: prediction of outcome after shunting by resistance to outflow of cerebrospinal fluid. *J Neurosurg,* **87**, 687-693.

Chu D., Levin D. N., Alperin N. (1998) Assessment of the biomechanical state of intracranial tissues by dynamic MRI of cerebrospinal fluid pulsations: a phantom study. *Magn Reson Imaging,* **16**, 1043-1048.

Czosnyka M., Batorski L., Laniewski P., Maksymowicz W., Koszewski W., Zaworski W. (1990) A computer system for the identification of the cerebrospinal compensatory model. *Acta Neurochir (Wien),* **105**, 112-116.

Deeren D. H., Dits H., Malbrain M. L. (2005) Correlation between intra-abdominal and intracranial pressure in nontraumatic brain injury. *Intensive Care Med,* **31**, 1577-1581.

Dhoondia H., Alperin N. (2003) Improved MR-Intracranial Pressure (MR-ICP) Measurement using a new Data Acquisition Technique. *In*: Proc Intl Soc Mag Reson Med. p. 793.

Dhungana S., Sharrack B., Woodroofe N. (2010) Idiopathic intracranial hypertension. *Acta Neurol Scand,* **121**, 71-82.

Egnor M., Rosiello A., Zheng L. (2001) A model of intracranial pulsations. *Pediatr Neurosurg,* **35**, 284-298.

Eide P., Brean A. (2006) Lumbar cerebrospinal fluid pressure waves versus intracranial pressure waves in idiopathic normal pressure hydrocephalus. *Br J Neurosurg,* **20**, 407-414.

Eklund A., Smielewski P., Chambers I., Alperin N., Malm J., Czosnyka M., Marmarou A. (2007) Assessment of cerebrospinal fluid outflow resistance. *Med Biol Eng Comput,* **45**, 719-735.

Ekstedt J. (1977) CSF hydrodynamic studies in man. 1. Method of constant pressure CSF infusion. *J Neurol Neurosurg Psychiatry,* **40**, 105-119.

Fedorow C., Moon M., Mutch W., Grocott H. (2010) Lumbar cerebrospinal fluid drainage for thoracoabdominal aortic surgery: rationale and practical considerations for management. *Anesth Analg,* **111**, 46-58.

Fridén H., Ekstedt J. (1982) Instrumentation for cerebrospinal fluid hydrodynamic studies in man. *Med Biol Eng Comput,* **20**, 167-180.

Gawthrop P. J., Bevan G. P. (2007) Bond-graph modeling. *IEEE CONTROL SYSTEMS,* **27**, 22.

Gilland O. (1965) CSF dynamic diagnosis of spinal block. II. The spinal CSF pressure-volume curve. *Acta Neurol Scand,* **41**, 487-496.

Glick R. P., Niebruegge J., Lee S. H., Egibor O., Lichtor T., Alperin N. (2006) Early experience from the application of a noninvasive magnetic resonance imaging-based measurement of intracranial pressure in hydrocephalus. *Neurosurgery,* **59**, 1052-1060; discussion 1060-1051.

Gu H., Lu H., Ye F., Stein E., Yang Y. (2006) Noninvasive quantification of cerebral blood volume in humans during functional activation. *Neuroimage,* **30**, 377-387.

Guinane J. E. (1972) An equivalent circuit analysis of cerebrospinal fluid hydrodynamics. *Am J Physiol,* **223**, 425-430.

Gücer G., Viernstein L. (1978) Long-term intracranial pressure recording in the management of pseudotumor cerebri. *J Neurosurg,* **49**, 256-263.

Hogan Q., Prost R., Kulier A., Taylor M., Liu S., Mark L. (1996) Magnetic resonance imaging of cerebrospinal fluid volume and the influence of body habitus and abdominal pressure. *Anesthesiology,* **84**, 1341-1349.

Johanson C., Duncan J. r., Klinge P., Brinker T., Stopa E., Silverberg G. (2008) Multiplicity of cerebrospinal fluid functions: New challenges in health and disease. *Cerebrospinal Fluid Res,* **5**, 10.

Karahalios D. G., Rekate H. L., Khayata M. H., Apostolides P. J. (1996) Elevated intracranial venous pressure as a universal mechanism in pseudotumor cerebri of varying etiologies. *Neurology,* **46**, 198-202.

Katzman R., Hussey F. (1970) A simple constant-infusion manometric test for measurement of CSF absorption. *Neurology,* **20**.

Kim J., Thacker N. A., Bromiley P. A., Jackson A. (2007) Prediction of the jugular venous waveform using a model of CSF dynamics. *AJNR Am J Neuroradiol,* **28**, 983-989.

Ko H., Park J., Shin Y., Baek S. (2004) Gross quantitative measurements of spinal cord segments in human. *Spinal Cord,* **42**, 35-40.

Kobayashi K., Akishita M., Yu W., Hashimoto M., Ohni M., Toba K. (2004) Interrelationship between non-invasive measurements of atherosclerosis: flow-mediated dilation of brachial artery, carotid intima-media thickness and pulse wave velocity. *Atherosclerosis,* **173**, 13-18.

Lakin W., Stevens S., Tranmer B., Penar P. (2003) A whole-body mathematical model for intracranial pressure dynamics. *J Math Biol,* **46**, 347-383.

Lee R., Abraham R., Quinn C. (2001) Dynamic physiologic changes in lumbar CSF volume quantitatively measured by three-dimensional fast spin-echo MRI. *Spine (Phila Pa 1976),* **26**, 1172-1178.

Lenfeldt N., Koskinen L., Bergenheim A., Malm J., Eklund A. (2007) CSF pressure assessed by lumbar puncture agrees with intracranial pressure. *Neurology,* **68**, 155-158.

Lindgren S., Rinder L. (1969) Production and distribution of intracranial and intraspinal pressure changes at sudden extradural fluid volume input in rabbits. *Acta Physiol Scand,* **76**, 340-351.

Ljung L. (1999) *System identification : theory for the user,* Upper Saddle River, NJ: Prentice Hall PTR.

Loth F., Yardimci M., Alperin N. (2001) Hydrodynamic modeling of cerebrospinal fluid motion within the spinal cavity. *J Biomech Eng,* **123**, 71-79.

Lu H., Law M., Ge Y., Hesseltine S., Rapalino O., Jensen J., Helpern J. (2008) Quantitative measurement of spinal cord blood volume in humans using vascular-space-occupancy MRI. *NMR Biomed,* **21**, 226-232.

Löfgren J., von Essen C., Zwetnow N. (1973) The pressure-volume curve of the cerebrospinal fluid space in dogs. *Acta Neurol Scand,* **49**, 557-574.

Löfgren J., Zwetnow N. (1973) Cranial and spinal components of the cerebrospinal fluid pressure-volume curve. *Acta Neurol Scand,* **49**, 575-585.

Magnaes B. (1989) Clinical studies of cranial and spinal compliance and the craniospinal flow of cerebrospinal fluid. *Br J Neurosurg,* **3**, 659-668.

Makki M., Sood S., Baledent O., Mody S., Grover K. (2007) Cine MRI Flow-Analysis in Phantom Model of Cranio-Spinal Axis In-vivo Studies. *In*: International Society for Magnetic Resonance in Medicine.

Mann J., Butler A., Rosenthal J., Maffeo C., Johnson R., Bass N. (1978) Regulation of intracranial pressure in rat, dog, and man. *Ann Neurol,* **3**, 156-165.

Marks M. P., Pelc N. J., Ross M. R., Enzmann D. R. (1992) Determination of cerebral blood flow with a phase-contrast cine MR imaging technique: evaluation of normal subjects and patients with arteriovenous malformations. *Radiology,* **182**, 467-476.

Marmarou A., Shulman K., LaMorgese J. (1975) Compartmental analysis of compliance and outflow resistance of the cerebrospinal fluid system. *J Neurosurg,* **43**, 523-534.

Marmarou A., Shulman K., Rosende R. (1978) A nonlinear analysis of the cerebrospinal fluid system and intracranial pressure dynamics. *J Neurosurg,* **48**, 332-344.

Marshall I., MacCormick I., Sellar R., Whittle I. (2008) Assessment of factors affecting MRI measurement of intracranial volume changes and elastance index. *Br J Neurosurg,* **22**, 389-397.

Maset A. L., Marmarou A., Ward J. D., Choi S., Lutz H. A., Brooks D., Moulton R. J., DeSalles A., Muizelaar J. P., Turner H. (1987) Pressure-volume index in head injury. *J Neurosurg,* **67**, 832-840.

Miyati T., Mase M., Banno T., Kasuga T., Yamada K., Fujita H., Koshida K., Sanada S., Onoguchi M. (2003) Frequency analyses of CSF flow on cine MRI in normal pressure hydrocephalus. *Eur Radiol,* **13**, 1019-1024.

Miyati T., Mase M., Kasai H., Hara M., Yamada K., Shibamoto Y., Soellinger M., Baltes C., Luechinger R. (2007) Noninvasive MRI assessment of intracranial compliance in idiopathic normal pressure hydrocephalus. *J Magn Reson Imaging,* **26**, 274-278.

Noback C. R., Ruggiero D. A., Demarest R. J., Strominger N. L. (2005) *The Human Nervous System: Structure and Function*.

Raabe A., Czosnyka M., Piper I., Seifert V. (1999) Monitoring of intracranial compliance: correction for a change in body position. *Acta Neurochir (Wien),* **141**, 31-36; discussion 35-36.

Reite M., Reite E., Collins D., Teale P., Rojas D., Sandberg E. (2010) Brain size and brain/intracranial volume ratio in major mental illness. *BMC Psychiatry,* **10**, 79.

Rekate H. (2008) The definition and classification of hydrocephalus: a personal recommendation to stimulate debate. *Cerebrospinal Fluid Res,* **5**, 2.

Rekate H. L., Brodkey J. A., Chizeck H. J., el Sakka W., Ko W. H. (1988) Ventricular volume regulation: a mathematical model and computer simulation. *Pediatr Neurosci,* **14**, 77-84.

Ryder H., Espey F., Kimbell F., Penka E., Rosenauer A., Podolsky B., Evans J. (1953) The mechanism of the change in cerebrospinal fluid pressure following an induced change in the volume of the fluid space. *J Lab Clin Med,* **41**, 428-435.

Schmidt J. M., Ko S. B., Helbok R., Kurtz P., Stuart R. M., Presciutti M., Fernandez L., Lee K., Badjatia N., Connolly E. S., Claassen J., Mayer S. A. (2011) Cerebral perfusion pressure thresholds for brain tissue hypoxia and metabolic crisis after poor-grade subarachnoid hemorrhage. *Stroke,* **42**, 1351-1356.

Shapiro K., Marmarou A., Shulman K. (1980) Characterization of clinical CSF dynamics and neural axis compliance using the pressure-volume index: I. The normal pressure-volume index. *Ann Neurol,* **7**, 508-514.

Shulman K., Marmarou A. (1971) Pressure-Volume Considerations in Infantile Hydrocephalus. *In:* pp. 90-95. Developmental medicine and child neurology.

Spilt A., Box F. M., van der Geest R. J., Reiber J. H., Kunz P., Kamper A. M., Blauw G. J., van Buchem M. A. (2002) Reproducibility of total cerebral blood flow measurements using phase contrast magnetic resonance imaging. *J Magn Reson Imaging,* **16**, 1-5.

Stevens S. A., Stimpson J., Lakin W. D., Thakore N. J., Penar P. L. (2008) A model for idiopathic intracranial hypertension and associated pathological ICP wave-forms. *IEEE Trans Biomed Eng,* **55**, 388-398.

Sundström N., Andersson K., Marmarou A., Malm J., Eklund A. (2010) Comparison between 3 infusion methods to measure cerebrospinal fluid outflow conductance. *J Neurosurg,* **113**, 1294-1303.

Tain R., Alperin N. (2009) Noninvasive intracranial compliance from MRI-based measurements of transcranial blood and CSF flows: indirect versus direct approach. *IEEE Trans Biomed Eng,* **56**, 544-551.

Tain R., Ertl-Wagner B., Alperin N. (2009) Influence of the compliance of the neck arteries and veins on the measurement of intracranial volume change by phase-contrast MRI. *J Magn Reson Imaging,* **30**, 878-883.

Tain R.-W., Alperin N. (2008) MRI-based Noninvasive Measurement of Intracranial Compliance Derived from the Relationship between Transcranial Blood and Cerebrospinal Fluid Flows: Modeling vs. Direct Approach. *In*: SPIE, Eds X. P. Hu & A. V. Clough San Diego.

Tain R. W., Bagci A. M., Lam B. L., Sklar E. M., Ertl-Wagner B., Alperin N. (2011) Determination of cranio-spinal canal compliance distribution by MRI: Methodology and early application in idiopathic intracranial hypertension. *J Magn Reson Imaging,* **34**, 1397-1404.

Takahashi S. (2010) Neurovascular Imaging: MRI & Microangiography. *In*.

Takemae T., Kosugi Y., Ikebe J., Kumagai Y., Matsuyama K., Saito H. (1987) A simulation study of intracranial pressure increment using an electrical circuit model of cerebral circulation. *IEEE Trans Biomed Eng,* **34**, 958-962.

Tsunoda A., Mitsuoka H., Sato K., Kanayama S. (2000) A quantitative index of intracranial cerebrospinal fluid distribution in normal pressure hydrocephalus using an MRI-based processing technique. *Neuroradiology,* **42**, 424-429.

Urchuk S., Plewes D. (1994) MR measurements of pulsatile pressure gradients. *J Magn Reson Imaging,* **4**, 829-836.

Ursino M. (1988) A mathematical study of human intracranial hydrodynamics. Part 1--The cerebrospinal fluid pulse pressure. *Ann Biomed Eng,* **16**, 379-401.

Ursino M., Colì L., La Manna G., Grilli Cicilioni M., Dalmastri V., Giudicissi A., Masotti P., Avanzolini G., Stefoni S., Bonomini V. (1996) A simple mathematical model of intradialytic sodium kinetics: "in vivo" validation during hemodialysis with constant or variable sodium. *Int J Artif Organs,* **19**, 393-403.

Ursino M., Giulioni M. (2003) Quantitative assessment of cerebral autoregulation from transcranial Doppler pulsatility: a computer simulation study. *Med Eng Phys,* **25**, 655-666.

Ursino M., Iezzi M., Stocchetti N. (1995) Intracranial pressure dynamics in patients with acute brain damage: a critical analysis with the aid of a mathematical model. *IEEE Trans Biomed Eng,* **42**, 529-540.

Ursino M., Lodi C. A. (1998) Interaction among autoregulation, CO2 reactivity, and intracranial pressure: a mathematical model. *Am J Physiol,* **274**, H1715-1728.

Ursino M., Lodi C. A., Rossi S., Stocchetti N. (1997) Intracranial pressure dynamics in patients with acute brain damage. *J Appl Physiol,* **82**, 1270-1282.

Ursino M., Lodi C. A., Russo G. (2000) Cerebral hemodynamic response to CO(2) tests in patients with internal carotid artery occlusion: modeling study and in vivo validation. *J Vasc Res,* **37**, 123-133.

Wagshul M., Chen J., Egnor M., McCormack E., Roche P. (2006) Amplitude and phase of cerebrospinal fluid pulsations: experimental studies and review of the literature. *J Neurosurg,* **104**, 810-819.

Wakeland W., Goldstein B. (2008) A review of physiological simulation models of intracranial pressure dynamics. *Comput Biol Med,* **38**, 1024-1041.

Wanifuchi H., Shimizu T., Maruyama T. (2002) Age-related changes in the proportion of intracranial cerebrospinal fluid space measured using volumetric computerized tomography scanning. *J Neurosurg,* **97**, 607-610.

Wåhlin A., Ambarki K., Birgander R., Alperin N., Malm J., Eklund A. (2010) Assessment of craniospinal pressure-volume indices. *AJNR Am J Neuroradiol,* **31**, 1645-1650.

Yallapragada N. (2003) *A model based description of the cerebrospinal fluid dynamics in the craniospinal system.* Master, University of Illinois at Chicago.

Yallapragada N., Alperin N. (2004) Characterization of spinal canal hydrodynamics and compliance using bond graph technique and CSF flow measurements by MRI. *In*: Proc Int Soc Magn Resonan Med. p. 2658.

Yanase M., Matsuyama Y., Hirose K., Takagi H., Yamada M., Iwata H., Ishiguro N. (2006) Measurement of the cervical spinal cord volume on MRI. *J Spinal Disord Tech,* **19**, 125-129.